# Tumor Infiltrating Regulatory T Cells – Phenotype and Expansion by Radiation Therapy

**by**

**Yuki Muroyama, MD**

A dissertation submitted to Johns Hopkins University in conformity with the requirements for the degree of Doctor of Philosophy

Baltimore, Maryland

November, 2017

**ABSTRACT**

Regulatory T cells (Treg) are the master immune-suppressor cells, with a double-edged sword. Treg protect us from autoimmunity, damages from excessive inflammation, and help us maintaining homeostasis in mucosal surface. On the other hand, Treg can be negative force against anti-tumor immunity in the tumor microenvironment (TME), which need to be targeted to maximize the effects of cancer immunotherapies. However, the exact phenotype and molecular basis of suppressive function of Treg in the TME have not been fully elucidated. Especially of translational relevance; what is the phenotype of tumor-infiltrating Treg (TIL-Treg) under the fundamental cancer therapy such as radiotherapy, and what is the determinant molecules for human TIL-Treg have not been fully elucidated.

To answer those questions, in my thesis projects, I have elucidated the TIL-Treg phenotype post radiotherapy (RT), and discovered novel human TIL-Treg targeting molecules.

In RT-Treg project, we have shown that RT significantly increased the phenotypically activated and, importantly functionally suppressive Treg in the TME. To the best of our knowledge, we were the first to demonstrate that irradiated TIL-Treg are indeed functionally suppressive, using the in vitro micro-suppression assay, using TIL post-RT. Our results also suggest that post-RT Treg expansion is likely independent of TGF-beta nor IL-33, but at least partly due to the proliferation of the Treg in the tumor.

In human TIL-Treg project, we performed RNAseq from prostate cancer, glioblastoma and renal cell carcinoma (and urothelial carcinoma as well) patients and identified novel targets highly expressed in TIL-Treg, including DUSP1, DUSP4, RGS1 (and RGS16).

Despite its high expression in Treg, DUSP1 showed unique downregulation upon activation, which presents a stark contrast with most Treg-associated molecules many of which increase their expression in activation. DUSP1 accordingly showed reciprocal expression pattern with DUSP4. From the data and close homology with DUSP1 and DUSP4, I hypothesized that DUSP1 and DUSP4 reciprocally regulate Treg activation and function. In depth *in vitro* and *in vivo* studies are underway to further elucidate the functional roles of these molecules in TIL-Treg (and TIL).

**Thesis readers:**

Dr. Charles G. Drake, MD, PhD (Thesis advisor; primary)

Dr. Drew M. Pardoll, MD, PhD (Thesis advisor; co-advisor)

Dr. Fan Pan, MD, PhD (Thesis committee member)

**Thesis committee members:**

Dr. Mark J. Soloski, PhD (Chair)

Dr. Jonathan D. Powell, MD, PhD

Dr. Fan Pan, MD, PhD

## PREFACE

This research will be humbly dedicated to all the patients and family members suffering from cancers and inflammatory diseases, and to the future/younger generations of doctors and scientists who are taking their courage to jump into the new frontier of global research world.

**ACKNOWLEDGEMENTS**

First and foremost, I would like to thank my outstanding mentors Dr. Charles Drake (Chuck; primary mentor) and Dr. Drew Pardoll (Drew). I cannot thank Chuck enough, a great scientist, physician and mentor, a role model of translational immunologists, and physician scientist. He has been constantly encouraging, positive, supportive, cheerful and nice to work with, respecting student's will and opinion, and gave me confidence in my research journey throughout my time in graduate school and in Drake lab. I would also like to thank Drew for his insightful comments and generous support for my research project. The experience in cancer immunology have widely opened up the great new research world and frontier to me. I would also like to thank my thesis committee members, Dr. Mark Soloski, Dr. Jonathan Powell and Dr. Fan Pan for their critical and insightful comments and suggestions, the great collaborative community of Bloomberg-Kimmel Institute (BKI) for Cancer Immunotherapy of Sidney-Kimmel Comprehensive Cancer Center (SKCCC), Graduate Immunology program at Johns Hopkins, School of Medicine and Columbia Center for Translational Immunology (CCTI) at Columbia University Medical Center, where Drake lab locates now.

This adventure was not possible without the tremendous support from my family and help from my friends; they are great friends as well as my life mentors.

My parents and brother in Japan, who supported me to make this adventure far away from my lovely hometown, have been always with me with their greatest love and support, believing in me more than I do, which really drove me keep moving forward.

I would like to give maximum acknowledgements to people who have supported me throughout my journey.

November 10th, 2017

New York

# Contents

LIST OF FIGURES

**LIST OF TABLES**

Table in CHAPTER I



Tables in CHAPTER II

# CHAPTER I: INTRODUCTION

# CHAPTER I: Introduction

## I-1: Cancer immunology, the tumor microenvironment and cancer immunotherapies

Today we are facing the unprecedented bursting development and the prime time of cancer immunotherapy; when the numbers of immunotherapies have been developed and approved in clinic, where the liaison of basic, translational and clinical research are making spiral progress and changing the clinical practice and patients outcome. The history of cancer immunology dates back in 1909, when Paul Ehrlich predicted that the immune system repressed the growth of carcinoma[1], revisited by Lewis Thomas and Frank Macfarlane Burnet in late 1950s[2-4]. The interaction of immune system and the tumor microenvironment (TME) was further systemized by Schreiber *et al*. as "cancer immunoediting" theory, which is a dynamic process composed of three phases: elimination, equilibrium, and escape[5,6].

Tumor progression or regression are determined by the tip of the balance of host anti-tumor immunity versus immune suppression in the TME (Figure I-1). Host anti-tumor effects come from the collaboration of innate and adaptive immune system; for innate immunity, danger signals released from tumors activate innate immunity including STING pathways, and release pro-inflammatory cytokines, and type I IFN. NK cell, M1 macrophage also play roles in tumor cell killing[7,8]. For adaptive immunity side, tumor antigen presentation followed by the tumor antigen specific activation of T cell response, leading to the secretion of IFN-g, Granzyme B for tumor killing, is of high importance. However, the TME also harbors numbers of immune suppressive mechanisms to evade

host immune attacks to protect themselves; including, lack of antigen presentation from tumor cells, impairment of T cell activation by expression of immune checkpoints (including CTLA-4, PD-1/PD-L1, LAG3, TIM-3, VISTA)[9], secretion of suppressive cytokines including TGF-beta, IL-10, IL-35, metabolic changes, and numbers of immune-suppressive cells such as tumor associated macrophages (TAM), Myeloid-derived suppressor cells (MDSC), and importantly, regulatory T cells (Treg)[10].

Cancer immunotherapy have been attempting to boost the anti-tumor immunity of host to eradicate tumors either by stimulating anti-tumor effects; the approaches include vaccines, adjuvant, agonists, or adoptive T cell transfer, or notably, by releasing breaks from suppressive immunity by targeting the above mentioned suppressive mechanisms, and the combination of both and with other pillars of cancer therapies including radiotherapy (RT) and chemotherapy. Among them, the most clinically successful approaches have been the immune checkpoint blockades[11-13], one of the latter approaches to releasing immunosuppressive breaks. Numbers of immune checkpoints, especially CTLA-4 and PD-1 targeted therapies to unleash the activated T cell responses, are now in clinic, and there have been floods of clinical trials of anti-CTLA4 and anti-PD-1/PD-L1 therapies and they have been approved by FDA in different types of tumors (Muroyama, LaFleur, Drake, Sharpe. *J. Immunol* (2018))[10,14] (Figure I-2, Table I)

## Table 1: FDA approved Anti-PD-1/PD-L1 Agents

| Target | Generic name | Isotype | Tumor types |
|---|---|---|---|
| PD-1 | Pembrolizumab | Humanized IgG4 (hinge region modified) | Melanoma, NSCLC, Hodgkin lymphoma, Urothelial carcinoma, HNSCC, MSI-H, dMMR |
| | Nivolumab | Fully human IgG4/kappa (hinge region modified) | Melanoma, NSCLC, Hodgkin lymphoma, RCC, Urothelial carcinoma, HNSCC, MSI-H, dMMR |
| PD-L1 | Atezolizumab | Humanized IgG1 (FcR-binding deficient) | NSCLC, Urothelial carcinoma |
| | Durvalumab | Humanized IgG1 (FcR-binding deficient) | Urothelial carcinoma |
| | Avelumab | Fully human IgG1 lambda | Urothelial carcinoma, Merkel cell carcinoma |

**Table 1: FDA approved Anti-PD-1/PD-L1 Agents**

Abbreviations: NSCLC: Non-Small Cell Lung Cancer, HNSCC: Head and Neck Squamous Cell Carcinoma, MSI-H: microsatellite instability-high, dMMR: mismatch repair deficient, RCC: Renal Cell Carcinoma

Despite the unprecedented successful cases and response rates of immunotherapies, numbers of cases are still refractory to the therapies; subsets of tumors are not immunogenic and with poor response rate (including prostate cancers, pancreatic cancers), and some patients experience relapse post immunotherapies. Therefore, understanding the mechanisms of resistance and developing the strategies to overcome resistance, making "cold/non-inflamed" tumors into "hot/inflamed" tumors have been huge challenges[7,10].

Many of the mechanisms of resistance overlap with the suppressive immune response

mentioned above, and recent clinical focus is also on mutational burden; low mutational burden could leading to low neo-antigen burden which could prime less tumor antigen specific T cells[10,15], and other factors of intervention are the active and intense area of research both in clinical and preclinical studies[10]. And among them, regulatory T cells (Treg) are the major immune suppressor of high importance, as described in the following section, and understanding the nature and molecular mechanism of Treg in tumors as well as developing Treg-targeted therapies are of vital translational and clinical importance to overcome resistance and maximize the effect of cancer immunotherapies.

**I-2: Regulatory T cells (Treg), especially in the tumor-microenvironment (TME)**

Regulatory T cell (Treg) is a subset of T cell with suppressive function, which plays an important role to avoid auto-immunity and maintain homeostasis by suppressing excessive inflammation. The key master regulator of Treg is Foxp3[16], which endows Treg the distinct gene signatures for their suppressive functions (including CTLA4, CD25…)[17]. Indeed, genetic mutations in Foxp3 are reported to impair Treg development and cause a fatal multi-organ autoimmune disease called immune dysregulation, polyendocrinopathy, enteropathy, and X-linked (IPEX) syndrome[18] in human. Treg depletion in mouse models also represent autoimmune diseases[19]. Treg exert immune suppressive functions in a variety of ways[20,21]; for example, Treg have high expression of CTLA-4, which interact with CD80/86 on antigen-presenting cells (APC), with higher affinity than CD28 on T cells, and down-regulating the co-stimulatory signal required for full T cell activation, making effector T cells anergic[22]. Treg can also deplete IL-2, a cytokine required for T

cell growth and activation, from surrounding environment via high expression of CD25 (IL-2R), outcompeting other T conventional cells (Tconv). Treg can also secrete numbers of immune-suppressive cytokines and molecules, including IL-10, TGF-beta, IL-35. Treg also express CD39 and CD73, converting ATP into adenosine, and some reports suggest that Treg can secrete granzymes to mediate killing of Tconv and APC[20,21].

This immune-suppressive nature of Treg is a double-edged sword. Treg play important roles in preventing auto-immunity, curtailing excessive inflammation, maintaining homeostasis including in the mucosa[23]. In human, adoptive transfer of Treg has actually ameliorated type I diabetes[24]. On the other hand, in the situation with cancers, as mentioned above, tumors take advantage of Treg suppression to protect themselves from the attacks from the host immune systems. In pre-clinical models, depletion of Treg results in better tumor control with activation of effector T cells[25-27]. In humans, Treg infiltration in tumor and low CD8/Treg ratio are reported to correlate with poor prognosis in patients in some types of cancers[20,28,29], depletion of Treg by low dose cyclophosphamide have shown better anti-tumor response[30,31] , and the treatments with anti-CTLA4 antibody have shown clinical response in different types of tumors including melanoma and now became established FDA-approved therapy[32,33].

Therefore, understanding the phenotype and molecular function of Treg in the TME and developing Treg-targeted immunotherapy are of high importance to maximize the anti-tumor immunity.

However, the nature of Treg in the TME has not been fully elucidated yet especially under the effects of cancer therapy including radiotherapy and the nature of Treg in human tumors.

Therefore, the objectives of my thesis projects are in two-fold;

(1) Elucidating the effect of radiotherapy (RT) on Treg in the TME

(2) Identifying the novel targets of human TIL-Treg

(1) The realistic and practical clinical approaches to optimize the efficacy of cancer immunotherapies will be combining them with other pillars of cancer therapies, such as chemotherapy and radiotherapy. With technical advancement, delivery of radiation become more targeted with better safety and efficacy profile. And accumulating evidence suggest that radiotherapy (RT) have numbers of anti-tumor immune-stimulatory effects, both in innate and adaptive immunity. However, not much has been known for the impact of suppressive immune phenotype including Treg, which needed to be targeted. Therefore, the overall goal of this project is to elucidate the effect of RT on Treg in the TME and characterize them both phenotypically, functionally and mechanistically.

(2) The nature of human TIL-Treg and the potential therapeutic targets selectively expressed in TIL-Treg or with beneficial immunomodulatory impacts have not been elucidated. From RNAseq data, we have identified novel HUMAN TIL-Treg targets with unique kinetics and of potential novel therapeutic targets, which are of important clinical and translational relevance.

# CHAPTER II: MATERIAL AND METHODS

## II-1: Material and Methods for Chapter III

### Experimental Animals

C57BL/6J and BALB/cJ mice were purchased from The Jackson Laboratory (Bar Harbor, ME). Female mice 4-8 weeks in age were used. To provide a congenic marker for cells used in suppression assays, 4-8 week-old, sex-matched CD45.1 (B6-Ly5.1/Cr) mice were purchased from Charles River Laboratories (Boston, MA). In some studies, Treg were isolated using sex-matched mice that express GFP under the control of the Foxp3 promoter (B6.129(Cg)-*Foxp3*$^{tm3(DTR/GFP)Ayr}$/J), referred hereafter as Foxp3 reporter mice[19]. A breeding pair was purchased from The Jackson Laboratories, and experimental animals were bred in-house. Animals were bred and housed in specific pathogen-free facilities accredited by the American Association for the Accreditation of Laboratory Animal Care (AAALAC) with protocols approved by the Animal Care and Use Committee of the Johns Hopkins University School of Medicine (Baltimore, MD).

### Cell lines

B16/F10, MC38, and RENCA cell lines were purchased from ATCC (Manassas, VA): B16/F10 and RENCA were cultured in complete RPMI (RPMI (Mediatech, Inc., Manassas, VA) with 10 % Fetal Bovine Serum (Gemini Bio-Products, West Sacramento, CA), 1 % anti-biotic/anti-mycotic solution (Sigma-Aldrich, St. Louis, MO), 1 % sodium pyruvate (Sigma-Aldrich), and 1 % MEM non-essential amino-acids (ThermoFisher Scientific, Waltham, MA). MC38 cells were cultured in complete DMEM (DMEM (Mediatech Inc.) with 10 % Fetal Bovine Serum (Gemini Bio-Products), 1 % anti-biotic/anti-mycotic solution (Sigma-Aldrich), 1 % sodium pyruvate (Sigma-Aldrich) and

1 % MEM non-essential amino-acids (ThermoFisher Scientific)) in 37°C, 5 % CO2 incubator.

**Flow cytometry**

Single-cell suspensions of tumor-infiltrating lymphocytes (TILs), draining lymph nodes (DLNs), and spleens were prepared as previously described[34]. Briefly, suspensions were prepared by mechanical dissociation, followed by density gradient centrifugation on an 80 % /40 % Percoll (GE Healthcare, Pittsburgh, PA) gradient. Cells were Fc-blocked with purified rat anti-mouse CD16/CD32 antibody (Clone: 2.4 G2, Becton Dickinson (BD), La Jolla, CA) for 30 minutes in 4°C. Dead cells were discriminated using the LIVE/DEAD® (LD) Fixable Near-IR Dead Cell Stain Kit (ThermoFisher Scientific) and samples were stained with the following antibodies: CD3 (Clone 17A2, Biolegend, San Diego, CA), CD4 (Clone RM4-5, ThermoFisher Scientific), CD8a (Clone 53-6.7, Biolegend), Foxp3 (Clone FJK-16s, eBioscience, San Diego, CA), CCR4 (Clone 2G12, Biolegend), 4-1BB (Clone 17B5, Biolegend), Ki-67 (Clone SolA15, Biolegend), CTLA-4 (Clone UC10-4B9, Biolegend), Helios (Clone 22F6, Biolegend). Stained samples were analyzed on an LSR II flow cytometer (BD). Flow data were quantified using FlowJo software (FlowJo, LLC, Ashland, OR).

**Radiotherapy (RT)**

Palpable tumors were irradiated with 10 Gy using the Small Animal Radiation Research Rlatform (SARRP; Xstrahl, Suwanee, GA) as previously described[35]. Briefly, mice with palpable subcutaneous tumors (B16/F10, RENCA, and MC38) were anesthetized with isoflurane and treated with SARRP radiotherapy (RT). 7-days post radiation, tumors,

DLNs and spleens were harvested, and analyzed by flow-cytometry.

**Tumor growth and TIL preparation**

On day 0, $5x10^5$ B16/F10, $1.5x10^6$ MC38 or $3x10^5$ RENCA cells were implanted subcutaneously (s.c.) to the flank of either wild-type C57BL/6J mice (in B16/F10 or MC38 experiments) or wild-type Balb/c mice (in RENCA experiments). On either day 7 (B16/F10), day 16 (RENCA) or day 10 (MC38), mice received 10 Gy of stereotactic radiation (RT) via the small animal radiation research platform (SARRP). 7 days after RT, mice were sacrificed. Tumors, DLNs, and spleens were harvested and used for flow cytometry analysis. Tumor diameters were measured every 2 to 3 days with an electronic caliper and are reported as volume using the formula $(W^2 \times L)/2$, where W represents the shorter diameter and L stands for the longer tumor diameter.

**Immunohistochemistry (IHC)**

Immunostaining for Foxp3 was performed on formalin-fixed, paraffin-embedded sections. Briefly, following dewaxing and rehydration, slides were immersed in 1% tween-20, and heat-induced antigen retrieval was performed in a steamer using Target Retrieval Solution (Dako, Santa Clara, CA) for 45 minutes. Slides were rinsed in PBST and endogenous peroxidase and phosphatase was blocked with Dual Endogenous Enzyme Block (Dako) and sections were then incubated with primary antibody; Foxp3 Rabbit monoclonal antibody (Clone D6O8R, Cell Signaling, Danvers, MA) for 45 minutes at room temperature. The primary antibodies were detected via a 30 minute incubation with HRP-labeled secondary antibody (Leica Microsystems, Buffalo Grove, IL) followed by detection with 3,3′-Diaminobenzidine (Sigma-Aldrich), counterstaining with Harris

hematoxylin, rehydration and mounting.

### *In vitro* suppression assays (micro-suppression assay)

Small-cell number suppression assays were performed as previously described[36]. To reliably sort Treg from spleen and tumors, Foxp3 reporter mice (B6.129(Cg)-*Foxp3*$^{tm3(DTR/GFP)Ayr}$/J) were used[19]. These mice were used for isolation of GFP-positive Treg, not for Treg-depletion. 5x$10^5$ B16/F10 cells were implanted s.c. into Foxp3 reporter mice. Mice were irradiated, and tumors and spleens were harvested as described above. TIL-Treg and spleen Treg from Foxp3 reporter mice were sorted as $CD4^+$ $GFP^+$ ($CD4^+$ $Foxp3^+$) cells; while congenically marked responder cells (Tresponder) from the spleen and inguinal lymph nodes of CD45.1 (B6-Ly5.1/Cr) mice were sorted as $CD45.1^+$ $CD4^+$ $CD25^-$ . Antigen presenting cells (APCs) were sorted as $CD4^-$ $Foxp3^-$ cells from spleen of Foxp3 reporter mice. Cells were sorted on a Fluorescence-Activated Cell Sorter (FACS) Aria II (BD, La Jolla, CA). Sorted responder cells were stained with CellTrace Violet (CTV; ThermoFisher Scientific) and plated in a in a 96-well round-bottom plate at a density of 2 x $10^4$ responder cells per well. $GFP^+$ Treg cells were added at 2-fold dilutions starting from 1 x $10^4$ cells, in the presence of mitomycin C-fixed (Sigma-Aldrich), 4 x $10^4$ APCs, and 1 μg/ml anti-CD3 (Clone: 145-2C11, Biolegend) and incubated for 80-90 hours. Proliferation of responder cells (gated as $L/D^-CD4^+CD45.1^+Foxp3^-$) was quantified by flow cytometry based on the dilution of Cell Trace Violet (CTV). Percent suppression (% Suppression) was calculated by the following formula. % Suppression = (1-(% divided cells of the condition/ the average of % divided cells of Tresponder only conditions)) x 100.

### TGF-β inhibition

Galunisertib (LY2157299; Selleck Chemicals, Houston, TX) or vehicle (10 g glucose, 30 g Cremophor, 30 g polyethylene glycol, 10 ml ethanol, and 30 ml distilled water) were delivered 300 mg/kg/day in a volume of 100 µl via oral gavage every 12 hours, starting one day prior to RT and continued until the day of harvest.

### IL-33 signaling blockade

Mouse anti-ST2/IL-33 R monoclonal antibody (Clone 245707, R & D, Minneapolis, MN) was diluted in PBS and administrated intraperitoneally at a concentration of 200 µg in a volume of 100 µl per mouse every three days[37], starting one day before RT, for a total of three doses.

### Fingolimod experiments

Fingolimod (FTY720, Enzo Life Sciences, Farmingdale, NY) was prepared and administered as previously described[38]. Briefly, mice received a dose of 25 µg FTY720 or vehicle (PBS containing DMSO) via oral gavage in a volume of 100 µl per mouse every 3 days, starting one day prior to RT, for a total of three doses. Sequestration of peripheral lymphocytes was monitored using the Hemavet whole blood cell counter (Drew Scientific, Miami Lakes, FL).

### Luminex assays and ELISA

Tumors collected at different post-radiation time points were minced, lysed in CelLytic™ MT (Sigma, St. Louis, MO) containing halt protease and phosphatase inhibitor (Thermofisher Science) in a 1:100 ratio, and incubated on ice for 30 minutes with

intermittent vortexing. Tumor lysates were assayed for raw protein concentration with Coomassie assay (Bio-Rad, Hercules, CA). A panel of cytokines and chemokines (IL-2, Exodus-2/CCL21/6Ckine, MCP-5/CCL12, Fractalkine/CXCL1, TARC/CCL17, MIP-3β, MCDC/CCL22, MIP-3α/CCL20, Eotaxin/CCL11, MIP-1α/CCL3, MIP1β/CCL4, MIP-2/CXCL2, MCP-1/CCL2, MIG/CXCL9, RANTES/CCL5, IP-10/CXCL10) was analyzed using a Millipore Mouse Cytokine/Chemokine Panel (Millipore, Billerica, MA). In addition, TGF-β and IL-33 were analyzed using a Milliplex map Kit (Millipore), and a Mouse/Rat IL-33 Quantikine ELISA Kit (R & D), respectively.

**NanoString**

RNA extraction was performed using the TRIzol reagent (ThermoFisher Scientific, Waltham, MA) as per manufacturer's instructions. For NanoString analysis, the nCounter mouse PanCancer Immune Profiling panel was employed using the nCounter Analysis System (both NanoString, Seattle, WA). Analysis was conducted using nSolver software (NanoString).

**Statistical Analyses**

Group means were compared with Student's t tests. Tumor growth and lymphocyte counts in the Fingolimod experiment were analyzed using two-way ANOVA with multiple comparisons. All statistical tests were two-sided, and p values equal or below 0.05 were considered statistically significant. All analyses were conducted using GraphPad Prism 5 (GraphPad Software Inc., La Jolla, CA).

## II-2: Material and Methods for Chapter IV

### Human tissue processing and RNAseq:

Details of RNAseq and human tumor sample processing will be described in the paper by Thomas Nirschl, Yuki Muroyama, Charles Drake et al (in preparation/ close to submission).

***PBMC Preparation***

30 CC's of whole blood was collected from each patient prior to surgery and was processed within 2 hours of collection. Whole blood was diluted with 10mL of 1X HBSS (Corning cellgro; Manassas, VA Ref. 21-022-CV) and underlayed with 10mL of Ficoll-Paque Premium (GE Healthcare; Pittsburgh, PA Ref. 17-5442-03), then centrifuged at 2000 rpm (913 RCF) for 20 minutes at room temperature (RT) without application of the break. The buffy coat was then extracted for downstream application.

***Tumor Dissociation***

Fresh tumor tissue from patients underwent prostatectomies was obtained immediately following the surgical procedure. On average, between 150mg and 250mg of tissue was obtained. Tissue was mechanically separated into 2-4mm cubes and transferred to gentleMACS C Tubes (Miltenyi Biotec; Bergisch Gladbach, Germany Ref. 130-093-237). Tissue samples were processed in accordance with the human tumor dissociation kit (Miltenyi Biotec; Bergisch Gladbach, Germany Ref. 130-095-929), then were placed on the gentleMACS Octo Dissociator (Miltenyi Biotec; Bergisch Gladbach, Germany Ref. 130-095-929) and run using the protocol 37C _h_TDK _1 per Miltenyi

protocol. Single cell suspensions were made for downstream applications.

***T cell Enrichment***

Cells from both PBMC and Tumor sources were then enriched using Dynabeads FlowComp Human CD4 Kits (Thermo Fisher Scientific; Waltham, MA Ref. 11331D) and Dynabeads FlowComp Human CD8 Kits (Thermo Fisher Scientific; Waltham, MA Ref. 11333D) simultaneously in accordance with kit protocols except for not using positive enrichment targeting the CD3 receptor to avoid accidental activation of T cells prior to FACS enrichment.

***FACS sorting***

Described in the following section.

***Ex-Vivo T cell Activation***

Described in the following section.

***RNA-Sequencing***

Whole transcriptome expression analysis (RNA-seq) was performed on an Illumina HiSeq instrument, using 100 bp paired end sequencing generating an average of 50 million reads per analyzed sample.

***Bioinformatic Analysis***

For data preprocessing, raw reads were cleaned for PCR artifacts and adapter trimmed then aligned with the human genomes using the bowtie2 algorithm. Gene and isoform expressions for each sample were obtained using the RSEM/EBseq tool suite. A generalized linear model approach was applied, incorporating patient information to identify genes differentially expressed between T-cell sub-populations. Gene Set Enrichment Analysis was used to identify pathways differentially expressed and social network analysis to pinpoint shared gene and pathway expression modules.

### Mouse

Dusp1 floxed mice and Rgs1 floxed mice were generated by Ozgene (Perth, Australia).

**Mouse tumor model:**

On day 0, $5x10^5$ B16/F10 cells were implanted subcutaneously (s.c.) to the flank of GFP-Foxp3 mice, which express GFP under the control of the Foxp3 promoter referred to as GFP-Foxp3 mice(ref). A breeding pair was purchased from The Jackson Laboratories, and experimental animals were bred in-house as described in Chapter I. And tumor, DLN and spleen were harvested as described in Chapter I.

### FACS sorting

Human cells; Enriched T cells from both PBMC and Tumor(TIL) sources, or thawed healthy donor-derived frozen PBMC were then stained with the following antibodies: Pacific Blue-CCR7 (BioLegend; San Diego, CA, Ref. 353210), Blue-CCR7 (BioLegend; San Diego, CA, Ref. 353210), Brilliant Violet 570-CD45RO (BioLegend; San Diego, CA, Ref. 304226), Alexa Fluor 488-CD127 (BioLegend; San Diego, CA, Ref. 351314), PE-CD25 (BioLegend; San Diego, CA, Ref. 302606), PerCP-Cy5.5-CD45RA (BioLegend; San Diego, CA, Ref. 304122), PE-Cy5-CD4 (BioLegend; San Diego, CA, Ref. 317412), PE-Cy7-CD8 (BioLegend; San Diego, CA, Ref. 300914), APC-CD28 (BioLegend; San Diego, CA, Ref. 302912), APC-Cy7-CD27 (BioLegend; San Diego, CA, Ref. 302816). Target populations were defined as following: PBMC CD4 naïve ($CD4^+CD25^{Low}CD127^{+/-}CCR7^+CD45RA^+CD27^+CD28^+$), PBMC CD4 regulatory T cell (Treg)($CD4^+CD25^{Hi}CD127^{Low}$), PBMC CD8 naïve ($CD8^+CD45RA^+CD45RO^-CD27^+CD28^+$), PBMC CD8 antigen experienced ($CD8^+$ $CD45RA^-CD45RO^+$), TIL CD4

regulatory T cell ($CD4^+CD25^{Hi}CD127^{Low}$) and TIL CD8 antigen experienced ($CD8^+CD45RA^-CD45RO^+$).

Mouse cells; Mouse splenocytes and TIL from GFP-Foxp3 mice (described below) were stained with the following antibodies: PerCP-Cy5.5-CD4 (Biolegend), PE-Cy7-CD8(Biolegend), Pacific Blue- CD44 (Biolegend), APC-CD62L (Biolegend).

Target populations were defined as following: CD4 naïve ($CD4^+CD62^+CD44^-$), Treg ($CD4^+Foxp3^+$), CD8 naïve ($CD8^+CD62^+CD44^-$) and CD8 antigen experienced ($CD8^+CD62^-CD44^+$).

Cells were sorted on a Fluorescence-Activated Cell Sorter (FACS) Aria II (BD, La Jolla, CA) or MoFlo (BECKMAN COULTER, Indianapolis IN).

**Frozen human PBMC:**

Frozen healthy human derived PBMC was obtained from the buffy coat of LeukoPak (New York Blood Bank Center, NY) and stored in liquid nitrogen tank with freezing media (10% DMSO and 90% FBS). In prior to use, they were thawed and incubated in cRPMI (the same as Chapter IV) overnight.

**In vitro T cell activation**

Human cells: PBMC CD4 naïve and PBMC CD8 naïve (both from fresh and frozen samples) were activated ex-vivo using anti-CD3/anti-CD28 activation beads (Thermo Fisher Scientific; Waltham, MA Ref. 111.32D). Cells were plated in 96 well round bottom plates (TPP; Trasadingen, Switzerland, Ref. 92097) at a concentration of 150,000 cells per well in complete RPMI media for 72 hours (or 12 hours in time-course experiments).

Stimulatory beads were used at a 5 Beads to 1 Cell ratio in accordance to previous experiments for maximal stimulation (unpublished).

Mouse cells: Dynabeads™ Mouse T-Activator CD3/CD28 for T-Cell Expansion and Activation (ThermomFisher Scientific) were used in accordance with manufacture's instructions.

### RNA extraction and qPCR

RNA extraction was performed using the TRIzol reagent (ThermoFisher Scientific, Waltham, MA), and the isolated RNA was used to synthesize cDNA with RNA to cDNA EcoDry Premix Random Hexamers (Takara Bio USA, Inc., Mountain View, CA) the and TaqMan probes (listed below) and Universal Master Mix No UNG (Both from ThermoFisher Scientific) were used for quantitative RT-PCR. PCRs were performed in triplicate. The following primers were used:

**Table 2: q-PCR primers used (ThermoFisher Scientific (lifetechnologies))**

pPCR was performed on Applied Biosystems StepOne Plus (ThermoFisher Scientific).

| | |
|---|---|
| Dusp1 TaqMan Probe (Human) | Hs00610256_g1 |
| Dusp1 TaqMan Probe (Mouse) | Mm00457274_g1 |
| Dusp4 TaqMan Probe (Human) | Hs01027785_m1 |
| Dusp4 TaqMan Probe (Mouse) | Mm00723761_m1 |
| Rgs1 Taqman PRgsobe (Human) | Hs01023772_m1 |
| Rgs1 Taqman PRgsobe (Mouse) | Mm00450170_m1 |
| Rgs16 TaqMan PRgsobe (Human) | Mm00803317_m1 |

| | |
|---|---|
| Rgs16 TaqMan PRgsobe (Mouse) | Hs00892674_m1 |
| Foxp3 TaqMan Probe (Human) | Hs01085834_m1 |
| Foxp3 TaqMan Probe (Mouse) | Mm00475162_m1 |
| Granzyme B Taqman Probe (Human) | Hs00188051_m1 |
| METRNL TaqMan Probe (Human) | Hs00417150_m1 |
| METRNL TaqMan Probe (Mouse) | Mm00522681_m1 |
| Tnfrsf9 Taqman Probe (Human) | Hs00155512_m1 |
| Tnfrsf9 Taqman Probe (Mouse) | Mm01268456_m1 |
| CCR6 Taqman Probe (Human) | Hs01890706_s1 |
| Gapdh Taqman Probe (Human) | Hs02758991_g1 |

**siRNA and Treg isolation**

siRNA oligos listed below, as well as positive control and negative control (Stealth RNAi™ siRNA GAPDH Positive Control, scramble oligos in BLOCK-iT™ Transfection Optimization Kit, respectively. ThermoFisher Scientific) were transfected to human PBMC (LeukoPak) at 200 nM by Amaxa® Human T Cell Nucleofector® Kit (Unstimulated) using Amaxa Nucleofactor II (both from LONZA, Basel, Switzerland) per manufacture's instructions. Transfection optimization was conducted using BLOCK-iT™ Transfection Optimization Kit (ThermoFisher Scientific). 24 hours post-transfection (in time-course experiments up to 96 hours), Treg were isolated by EasySep™ Human $CD4^{+}CD127lowCD25^{+}$ Regulatory T Cell Isolation Kit (STEMCELL, Vancouver, BC, Canada) and used for the downstream application including RNA extraction.

**Table 3: siRNA oligo used for transfections**

| Target gene | siRNA oligo |
|---|---|
| Dusp1 | Human stealth siRNA HSS102983 |
| Dusp1 | Human stealth siRNA HSS102984 |
| Dusp1 | Human Stealth siRNA VHS40581 |
| Dusp1 | Human Stealth siRNA VHS40583 |
| Dusp4 | Human Stealth siRNA VHS40973 |
| Dusp4 | Human Stealth siRNA VHS40975 |
| Rgs1 | Human Stealth siRNA HSS143614 |
| Rgs1 | Human Stealth siRNA HSS143615 |
| Rgs1 | Human Stealth siRNA HSS143616 |
| Foxp3 | Human Stealth siRNA HSS121456 |
| Foxp3 | Human Stealth siRNA HSS121458 |
| Foxp3 | Human Stealth siRNA HSS181786 |
| Ikzf2 (Helios) | Human Stealth siRNA HSS117670 |
| Ikzf2 (Helios) | Human Stealth siRNA HSS117672 |
| Ikzf2 (Helios) | Human Stealth siRNA HSS176945 |

(Note: The purity post Treg isolation by the above mentioned kit was poor.)

### *In vitro* micro-suppression assay for human Treg

Healthy donor derived frozen PBMC (LeukoPak) were thawed and rest overnight in cRPMI for recovery. Treg were sorted as $CD4^+CD25^+CD127^-$ population, APC were sorted as the size of myeloid gate based on forward and side scatter. Responder cells were sorted as $CD8^+CD45RO^-$ cells or isolated by CD8 T cell naïve selection kit (STEMCELL).

Cells were sorted on a Fluorescence-Activated Cell Sorter (FACS) Aria II (BD, La Jolla, CA) or MoFlo (BECKMAN COULTER, Indianapolis IN). When frozen samples were used, Treg were treated with 200 U/ml of human recombinant IL-2 (Peprotech, Reckey Hill, NJ) for 1-2 days before setting up the assay for recovery and treat the CD8 T cell responder population with 20 U/ml of IL-2 for 1-2 days for recovery of the population. Sorted responder cells were stained with CellTrace Violet (CTV; ThermoFisher Scientific) and plated in a in a 96-well round-bottom plate at a density of 2 x $10^3$ responder cells per well. Treg cells were added at 2-fold dilutions starting from 1 x $10^3$ cells, in the presence of 2 x $10^3$ APCs, and 0.5-1 μg/ml anti-CD3 (Clone: OKT3, eBioscience) and incubated for 72-96 hours. Proliferation of responder cells was quantified by flow cytometry based on the dilution of Cell Trace Violet (CTV). Percent suppression (% Suppression) was calculated by the following formula. % Suppression = (1-(% divided cells of the condition/ the average of % divided cells of Tresponder only conditions)) x 100.

# CHAPTER III: STEREOTACTIC RADIOTHERAPY INCREASES FUNCTIONALLY SUPPRESSIVE REGULATORY T CELLS IN THE TUMOR MICROENVIRONMENT

## INTRODUCTION

Radiotherapy (RT) is an important component of cancer treatment, with approximately 50% of cancer patients receiving RT as part of their treatment regimen[39]. Although the primary anti-tumor effects of RT involve the induction of single and double stranded DNA breaks with downstream apoptosis [40], important studies by several groups[41,42] showed that RT has clear immunological effects, including the occasional induction of a systemic anti-tumor response, the so-called abscopal effect[43]. RT modulates several elements of the immune response; it promotes the secretion of pro-inflammatory cytokines such as IL-1 and IL-6[44]; it enhances expression or release of damage-associated molecular patterns (DAMPs), including calreticulin, high mobility group box 1 (HMGB1) and ATP from affected tumor cells[42,44,45]; it increases MHC-I expression on tumor cells[44,46]; and it activates the stimulator of interferon genes (STING) pathway leading to type I interferon secretion[47]. Together, these factors may lead to the maturation of dendritic cells, resulting in improved cross-presentation of tumor antigens and subsequent antigen-specific CD8 T cell responses[34,42].

Despite these multiple pro-inflammatory effects, the abscopal effect is clinically rare - suggesting that RT may also exert immunosuppressive effects, or amplify pre-existing suppressive components of the tumor microenvironment (TME)[5,48]. The pro-tumor microenvironment incorporates numerous mechanisms by which tumors evade host anti-tumor immune responses: for instance, RT has been correlated with increased levels of TGF-β[49], a pluripotent cytokine which generally suppresses immune responses[50]. Another evasion method involves regulatory T cells (Treg), which play an important role in suppressing immune responses and are of clinical relevance[20]. Accordingly, Treg depletion has been shown to enhance CD8 T cell activity and limit tumor growth in animal

models[26], and treatments targeting these cells are in various stages of clinical development[51]. However, the effects of RT on suppressive immune cells, especially Treg, have not been fully elucidated. Several reports suggest an increase of Treg post-radiation, both in animals and humans[34,52-55], but whether radiotherapy may render tumor-infiltrating Treg (TIL-Treg) both phenotypically and/or functionally more suppressive, has yet to be determined.

To test the hypothesis that stereotactic radiotherapy increases phenotypically and functionally suppressive TIL-Treg, we used the Small Animal Radiation Research Platform (SARRP), which directs CT-image-guided radiation to selectively target tumors[35] and models stereotactic radiotherapy in human patients, thus enabling us to investigate the phenotype and functional ability of TIL-Treg. We also evaluated several potential mechanisms underlying the observed post-RT Treg increase, including TGF-β and IL-33, and the role of trafficking versus intratumoral proliferation.

## RESULTS

### Stereotactic radiation increases Treg in multiple tumor types

We first sought to investigate whether the previously observed RT-mediated increase in intratumoral regulatory T cells (Treg) [34,52-55] was a general phenomenon, i.e. whether it occurred across multiple tumor types. For these studies, we used the Small Animal Radiation Research Platform (SARRP)[35] (Figure III- 1A). At the dose studied, RT suppressed B16/F10 (melanoma) tumor growth, but did not completely eradicate the tumors (Figure III- 1B). Similar trends were observed in the RENCA (kidney cancer) and

MC38 (colorectal cancer) models (Supplementary Figure III 1A, 1B). These effects were confirmed by a comprehensive profiling of the post-RT TME; which revealed additional changes in the immuno-biology of the TME involving $CD4^+$ T cells, $CD8^+$ T cells and myeloid cells (Supplementary Figure III- 2). In all three tumor types studied, RT significantly increased both the proportion (Figure III- 1D, 1E) and absolute numbers of Treg (Figure III- 1C and data not shown). This effect was local; no significant increases in Treg were observed in either the DLN or spleen in any of the three models examined (Supplementary Figure III- 3). This increase in Treg was accompanied by an increase in Foxp3 levels as assayed by MFI (Figure III- 1F) and was verified by IHC (Figure III- 1G). In addition, the Treg increase was persistent and was still present two weeks after the administration of RT (Supplementary Figure III- 4). Taken together these data established a model to study Treg following RT.

**The Phenotype of Treg Post-RT is Consistent with Activation**

We next tested whether RT treated TIL-Treg developed a phenotype different from that observed in untreated tumors. For this, we focused on: CCR4, which has been associated with Treg trafficking[56]; the checkpoint molecule cytotoxic T-lymphocyte-associated protein 4 (CTLA-4)[57]; the transcription factor Helios (IKZF2), which is up-regulated with activation[58-60]; and 4-1BB (CD137), which also increases with T cell activation[61]. As shown in Figure III- 2, in the B16/F10 model, CCR4 was not significantly altered post-RT. By contrast, CTLA-4, Helios and 4-1BB expression were all significantly up-regulated post-RT, potentially consistent with a more activated Treg phenotype. Similar trends were noted in the RENCA and MC38 models (Supplementary Figure III 5 and 6).

Supporting a local immunological role for RT, none of these 4 markers were significantly altered in either the DLN or the spleen of RT-treated mice (Supplementary Figure III 7 and 8). We also quantified expression of these markers in the non-Treg CD4 T cells (Tconv) and found that in both the B16 and RENCA models, 4-1BB and CTLA-4 were induced post-RT on T conv as well; this was not observed in the MC38 model (Supplementary Figure III 9-11). In none of the 3 models was 4-1BB significantly induced on CD8 post-RT (Supplementary Figure III- 12).

**TIL-Treg Retain Suppressive Function Post-RT**

Based on their increased expression of CTLA-4[57] and Helios[58-60], we queried whether TIL-Treg demonstrated increased suppressive function after RT. To investigate the suppressive capabilities of post-RT Treg, we conducted micro-suppression assays[36]. Briefly, GFP-labeled TIL-Treg were sorted from Foxp3 reporter mice (B6.129(Cg)-*Foxp3*$^{tm3(DTR/GFP)Ayr}$/J ), which express GFP under the Foxp3 promoter[19]. As shown in Figure III- 3, we found that TIL-Treg from irradiated mice (RT TIL-Treg) were more suppressive than those from non-irradiated tumors (Control TIL-Treg) or un-manipulated spleens at low Treg:Tresponder ratios, but that at a higher ratio the three populations were functionally indistinguishable (Figure III- 3A and 3B). Collectively, these data show that the post-RT Treg from TILs are indeed functional and demonstrate enhanced suppression in standard *in vitro* suppression assays.

### RT-Induced Expansion of TIL-Treg is Not TGF-β Dependent

Given the well-described influence of TGF-β on Treg induction[62], we next investigated whether the post-RT Treg expansion observed above was dependent on TGF-β signaling. To test this hypothesis, we treated B16/F10 tumor-bearing mice with Galunisertib (LY2157299), a small molecule TGFβR1 kinase inhibitor that nearly completely abrogates TGF-β signaling[63-65]. To optimize potential treatment effects, we began treatment with daily oral gavage (every 12 hours) one day prior to RT (Figure III- 4A). As expected, treatment with Galunisertib did not significantly alter tumor outgrowth, independent of the presence or absence of RT (Figure III- 4B). Interestingly, blockade of TGF-β did not significantly abrogate the RT-induced TIL-Treg increase as compared to the vehicle-treated control groups (Figure III- 4C). Neither the proportion of $Foxp3^+$ cells (Figure III- 4D) nor the absolute numbers (Figure III- 4E) decreased, suggesting the post-RT TIL-Treg increase was not strongly dependent on TGF-β in this model. In addition, the overall composition of the T cell infiltrate in these aggressive B16/F10 tumors was not significantly affected by Galunisertib; there was no significant difference in total CD3, CD4 or CD8 proportions (Supplementary Figure III- 13). We also tested whether RT was associated with increased levels of TGF-β1 or β2. As shown in Supplementary Figure III- 14, levels of both TGF-β molecules increased as tumors progressed, but significant differences were not observed between irradiated and non-irradiated tumors.

### RT-Induced Expansion of TIL-Treg is Not IL-33 Dependent

Since recent data suggest the possibility of an increase in IL-33 levels after RT[66], we next tested whether this cytokine might be responsible for the increment of TIL-Treg after RT treatment. To investigate this hypothesis, we quantified IL-33 levels in B16/F10 tumors post RT. As show in in Figure III- 5A, IL-33 levels increase after RT, consistent with

previous data. Therefore, we treated mice with a neutralizing anti-ST2 (IL-33R) antibody[37], starting one day prior to RT (Figure III- 5B). Anti-ST2 treatment did not significantly affect tumor outgrowth (Figure III- 5C). In addition, the blockade of ST2 did not significantly abrogate the post-RT TIL-Treg increase (Figure III 5D-F). Furthermore, there was minimal expression of ST2 (IL-33R) on intra-tumoral Treg and that expression is not increased by RT (Supplementary Figure III- 15). Taken together, these data suggest that, in this model, the post-RT Treg increase is most likely not dependent on either TGF-β or IL-33.

**Radiation enhances the proliferation of TIL-Treg**

We next tested whether the observed increase in TIL-Treg post RT was due to Treg migration into tumors as opposed to being driven by intratumoral proliferation of pre-existing TIL-Treg. To perform these studies, we treated B16/F10-bearing mice with Fingolimod (FTY720), a blocker of the sphingosine 1-phosphate receptor 1; this drug effectively blocks T cell egress from lymphoid organs[38,67]. As in the studies above, treatment was initiated one day prior to radiation (Figure III- 6A). As expected, administration of Fingolimod resulted in an approximately 75-80% decrease in peripheral blood lymphocytes counts from baseline (Supplementary Figure III- 16), and did not significantly affect tumor growth (Figure III- 6B). Fingolimod seemed to slightly blunt the TIL-Treg increase, but did not abrogate it completely (Figure III- 6C and 6D). Accordingly, we next investigated the proliferation of intratumoral Treg via Ki-67 staining. RT consistently increased Treg proliferation within tumors both in the presence or absence of Fingolimod (Figure III 6E - 6G). Of note, although post-RT proliferation

occurred to some extent in all T cell subsets, the increased proliferation of Treg was more pronounced than in the other subsets examined (Figure III- 6G). Of note, nearly all T cell subtypes in the tumor had increased proliferation post-RT, however, TIL-Treg have a higher baseline proliferation rate, making the ratio of Treg increase post-RT (Figure III- 6 H, I)

## DISCUSSIONS

Radiation therapy is a mainstay of cancer treatment and is broadly used across a spectrum of tumor types. The basic mechanism of action of RT is to induce single and double-stranded DNA breaks, leading to apoptotic cell death, with tumor cells being preferentially affected [40,68]. However, accumulating evidence suggests that RT has clear immunological effects as well - including the occasional induction of a systemic anti-tumor response, the so-called abscopal effect [41,42].

Here we found an increased frequency of Treg in the TME of several tumor types (B16/F10, RENCA and MC38) following treatment with RT (Figure III- 1). The consistency across these disparate tumor types (using two separate mouse strains) is in agreement with prior results[34,52-55].

We investigated Treg-specific expression of several molecules post-RT: chemokine receptor CCR4[56], the checkpoint molecules CTLA-4[57] and 4-1BB[61], and the transcription factor (Helios). Post RT, we found increased expression of CTLA-4, 4-1BB and Helios, consistent with an activated/ suppressive phenotype (Figure III- 2). Based on the increased expression of CTLA-4[57] and Helios[58-60] observed in RT treated TIL-Treg, we next sought to investigate whether these cells demonstrated greater suppressive capability than their non-treated counterparts. Interestingly, Treg from RT treated tumors

not only retained their ability to suppress effector cell proliferation, but were in fact more suppressive at a low Treg: Tresponder ratios (Figure III- 3). To our knowledge, these data represent the first report of a micro-suppression assay using sorted TIL-Treg from mice treated with stereotactic RT; and may be important in understanding a potential counter-balance to RT-induced immune activation [42,69-71].

We interrogated several potential molecular mechanisms underlying the RT mediated increase in the frequency of TIL-Treg. A primary consideration was TGF-β for three reasons. First, TGF-β induces the expression of Foxp3, the master transcription factor for Treg[72], in traditionally $CD4^{+}Foxp3^{-}$ effector CD4 T-cells[62,73]. Second, RT has been shown to correlate with increased TGF-β expression[49]. Lastly, several prior studies suggest synergistic anti-tumor effects when RT is combined with TGF-β blockade[74-76]. Thus, we blocked TGF-β signaling using the small molecule inhibitor Galunisertib (LY2157299), which prevents phosphorylation of SMAD2 by inhibiting TGF-β receptor I kinase [63-65]. Surprisingly, we were not able to influence the TIL-Treg increase induced by RT with TGF-β blockade (Figure III- 4). These results are not consistent with previous studies by Wu *et al.* [77] in which TGF-β blockade was shown to mitigate the TIL-Treg increase after irradiation in a murine prostate cancer model. The reasons for the discrepancy between these results are not obvious, but may include differences in the models used, or in agents used - prior studies used intraperitoneal delivery of a neutralizing antibody against TGF-β1 or transfection with TGF-β1 shRNA, whilst we orally administered a small-molecule inhibitor currently under investigation in a number of clinical trials[64].

In addition, we investigated IL-33, a cytokine that has recently been described to be important in Treg expansion in several models[78-80]. Consistent with a previous

report[66], we found that RT increased the levels of IL-33 in the TME. We thus blocked IL-33-IL-33R (ST2) signaling using antibodies against ST2 to test whether IL-33 might play a role in the observed increment of TIL-Treg post RT. IL-33 blockade did not abrogate the TIL-Treg increase after irradiation (Figure III- 5), leaving the precise molecules or signaling pathways driving Treg expansion in our models a matter for ongoing investigation. We also found that the post-RT TME includes a number of dynamic changes in the expression of multiple immunological transcripts involving diverse immune cell subsets. This not only highlights the complexity and dynamics of the TME, but also suggests additional avenues for intervention (Supplementary Figure III-2). Some of the effects of RT appeared to transcend cell subtype; for example, we noted increased proliferation of CD4, CD8 and Treg post-RT. By contrast, some cell surface proteins were differentially affected, with 4-1BB expression up-regulated post-RT on Treg but not on CD8 T cells. These data highlight the complex effects of RT on the immune components of TME.

We next sought to determine whether the observed increase was due to Treg proliferation *in situ*, or due to an increased trafficking of peripheral Treg to the TME. For these studies, we used Fingolimod, a small-molecule S1P signaling inhibitor that largely blocks T cell emigration from lymph nodes. We hypothesized that if the RT TIL-Treg increase was due to an influx of new immune cells into irradiated tumors, then it would be blocked or at least significantly blunted by Fingolimod treatment. In multiple iterations, the post-RT Treg increase appear to be blunted but not abrogated in the presence of this agent (Figure III- 6). From a technical standpoint, Fingolimod treated mice displayed less infiltration when considering the density of T cells (ubiquitously across all immune cell types) in the TME, these low numbers may be a source of variation

in population frequencies. Therefore, it is formally possible that at least partially, trafficking of Treg may play a role in the increased Treg frequency in the TME, as suggested by an increased level of the CCR4 ligands: CCL17 and CCL22 in RT-treated tumors (Supplementary Figure III- 17). Finally, we turned our attention to the possibility of Treg expansion/proliferation driving the post-RT increase of TIL-Treg. Of note, we found a consistent increase in TIL-Treg proliferation post-RT, suggesting that proliferation likely explains a significant fraction of the post-RT Treg increase. Interestingly, nearly all T cell subtypes in the tumor had increased proliferation post-RT, however, TIL-Treg have a higher baseline proliferation rate, making the ratio of Treg increase post-RT (Figure III- 6 H, I), leading to a potential suppressive counterbalance to the well-described stimulatory effects of RT[42,69,70,81]. And we did not see the difference in death rate between non-irradiated tumor-derived TIL versus irradiated tumor derived TIL (Supplementary Figure III- 18), which further support the roles of proliferation rather than the difference in cell death rate.

Underlying mechanism for the above phenomenon has not been clear yet. One potential candidate could be IL-2, considering the global proliferation among T cell subsets post-RT, and the dependence of Treg on IL-2 for their survival and suppressive functions[82,83]. Although the IL-2 level in tumor lysate was not significantly different in protein level and transcription level between irradiated and non-irradiated tumors (Supplementary Figure III- 2, 17), kinetics of IL-2 secretion from immune cells, or the experiments in IL-2 knockout mice or with IL-2 blockade as well as a changes in signaling with phosphorylation of STAT5 will follow. In addition, origin of the Treg; whether they are thymic-derived or periphery-induced Treg, as well as novel molecules upregulated

post-RT for Treg-targeted immunotherapy (Supplementary Figure III- 19) are also worth investigating.

Another important question would be whether the RT-induced Treg expansion was due to the primary impact of RT to Treg (i.e. radio-resistance of Treg) or the secondary impact from RT to the TME. The parallel adoptive transfer experiments where tumor-implanted RagKO mice (or Foxp3DTR mice depleted Treg with DT) are adoptively transferred with irradiated Treg or the tumors were irradiated and non-irradiated Treg are adoptively transferred and see in which condition Treg would expand. As the nanostring data showed, complex and dynamic immunological changes occur in the TME; thus we cannot underestimate the impact of irradiated TME. But interestingly, TIL, especially TIL-Treg proliferate under RT and still survive; although typically proliferative cells are more sensitive to radiation induced cell death, suggesting there is a cell intrinsic mechanism especially for TIL-Treg to be radio-resistance. Along those lines, it is suggested that TIL-Treg has higher expression of cFLIP, anti-apoptotic molecule, making them resistant to FasL-induced cell death.[84] Considering the known effect of RT to induce FASL expression on tumor cells (and could be stromal cell as well)[42], it is possible that TIL-Treg, especially post-RT, have higher expression of cFLIP and counter act with the FASL induced cell death. Adoptive transfer experiment experiments using c-FLIP KO/KD T cells or conditional KO mouse (especially temporal KO) of c-FLIP in Treg[85] might help to elucidate the impact of this molecule.

In addition, along the lines of migration and the secondary impact from TME, common lymphatic endothelial and vascular endothelial receptor 1 (CLEVER1) on blood endothelial cells (BEC) has been suggested to preferentially mediate Treg extravasation[84], which might also explain the increased Treg population in the TME post-RT, if RT

increased the expression of CLEVER. Thus the impact of stromal cells in the TME cannot be underestimated as well.

Furthermore, exploring other immune-suppressive cells post-RT, and relation to Treg would be also interesting area to explore further. It has been suggested that RT could also increase MDSCs in the TME[86] (and Weichselbaum's group personal conversation). Interestingly, our preliminary data from B6/F10 tumor-bearing mice showed the almost diminished population of $LD^{-}CD45^{+}Ly6C^{+}Ly6G^{+}$ population ("(Granurocytic) G-MDSC" population), leading to increased monocytic/granurocytic -MDSC ratio (M/G-MDSC ratio) (Supplementary Figure III- 20). Further characterization in different time points (especially early time points) or different types of tumors, and delineation of specific myeloid population (as the above population could include neutrophils), underlying mechanisms (different apoptosis ratio, for example), and how they could affect TIL-Treg are needed, but this data suggest that RT could modulate the population of MDSC (and myeloid cells) as well.

The strengths of these studies include a well-defined, localized and consistent RT treatment regimen using the SARRP platform[35], which we used to model single-dose stereotactic radiation. In addition, we carefully controlled for tumor size at the time of treatment. Potential limitations include the use of implanted tumor models, which may or may not accurately recapitulate the TME in human tumors, and that we did not thoroughly test other radiation doses or fractionation regimens. Thus, it is possible that our results may not translate to other treatment regimens. Nevertheless, the results obtained here are consistent with prior work[34,52-55] showing that RT may have Treg inducing affects which may need to be considered in clinical regimens that combine RT with immunotherapy. In addition, we clearly documented that the post-RT intratumoral

Treg have suppressive function, providing a rationale for regimens combining Treg-targeted strategies with RT. Indeed, such combination regiments may be required to optimize the immune effects of RT in patients.

FUTURE PLANS

(I am writing RO1 grant draft with Dr. Drake based on this project.)

The following are the future plans of the project. Mainly three-folds.

(1) To determine the mechanism(s) by which RT induces Treg expansion in the tumor microenvironment.

1.1 Test the hypothesis that TIL-Treg are more radio-resistant

To test this hypothesis, we will perform clonogenic survival assay to compare the sensitivity to RT of Treg, especially TIL-Treg with other T cell subsets (conventional T cells (Tconv)). If we proved TIL-Treg are more radioresistant, we will determine the mechanisms; whether the radioresistant is dependent on cell cycle or apoptosis, and whether they are linked to DNA damage response.

1.2 Determine the mechanism by which RT triggers proliferation (and activation) of TIL-Treg

It is hypothesized that enhanced IL-2 signaling post-RT will trigger the proliferation of TIL-Treg. To test the hypothesis, we will evaluate the enhancement of IL-2 signaling via phosphor-flow and immunoblot of downstream target of IL-2R, including STAT5, as well as directly evaluate the impact of IL-2 in vivo by combination therapy of IL-2 blockade with RT and transgenic mice model where we conditionally and inducibly knockout the IL-2R signaling in Foxp3+Treg.

(2) To optimize RT combined with Treg modulating immunotherapy in physiologically

relevant animal models

2-1 RT increases the expression of immune-checkpoint molecules on TIL-Treg (CTLA4, 41-BB, CCR8) and targeting the molecules in combination with RT results in better anti-tumor immunity

2-2 RT dose and fractionation optimization will affect TIL-Treg expansion

(3) To test the hypothesis that RT increases Treg infiltration and/or alters phenotype in patients receiving palliative SBRT with biopsy accessible lesions

3-1 RT increases Treg expansion in the tumors of cancer patients (renal cell carcinoma, prostate cancer, and bladder cancer)

3-2 Comprehensively profile TME pre- and post- RT lesions

(1) To determine the mechanism(s) by which RT induces Treg expansion in the tumor microenvironment.

1.1 Test the hypothesis that TIL-Treg are more radio-resistan

Our preliminary data suggest that TIL-Treg proliferate robustly post-RT and maintain their suppressive function[87]. This appears counter-intuitive because as a general trend, more proliferative cells tend to be more vulnerable to the RT-induced cell death, which does not necessarily seem to apply for TIL-Treg. This led us to the hypothesis is that Treg in the TME are radioresistant. Separately, we will also determine the mechanism by which RT triggers the proliferation (and activation) of TIL-Treg.

To test the hypothesis, we will conduct in vitro clonogenic survival assay both in mouse and human cells. For mouse, we will isolate Foxp3+Treg and CD4 and CD8 T

conventional cells from spleen, draining lymph node and tumor of tumor-implanted or control YFP-Foxp3-CRE mice, cultured in FBS-containing media in round 96 well plate supplemented with IL-2. We will irradiate them (0-20 Gy) and evaluate the cell death rate) 7 days post-RT. For translational relevance, we will do the same setting of experiment evaluating the radioresistance in vitro by using human PBMC (Leukopak) derived Treg (CD4+CD25+CD27-) as well as other non-Treg T conventional cells (CD4, CD8) subsets.

We will use the Curve and DER (dose-enhancement ratio (DER) at 10% cell survival) as readout. We expect to observe that Treg, especially TIL-Treg are more radioresistant, with the shifter curve toward upright and DER greated than 1 compared with other Tconv subsets. If this was true, the hypothesis will be confirmed and this would offer significant insight in to one of the mechanism for patients refractory to RT. Then, we will further pursue to determine if those cells respond differently to RT based on cell cycle (like "Mitotic Catastrophie" like the ways tumor cells die by radiologists) by G2 block (to test check point function different) and by examining the markers of cell cycle (to test if there was any difference in distribution in cell cycles (i.e. less cells are in G2/S (radiosensitive) but in G0 (radioresistant) suggesting radioresistant), by the expression of CDKs by Westernblot, flowcytometry. We will also examine if Treg die more by apoptosis (just like "lymphocytes' way of death by RT by radiologists) using Live/Dead, 7-AAD, annexin-V, caspase-1,8 by Western, flowcytometry as readouts. The potential pitfall could be other types of cell death than mitotic catastrophie and apoptosis might be involved. If we did not see the difference, we could further expand our search into other types of cell death such as necrosis, pyroptosis, autophagy.

We will also determine if this is related to DNA damage or test the hypothesis that

Treg are radio-resistant because they have better DNA damage response (DDR). To test the DNA damage, by flow cytometry and IF, we will stain gamma-H2AX. TO test if Treg has better recovery from DNA damage (better DNA damage response (DDR)), we will perform Comet assay and test the Markers of NHEJ (DNA PKCs, XRCC4 by Western blot). We will expand our investigation into cGAS-STING-type I IFN pathway as well.

If DNA damage (1-3) was true, we could also look into the effect of TGF-b and adenosine, suggested to dampen radiosensitivity of tumor cells[75] and protect the normal tissue cells[88], respectively.

To test the relevance in vivo, we could use double reporter mice from Rudensky group[89] and we could generate Foxp3eGFPCD4 Cre-ERT2 R26Y mice so that tamoxifen administration can label all T cells and can distinguish Treg vs Tconv by GFP expression. We could also make Ebi3 CRE to make it CD8 specific. We will monitor the survival of the YFP-labelled Treg (as well as other YFP-labelled Tconv in second model) by cell numbers, ratio of the cell death, as well as examine the pro- and anti-cell death markers listed in Table I over the time course using flow-cytometry and immunoblots. We are expecting to see the high survival and increased anti-apoptotic protein expression for YFP+Treg from irradiated tumors.

We are also considering the possibility of Treg becoming radio-resistant by the irradiated TME-derived factors. We hypothesized that Treg are radioresistant because they make adenonosine which protects them from RT and (oxidative) stress. TME is rich in generally immunosuppressive adenosine, and evidence suggest the expression of A2AR CD39, 73 on Treg make them suppressive and Treg secretion of adenosine further contribute to the immune suppression in the TME. RT increase release of ATP

as a DAMP, the source of adenosine4, and the adenosine pathway blockade revealed anti-tumor in multiple tumor types, suggesting the potential efficacy of combination therapy of RT and adenosine blockade pathway, which might involve TIL-Treg. Treg-derived Adenosine could counteract ROS to make the cells radioresistant (Treg protect HSC as niche in bone marrow, and adenosine from Treg stop cell cycle in G0 in HSC in bone marrow. (Hirata, Fujisaki et al unpublished) These data led us to hypothesize that Treg protect themselves from RT-induced cell death by counteracting ROS by adenosine pathway. We will be testing this hypothesis using pharmacological approach and genetic approach both in vitro and in vivo. To determine the impact of RT-induced adenosine pathway on TIL-Treg survival and dissect the contribution from (1) the production of adenosine by Treg and (2) the sensitivity/downstream signaling of adenosine receptor on Treg (A2AR), we will use treatment both of blocking antibody and small molecule antagonists of adenosine-producing enzyme (CD73 and CD39) and A2AR in combination with radiation and measure the survival rate, and pro- and anti-cell death markers, both in vitro and in vivo, using pharmacological (mAb, small molecule inhibitors against CD37, A2AR etc.). For transgenic model approach, we will cross A2AR floxed mice (Adora2a$^{tm1Dyj}$ ; available from Jackson might need extra breeding to B6 as B6;129-*Adora2a*$^{tm1Dyj}$/J) and CD39 floxed mice (with Foxp3$^{YFP\text{-}CRE}$ mice to generate Treg specific knockout of A2AR (receptor of adenosine) and CD39 (enzyme required for conversion of ATP into adenosine). We will use Foxp3 $^{YFP\text{-}CRE}$ mice as control. For *in vitro* experiment, we will isolate CD39 (or A2AR) KO Treg from CD39$^{fl/fl}$Foxp3$^{YFP\text{-}CRE}$ mice (or A2AR$^{fl/fl}$Foxp3$^{YFP\text{-}CRE}$ mice) or WT Treg isolated from Foxp3$^{YFP\text{-}CRE}$ mice from tumor, draining lymph node and spleen of tumor(MC38, B16/F10)-bearing mice, and culture followed by irradiation in the method used in 1.1

and evaluate the survival, death rate, proliferation and pro/anti-cell death markers expression listed in Table 1, as well as suppressive function of CD39/A2AR KO Treg and compared with the WT control, by immunoblot and flowcytometry and *in vitro* suppression assay. We expect to observe the impaired survival of CD39/A2AR KO Treg upon irradiation, especially in TIL-Treg. For *in vivo* approach, we will implant tumors (B16/F10, MC38) in CD39$^{fl/fl}$ Foxp3$^{YFP\text{-}CRE}$ and A2AR $^{fl/fl}$ Foxp3$^{YFP\text{-}CRE}$ mice, and irradiate the tumors with SARRP RT and YFP+Foxp3+ TIL-Treg will be evaluated for the survival, apoptosis markers over the time. We will use Foxp3$^{YFP\text{-}CRE}$ mice as a WT control and Foxp3-DTR mice as negative control for the experiment. We will evaluate the tumor growth with measuring tumor volumes and weight, as well as the survival and markers of TIL-Treg as well as in vitro suppression assay. We expect to observe the impaired survival of CD39/A2AR KO Treg upon irradiation, especially in TIL-Treg leading to the better tumor control and enhanced CD8 response measured by intracellular staining of IFN-g, TNF-a, GzmB (and Elispot assay).

To further investigate and delineate the impact of Treg-derived adenosine itself (using CD39 floxed and adenosine signaling (using A2AR floxed) on TIL-Treg's radio-resistance, we will generate heterozygous CD39 $^{fl/fl}$ Foxp3$^{Cre\text{-}YFP/DTR\text{-}GFP}$ female mice (and A2AR $^{fl/fl}$ Foxp3$^{Cre\text{-}YFP/DTR\text{-}GFP}$), where 50% of Tregs have a Cre-mediated deletion of CD39 (A2AR), are marked with YFP, whereas the other 50% express DTR-GFP and are WT Treg, as they carry the CD39 $^{fl/fl}$ allele (or A2AR allele) but not Foxp3$^{Cre\text{-}YFP}$ within the same mouse without the administration of DT (as Foxp3 in on X chromosome and only one allele will be expressed due to the random inactivation). And we will use Foxp3 $^{CRE\text{-}YFP/CRE\text{-}YFP}$ mice and CD39 $^{fl/fl}$ Foxp3 $^{CRE\text{-}YFP/CRE\text{-}YFP}$ mice (or A2AR $^{fl/fl}$ Foxp3 $^{CRE\text{-}YFP/CRE\text{-}YFP}$) as controls[90,91]. The strength of this genetic model

is that we could compare the WT and KO Treg population within the same mouse, so WT Treg can serve as an internal control. We will subcutaneously implant immunogenic MC38 or less-immunogenic B16/F10 to these mice, and irradiate the tumors with SARRP, and follow up the survival, apoptosis markers of YFP+CD39KO Treg versus GFP+CD39WT Treg (or A2AR KO vs WT TIL-Treg) in the tumor over time just as above. If the adenosine from Treg was important for the survival of TIL-Treg post-RT, not only YFP+CD39 KO Treg will more sensitive to RT-induced cell death but also GFP+CD39KO Treg will become more sensitive to RT-induced cell death due to the less availability of adenosine provided from irradiated tumor-derived Treg, whereas if the adenosine signaling on Treg make them radioresistance, GFP+A2AR WT Treg will outnumber YFP+A2AR KO Treg and show increased survial and anti-apoptotic molecule expression in post-RT TME.

Other than adenosine, another TME derived factors potentially make Treg radioresistant and /or make them proliferate could be TGF-beta. It is well-known that RT-increase TGF-b and TGF-b induce Treg. Although our data using Galunisertib (LY2157299 monohydrate), small-molecule TGFbR1 kinase inhibitor did not abrogate Treg expansion post-RT[87], it is still possible that TGF-b impacts TIL-Treg in TGFbR1-independent mechanism including the “non-classical” pathways of TGF-b other than TGF-bR/Smad3/4 pathway, including LRP1. To explore the possibilities, we will use other TGF-b blockade approach and genetic mouse model. For pharmacological approach, we will use pan-TGF-beta blockade antibody (1D11 (a pan-isoform, TGFβ-neutralizing mouse mAb that binds only to active TGFβ) [74]in combination with RT. We will treat the tumor-bearing mice with 1D11 or isotype control starting from a day prior to the RT every other day (200 ug) and evaluate the impact of TGF-b neutralization to

RT-induced Treg (expansion and the pro- and anti-apoptotic markers (such as caspase-1/3, or Bcl-2 respectively) of TIL-Treg and other conventional T cells. We will also conduct the same experiment using LRP inhibitors. For genetic approach, we will generate Treg-specific knockout of Smad4 mice by crossing $Foxp3^{YFP\text{-}CRE}$ with Smad4 fl/fl mice (Smad4tm2.1Cxd/J)). We will implant B16/F10 and MC38 in $Smad4^{fl/fl}Foxp3^{YFP\text{-}CRE}$ mice followed by SARRP radiation, and evaluate the Treg increase post-RT. We will also generate $Smad4^{fl/fl}Foxp3^{Cre\text{-}YFP/DTR\text{-}GFP}$ and conduct the similar experiment as mentioned in adenosine section.

(2) To optimize RT combined with Treg modulating immunotherapy in physiologically relevant animal models

Our previous study showed that RT expand TIL-Treg with activated and functionally suppressive phenotype post-RT[92], which gave a rationale to develop TIL-Treg targeted immunotherapy in combination with RT to maximize the anti-tumor response. In addition, although single fraction irradiation gives great insights and opportunity for well-controlled experiments with clinical relevance in SBRT, recent study also suggests the that changing dose and fractionation schemes could result in different impact to trigger innate and adaptive anti-tumor immune response including c-GAS-STING pathway followed by DNA damage, leading to the activation of type I IFN pathway[93], supporting modulation of dose and fractionation scheme will be another parameter to optimize the efficacy of the treatment. Therefore, in order to optimize the RT combined with Treg modulating immunotherapy, we will test the different immunotherapy targeting relatively specifically expressed on TIL-Treg, and also test the different dose and fractionation scheme, separately and in combination in vivo, using transgenic mouse models for different tumor types with phygiological relevance

as well as xenograft tumor models.

2-1: RT increases the expression of immune-checkpoint molecules on TIL-Treg (CTLA4, 41-BB, CCR8 (CCR4)) and targeting the molecules in combination with RT results in better anti-tumor immunity.

(And DUSPs and RGSs described in Chapter IV might fit into this.)

Earlier studies suggest the augmented anti-tumor effect with Treg-depletion in combination with RT[26,34]. One of the challenges of Treg-targeted immunotherapy is the side effects of autoimmunity especially if the depletion of Treg was systemic, supporting the importance of selectively targeting TIL-Treg. Recently, using RNAseq from different cancer patients (prostate, RCC, bladder, glioblastoma), we have identified some molecules relatively specifically and highly expressed in TIL-Treg (Nirschl, Muroyama, Drake at al (refer Chapter IV for details)), which was also validated in protein levels, including CTLA-4, 4-1BB and CCR8, which are expressed on the surface of TIL-Treg thus more targetable by mAb and clinically applicable. We showed that CTLA4 and 41-BB expression in TIL-Treg increased post-RT[92]. Using the same approach, we will test the CCR8 expression on TIL-Treg post-RT *in vivo*.)Our preliminary data showed, using the monoclonal antibody against CTLA4 whose isotype is IgG2a, in which FcR-dependent ADCC are relatively strong compared to the other isotypes, serving as depleting antibody of the targets, that selective TIL-Treg depleting aCTLA4 Ab in combination with RT eradicated the established tumors in more than 80 % of the MC38-bearing mice, with better survival and long- lasting immune response with increased CD8 effector/Treg ratio, and overcome second tumor challenge, compared with single treatment (RT alone, aCTLA4 alone) and untreated group. (Marsiscano, …Muroyama, …Drake at al (in submission)) Using this model,

we will also expand our search in combination therapy of other targets, 4-1BB and CCR8 *in vivo*. We will use MC38 (-OVA), B16/F10 (-OVA), RENCA (-HA), and 4T1 (-HA) subcutaneous models as well. Furthermore, with the collabolation, we will test the antibody in physiologically relevant transgenic mouse models of other tumor types; Melanoma (Bosenburg mice), Prostate cancer, Pancreatic cancer; KPC model, Gastric cancer, as well as human cell line or human tumor xenograft implanted in humanized mice. For the treatment groups, we will have untreated (isotype control as negative control), RT (+ isotype control), mAb alone, and use Foxp3-DTR mice treated with DT for genetic depletion of Treg, insetead of mAb as "positive control". We expect the see that combination therapy of TIL-Treg targeted immunotherapy with RT showed improved survival, tumor eradication with anti-tumor immune response. (If we did not observe the significant and improved anti-tumor response, we will further looking into other TIL-Treg targeting molecules found in our RNAseq data., including CD177.)

2-2: RT dose and fractionation optimization will affect TIL-Treg expansion

Recent study showed that the dose of RT and fractionation scheme can significantly impact the immunogenicity of tumor cells. One study suggest that radiation dose above 12-18 Gy induce Trex1 to degrade cytosolic DNA, which activate STING pathway and type I IFN flowed by Batf3+ DC enhancing CD8 effector response, leading high dose RT less immunogenic to induce abscopal effect. And hypofractionation (8 Gy x3) will help to accumulate the cytosolic DNA and further make the tumor immunogenic [93](The dose we have been using, 10 Gy, fits into "immunogenic" range inducing dsDNA without significant induction of Trex1.) However, the impact of dose and hypofractionation on TIL-Treg induction post-RT has not been fully elucidated. We hypothesized that TIL-Treg will still increase post-RT in different doses and

fractionation scheme, but the most “immunogenic” regimen could increase the TIL-Treg most because those tumors would by highly “Hot” or “T-cell inflamed” tumors, and if so the combination with TIL-Treg targeted immunotherapy above would significantly augment the anti-tumor response. (Test abscopal effect too??) To test the impact of dose, we will first irradiate tumor-bearing mice (B16/F10, MC38) by different dose of RT (0 – 30 Gy) by single fraction, and determine the number, ratio, phenotype (activation marker CTLA4, 41BB, Helios), proliferation (Ki-67) and function (in vitro suppression assay) of Treg (especially TIL-Treg), as well as effector CD8 (and CD8/Treg) by flow cytometry (and IHC) and tumor volume and survival. We will determine the dose of best anti-tumor response. Next, using that dose or 8 Gy as Demaria’s paper, we will compare the impact of fractionation on the expansion of TIL-Treg, by using 8,10 Gy x1, 8 Gy x3, 20 Gy x1, 30 Gy x1 using the same readout as above. We expect to observe the increase of suppressive Treg even in different dose and fractionation scheme. But expect to see the most increased and suppressive TIL-Treg in “immunogenic” regimen. If this worked, we will further pursue to test the combination therapy of that RT scheme with TIL-Treg depletion strategies developed above to see the additive and synergistic anti-tumor effect.

(3) To test the hypothesis that RT increased Treg infiltration and/or alters phenotype in patients receiving palliative SBRT with biopsy accessible lesions

3-1: RT increases Treg expansion in the tumors of cancer patients (renal cell carcinoma, prostate cancer, and bladder cancer)

My study showed above in multiple preclinical mouse models that RT increased Treg infiltration and make them into more suppressive phenotype[23]. And numbers of clinical reports support the improved anti-tumor response in combination therapy of

radiation and ipilimumab. We hypothesized that RT induce the increase and activated/suppressive phenotype of TIL-Treg in patients received SBRT. To test the hypothesis, we will obtain biopsy samples of pre-RT tumor and post-RT tumors from RCC, prostate cancer and bladder cancer patients, with written informed consent. We will use both flow cytometry and IHC with Foxp3 staining for the evaluation of TIL-Treg. For flowcytometry experiments, the fresh tumors will be digested using Human tumor dissociation kit and gentle MACS dissociator (Milteniyl), single cell suspention will be stained for L/D, CD3, CD4, CD8, CD25, CD127, Foxp3 and markers of interest (CTLA4, 41-BB and Helios), Ki-67 for the analysis of the numbers, ratio, survival, and expression of the markers of "activated Treg" of TIL-Treg (LD-CD3+CD4+CD25+CD127-Foxp3+) population. We will use corresponding peripheral blood T cell populations as control. For IHC staining, the samples fill be FFPE-fixed and stained for Foxp3 expression with pathologist's evaluation. (If possible) biopsy samples from non-tumor and non-irradiated surrounding tissues will be used as a control. We expect to see that, as the same as preclinical model, TIL-Treg will increased in post-RT tumors with increased expression of CTLA4, 41BB, Helios and Ki-67, which will validate the clinical relevance of the impact of RT on TIL-Treg. One of the technical challenges of this approach will be the paucity of cell components obtained from small and limited biopsy samples. If we encounter the pitfalls, we will use an alternative approach of single cell RNAseq or Nanostring immune assay for the evaluation of transcriptional signature of the whole TME using the whole obtained tumor samples and de-convolute and evaluate the Treg-gene signatures using computational approach. Another pitfall of this approach will be the potential sample bias, as a nature of biopsy and of the intratumoral heterogeneity of the immune

signature in the TME depending on the regions within the tumor. To minimize the sample bias and to obtain the representative tumor samples, we will be using CT/MRI-guided targeted biopsy and target multiple regions of tumor parenchyma, and analyze the samples from multiple locations.

3-2: Comprehensively profile TME pre- and post- RT lesions

My study shown that RT induce dynamic and complex immunological changes in the tumormicroenvironment in preclinical mouse model using Nanostring.[23] To evaluate the immune profile of the TME in HUMAN patients, using the biopsy samples pre- and post-RT as described above, we will characterize both 3-2-1: immune profiling and 3-2-2: immune cell subsets location in the tumor, taking into the heterogeneity of the TME into account.

3-2-1: We will perform single cell RNA sequenencing. We will sort out the immune cell population from patients samples as a bulk and conduct scRNAseq using 10x platform, and de-convult immune signature with computational approach.

3-2-2: To test the distribution of immune cells, especially CD8 effector cells and phenotypically suppressive TIL-Treg in the TME, we will conduct Poly chromatic IF with immune monitoring core. Potenaial pitfall could be small sample size. Alternative approach could be using surgery case taking RT to reduce tumor size pre-operation followed by surgical resection to increase the size of sample.

**SUMMARY**

Radiotherapy (RT) enhances innate and adaptive anti-tumor immunity; however, the effects of radiation on suppressive immune cells, such as regulatory T cells (Treg), in the tumor microenvironment (TME) have not been fully elucidated. Although previous reports suggest an increased Treg infiltration post-radiation, whether these Treg are functionally suppressive has not been determined. To test the hypothesis that RT enhances the suppressive function of Treg in the TME, we selectively irradiated implanted tumors using the Small Animal Radiation Research Platform (SARRP), which models stereotactic radiotherapy in human patients – followed by flow-cytometric and functional analyses of tumor-infiltrating lymphocytes (TILs). Our data showed that RT significantly increased tumor-infiltrating Treg (TIL-Treg), which had higher expression of CTLA-4, 4-1BB, and Helios as compared to non-irradiated tumors. This observation held true across several tumor models (B16/F10, RENCA, and MC38). Notably, we found that post-RT, TIL-Treg had equal or improved suppressive capacity compared to non-irradiated tumors. Our data also indicated that post-RT, Treg proliferate more robustly than other T cell subsets (CD3, CD4, and CD8) in the TME. In addition, the post-RT Treg expansion occurred when T cell migration was inhibited using Fingolimod - suggesting that the increased Treg frequency was likely due to preferential proliferation of intratumoral Treg post-radiation. Our data also suggested that post-irradiation Treg expansion was independent of TGF-β and IL-33. Collectively, these data demonstrate that RT increases phenotypically and functionally suppressive Treg in the TME, and provide a rationale for treatment regimens that combine RT with Treg-targeting agents to maximize anti-tumor efficacy.

“Intended to be blank”

# CHAPTER IV: NOVEL TREG-ASSOCIATED TARGETS FROM HUMAN TUMOR INFILTRATING LYMPHOCYTES (TIL)

## INTRODUCTION

Accumulating evidence suggests that Treg are the negative force against tumor immunity. In pre-clinical models, depletion of Treg results in better tumor control with enhancement of effector T cell response[25-27]. In humans, Treg infiltration in tumor and low CD8/Treg ratio are reported to correlate with poor prognosis in patients in some types of cancers[20,28,29], and the depletion of Treg by low dose cyclophosphamide have shown better anti-tumor response[30,31] , and the treatments with anti-CTLA4 antibody, which at least partly exerts its anti-tumor effect via Treg depletion through ADCC, have shown clinical response in different types of tumors[32,33]. Despite the potential importance of Treg in the tumor progression and resistance to anti-tumor immunity, and its importance as a therapeutic target, the exact properties of TIL-Treg, and the determinant molecule for the function of Treg in human tumor, have not been clear yet. This has been a challenging question as numbers of molecules expressed on TIL-Treg, which have activated phenotype[20,94,95], and are overlapped with activated effector T cells, and targeting those molecules could potentially affect activated T effector cells, which are important for anti-tumor effect, as well. In addition, even the molecules were expressed on Treg, systemic depletion of Treg will lead to auto-immunity thus targeting molecules selectively expressed on TIL-Treg will be important[20]. Therefore, finding out the targetable molecules selectively expressed on TIL-Treg or effectively modulate TIL-Treg functions, especially in human, are of vital importance with clinical significance. Here, we have performed RNA sequencing (RNAseq) of the peripheral blood mononuclear cells (PBMCs) and TILs from prostate cancer, glioblastoma and renal cell carcinoma patients (and urothelial carcinoma (bladder cancer) in progress), and conducted extensive profiling of TIL-expressing molecules. Of note, we have included activated conventional

T cells in PBMC as control as well as naïve T cells, which enable us to distinguish the markers for activation and the markers of TIL-Treg, and to profile the kinetics of molecules upon activation. From the dataset, we have identified novel molecular targets for human TIL-Treg, including DUSP1, DUSP4, RGS1 and RGS16, which are highly expressed on TIL-Treg and showed unique expression patterns. Notably, DUSP1 and DUSP4 showed reciprocal expression pattern, where the expression of the former was downregulated upon activation. Expression of the molecules was confirmed by qPCR both in mouse and human, and we are further characterizing their roles in Treg *in vitro* and *in vivo*.

## RESULTS

### RNA sequencing data revealed genes highly expressed in TIL-Treg

We sorted out the following populations; from PBMC, we isolated naïve CD4 cells ($CD4^+CD45RA^+CCR7^+CD27^+CD28^+$), Treg ($CD4^+CD25^+CD127^+$), naïve CD8 cells ($CD8^+CD45RA^+CD27^+CD28^+$), and antigen-experienced CD8 cells ($CD8^+CD45RO^+$), and from tumor infiltrating cells, we isolated Treg and antigen-experienced CD8 cells (Supplementary Figure IV-1). We also prepared activated CD4/CD8 population, by stimulating naïve CD4/CD8 with anti-CD3 and CD28 *in vitro*. We included these activated populations as control as well, since large population of Treg-associated genes are also upregulated in activated T cells[17,96]. Thus, we expected these control groups will help identifying the genes selectively expressed in TIL-Treg or help finding out the genes

with unique expression patterns.

To identify the candidate target genes, we looked into the expression patterns of the genes which are highly expressed in TIL-Treg, compared to the three different controls, namely PBMC CD4 naïve cells, PBMC CD4 activated cells, and PBMC Treg (Figure IV-1A, B, C, respectively). We used FPKM (Fragments Per Kilobase Million) as readouts.

The expression patterns of the genes from prostate cancer RNAseq are shown in Figure IV-1 and Figure IV-2. CCR4, which is a chemokine receptor expressed in activated Treg, which recruit Treg in the TME via chemokine ligands CCL17 and CCL22[95] are relatively selectively highly expressed in Treg and TIL-Treg, consistent with the previous finding. (Figure IV-2A) (As shown in Figure 2 in Chapter III, we confirmed the expression of CCR4 in mouse tumors as well.) CCR6, another chemokine receptor for CCL20, is relatively selectively expressed in TIL-Treg. (Figure IV-2B) (Along the lines of chemokine receptors, we and others have shown the selective expression of CCR8, CD177 and IL1R2 in TIL-Treg (Thomas Nirschl, Yuki Muroyama, Charles Drake et al. unpublished data)[97,98]. METRNL (Meteorin Like, Glial Cell Differentiation Regulator), which is not-well characterized gene associated with beige fat and improving glucose intolerance[99-102], is highly expressed in TIL, which could be a potential target for tumor metabolism (Figure IV-2C). RGS16, a negative regulator for G-protein coupled receptor were associated with activation (Figure IV-2D). For fucosyltransferase 7 and 9 (FUT7 and FUT9), which mediate the systhesis of CD15s (sialyl Lewis x), which is reported to define suppressive Treg in human[103], expression level was low, but show a trend for higher expression in more aggressive prostate cancer (Figure IV-2E, F). Solute carrier family 1 member 2 (SLC1A2) is a glutamate transporter reported to be expressed in central nervous system[104] were highly expressed in TIL (Figure IV-2G), suggestive for

the potential role in modulating tumor metabolism. Fibrinogen-like protein2 (FGL2), reported to be downstream suppressive effector molecule of TIGIT[105,106] was also highly expressed in TILs (Figure IV-2H).

Among them, the interesting expression patterns were seen in DUSP1, DUSP4 and RGS1. (Figure IV-3)

**Unique expression pattern of DUSP1, and reciprocal pattern with DUSP4**

DUSP1 (dual specificity phosphatase 1), showed an unique expression pattern; DUSP1 was expressed in naïve CD4 T cells, and down-regulated upon activation despite of high expression in Treg and TIL-Treg. (Figure IV-3).

Whereas DUSP4 showed the reciprocal pattern with DUSP1; which is upregulated activation, highly expressed in Treg. This expression pattern held true across different types of tumors analyzed; prostate cancer (Figure IV-3A), glioblastoma (Figure IV-3B) and renal cell carcinoma (Figure IV-3C), supportive for the expression pattern being global phenomenon. To verify the expression pattern shown in RNAseq, we conducted the qPCR both in human and mice, with designated time course (from 12 hours to 72 hours post activation) and saw the similar pattern: DUSP1 showed down regulation upon activation in time-dependent manner both in conventional T cells and in Treg. And DUSP4 showed the reciprocal pattern. (Figure IV-3 D, and Supplementary Figure IV-2A, B (with preliminary tumor-derived sample data)). Next, we examined whether this pattern would hold true for the corresponding mouse T cell population, whether we could develop the mice model. Using GFP-Foxp3 mice, we isolated naïve CD4 T cells ($CD4^+CD62L^+CD44^-$), naïve CD8 T cells ($CD8^+CD62L^+CD44^-$), Treg ($CD4^+Foxp3^+$), antigen-experienced CD8 T cells ($CD9^+CD62L^-CD44^+$) (Supplementary Figure IV-3). *In*

*vitro* activation was performed with the stimulation with CD3 and CD28 just like in human experiments. We saw the similar expression pattern of DUSP1 and DUSP4 in mouse as well (Figure IV-3E, and Supplementary Figure IV-3 B-G (with preliminary TIL and DLN data)).

This reciprocal expression pattern of DUSP1 and DUSP4 led me the hypothesis that these two molecules reciprocally regulate Treg activation/function.

In addition, DUSP1 and DUSP4 showed similar expression pattern in CD8 cells; where DUSP1 expression decreased upon activation, high expression in antigen-experienced cells, especially in tumor, and DUSP4 showed reciprocal patterns (Figure IV-4, Supplementary Figure IV-3 B-G (with preliminary TIL and DLN data)), suggestive for the multifold action of those molecules in TIL.

**High RGS1 expression in TIL**

Another gene which is one of the top genes highly expressed in TIL-Treg was RGS1 (Figure IV-1), a negative regulator of G-protein coupled receptors[107,108]. RGS1 was selectively highly expressed in TIL (TIL-Treg and TIL-Ag-experienced cells) in prostate cancer, glioblastoma and renal cell carcinoma RNAseq (Figure IV-5 A-C). We also confirmed its expression pattern by qPCR both in human and mice as described above (Figure IV-5 D, E).

**Generation of selective knockout mice for Dusp1 and Rgs1**

To further characterize the role of DUSP1, DUSP4 and RGS1 *in vivo*, we generated the floxed mice for DUSP1 and generating RGS1. The schemes are shown in Figure IV-6A and B, respectively. We are crossing these mice to Foxp3-Cre and CD4-Cre mice to

generate Treg or T cell specific knockout of those genes, and characterize their role in vivo. We are planning to test in vivo suppression assay, tumor models and autoimmune models including colitis and EAE to test the genes function in Treg in vivo. We will make additional knockout mice depending on the phenotype observed (including double reporter mice (Foxp3-GFP-Cre BAC transgenic mice were crossed to Rosa26-loxP-Stop-loxP-YFP (R26-YFP) reporter mice) or temporal knockout (with ERT) or depletion of Treg (Foxp3-DTR) to test the effect of those genes for stability of Treg.

**The impact of DUSP1, DUSP4 and RGS1 on suppressive function of Treg *in vitro***

To test the role of the selected genes on suppressive function of Treg *in vitro*, we are performing knocking down those genese via siRNA in human PBMS, followed by in vitro suppression assay. (Supplementary Figure IV-4A)

The siRNA transfection with electroporation knocked down the Foxp3 expression (positive-control) for up to 72 hours (Supplementary Figure IV-4B) and downregulated of Rgs1 RNA expression (and Helios) but not for Dusp1 and Dusp4 (Supplementary Figure IV-4C), where further optimization is required. We are also considering other approach including CRISPR-Cas9 knockout, and lipid-free transfection reagent. We are also working on improving the suppression assay using human PBMC. (primary data shown in Supplementary Figure IV-4D, E).

**DISCUSSIONS**:

Here we identified novel genes associated with human tumor-infiltrating Treg (TIL-Treg), including DUSP1, DUSP4 and RGS1 in different types of tumors; prostate cancer, renal cell carcinoma, and glioblastoma (urothelial carcinoma in progress). Those genes are highly expressed in TIL-Treg and could be a potential therapeutic target.

Notably, expression of DUSP1 is downregulated upon activation via stimulation through CD3 and CD28, both in T conventional cells and in Treg. This is of special interest as many Treg-associated genes are also upregulated upon T cell activations, including CTLA-4[17,22,96], but the expression pattern of DUSP1 was actually the opposite; down-regulated upon activation despite of high expression in Treg. Furthermore, the expression pattern of DUSP1 and DUSP4 was reciprocal; DUSP1 expression was observed in naïve T conventional cell, was down-regulated upon activation in time-dependent manner and was high in Treg and down-regulated upon activation of Treg, and its expression was especially high in TIL-Treg. On the other hand, DUSP4 expression was up-regulated upon activation, its expression was high in Treg and further up-regulated upon activation, and high expression in TIL-Treg was observed. In addition, DUSP1 and DUSP4 are very homologous, they are 78% homologous and form the closest cluster in alignment tree of DUSP proteins[109], suggestive of the common ancestor molecule. These data drove me a hypothesis that DUSP1 and DUSP4 were derived from a common ancestor molecule, and with some mutations, they diverged into different molecules which reciprocally modulate Treg activation and function.

To test this hypothesis of reciprocal regulations, we will be working on double knockdown/knockdown in vitro to see the Treg function, titration experiments by knock-

in, and making double knockout mouse by crossing DUSP1, DUSP4 floxed mice to Treg specific, T cell specific CRE mice.

Dual specificity phosphatases (DUSPs) are also known as MAPK phosphatases (MKPs), which are the primary phosphatases responsible for dephosphorylation/deactivation of MAPKs in vivo[109-111]. As the name suggest, they dephosphorylate both threonine/serine and tyrosine. Their targets are p38, c-jun N-terminal kinase (JNK), and ERK, but the target specificity depends on the cell types. For example, in macrophage, DUSPs are reported to dephosphorylate p38 and JNK upon activation, but had little effect on ERK, whereas in T cells, DUSPs primary regulate JNK activities, perhaps ERK but not p38[109,110].

In relation to immune system, DUSP1 has been known as a negative regulator of innate immunity. DUSP1 knockout macrophage have higher secretion of pro-inflammatory cytokines upon TLR stimulation, and DUSP1 knockout mice are more susceptible to systemic inflammation such as sepsis upon LPS [112,113]. Less is known for the roles of DUSP1 in adaptive immunity. Global DUSP1 knockout mice revealed normal thymocytes development, and CD4/CD8 ratio were comparable to wild type (WT)[109,114]. And in dendritic cells, DUSP1 is shown to reciprocally regulate Th1/17 differentiation of T cells in cytokine dependent manner and downregulating iTreg generation via reduced TGF-beta2 secretion from dendritic cells (DC)[115]. However, the role of DUSP1 in Treg, especially in the context of tumor microenvironment and its interactions with other DUSPs have not been elucidated.

Of translational relevance, in addition to immune cells, DUSP1 is highly expressed in prostate, breast, gastric, renal cancer, and non-small cell lung cancer (NSCLC)[109], and has been shown to inhibit cisplatin-induced apoptosis in NSCLC cells, osteosarcoma cells,

and breast cancer cells in JNK dependent manner. Indeed, numbers of DUSP inhibitors have been under development[116-118] as anti-tumor drug to augment the therapeutic effects of chemotherapy. Thus, if DUSP1 is necessary for suppressive function in Treg, DUSP1 inhibition could not only blocking suppressive Treg but also help inducing tumor cell apoptosis, which could result in synergistic anti-tumor effects.

In addition, DUSPs are known to be induced by glucocorticosteroid, and are suggested to play roles in anti-inflammatory effects of steroids, although involvement of multiple DUSPs with compensatory roles each others have been suggested as well[109]. Therefore, in future direction, relation to the signaling of glucocorticoid-induced TNFR-related protein (GITR), or TNFRSF18, might be of interest as well, considering the high expression and potential roles of GITR in Treg[119]. (Experiments comparing transcriptional profiles of GITR positive and negative were underway (data not shown)).

DUSP4 shares some common DUSP features mentioned above. Phenotype of global knockout mice varies among different deletion strategies. One study suggests that, ERK signaling, which has been suggested to be a primary target for DUSP4, in Treg/Tconv was comparable to WT[120], and so does the generation of induced Treg (iTreg). However, DUSP4 has been suggested to be one of the few genes with Treg-specific epigenetically active landscape (H3K27ac), both in mouse and human, suggestive for Treg lineage identifier[96] . Nevertheless, the exact functional role of DUSP4 in Treg especially in the context of the TME, as well as the interaction with other DUSPs including DUSP1 have not been elucidated yet.

Therefore, understanding the role of DUSP1 and DUSP4 in Treg, especially in the context of the TME, and the reciprocal regulation with molecular mechanisms will not only offer the unique opportunity to understand the TIL-Treg function as well as to develop the

novel therapeutic strategies for cancer immunotherapy as well as autoimmune disease as the opposite side of the coin.

Once the reciprocal regulation between DUSP1 and DUSP4 has been established *in vitro* and *in vivo*, we will further look into the underlying mechanisms. One potential mechanism for reciprocal regulation, suggested from the previous literature could be the negative feedback of DUSP4 to inhibit ERK1/2, which is one of the inducer of DUSP1 transcription shown in macrophage[121,122].

RGS1 is a negative regulator of G-protein coupled receptor (GPCR), including chemokine receptors, serving as a GTPase-activating protein (GAP)[107]. In T cells, RGS1 is known to downregulate the signaling of CXCR4-CXCL12 in bone marrow, and CCR7-CCL19 in lymph node[108]. Thus, it is possible that RGS1 might help retaining T cell/Treg in tissue such as gut. And considering the high expression in TIL from our RNAseq data, we could speculate that RGS1 in TIL might help them stay in tumor, keeping Treg infiltration. RGS1 expression in tumor is either increased or decreased depending on tumor types[123]. For example, RGS1 upregulation is reported in esophageal adenocarcinoma, renal cell carcinoma (RCC), Head and neck squamous cell carcinoma (SCC), Brain tumors, Melanoma, Diffuse Large B Cell Lymphoma (DLBCL), Follicular lymphoma (FL), and downregulation is reported in bladder cancer and Chronic Lymphocytic Leukemia (CLL). Global RGS1 knockout mice revealed a normal distribution of CD4 and CD8 expression on thymocytes, but decreased B cell migration to CXCL12, 13[124]. However, its role in Treg especially in the context of the TME has not been elucidated. To test that, like DUSP1/4, in vitro suppression assay via knockdown/knockout of the RGS1 gene is under progress, and we generated RGS1 floxed

mice to be able to perform experiments in Treg, T cell specific knock out mice by crossing the mice with the specific CRE-expressing mice.

Nevertheless, this research will elucidate the roles of novel targets associated with human TIL-Treg, which will help understanding their roles in different disease settings, such as tumors and autoimmunity, and will help developing the Treg-targeted immunotherapy to maximize anti-tumor effect, or contrary, to protect against autoimmunity.

## SUMMARY

Treg has been implicated as negative force and protective for tumor growth. Numbers of preclinical studies suggest that depletion of Treg have better outcome for tumors, and clinical data with anti-CTLA4 blockade, which is known to block or deplete Treg have support this notion[25-27,29,32]. However, what is exactly the determinant molecule for Treg in human TIL, which has much more clinical relevance and of large therapeutic target, has not been clear.

Here, using RNAseq data from prostate cancer, renal cell carcinoma, and glioblastoma (and urothelial carcinoma) patients, we have identified DUSP1, DUSP4 and RGS1 as well as other genes which are highly expressed in human TIL-Treg and have unique expression pattern; especially DUSP1 expression is down-regulated upon T cell activation, contrary to majority of Treg-associated genes whose expression will increase upon activation[17], and shows reciprocal expression pattern with DUSP4. These gene expression was confirmed by q-PCR both in human and mice and *in vitro* functional studies and *in vivo* characterization by knockout mice are underway. In addition, I hypothesized that, from the reciprocal expression pattern and homology, DUSP1 and DUSP4 are reciprocally regulating Treg activation and function, and RGS1 plays a

regulatory role in TIL.

Further *in vitro* and *in vivo* studies will follow to delineate the roles and interactions of those genes in TIL-Treg, and will give new frontiers for Treg-targeted immunotherapies.

**REFERENCES:**


1 Ehrlich, P. Über den jetzigen Stand der Karzinomforschung. *Ned Tijdschr Geneeskd.* **5**, 273–290 (1909).

2 Burnet, M. Cancer—A Biological Approach: III. Viruses Associated with Neoplastic Conditions. IV. Practical Applications. *British Medical Journal* **1**, 841-847 (1957).

3 Thomas, L. On immunosurveillance in human cancer. *The Yale Journal of Biology and Medicine* **55**, 329-333 (1982).

4 Thomas, L. Discussion. In Cellular and Humoral Aspects of the Hypersensitive States. *H. S. Lawrence (ed.), Hoeber-Harper, New York,* , pp. 529–533 (1959).

5 Schreiber, R. D., Old, L. J. & Smyth, M. J. Cancer Immunoediting: Integrating Immunity's Roles in Cancer Suppression and Promotion. *Science (New York, N.Y.)* **331**, 1565-1570, doi:10.1126/science.1203486 (2011).

6 Dunn, G. P., Old, L. J. & Schreiber, R. D. The Immunobiology of Cancer Immunosurveillance and Immunoediting. *Immunity* **21**, 137-148, doi:http://dx.doi.org/10.1016/j.immuni.2004.07.017 (2004).

7 Gajewski, T. F., Schreiber, H. & Fu, Y.-X. Innate and adaptive immune cells in the tumor microenvironment. *Nature immunology* **14**, 1014-1022, doi:10.1038/ni.2703 (2013).

8 Corrales, L., Matson, V., Flood, B., Spranger, S. & Gajewski, T. F. Innate immune signaling and regulation in cancer immunotherapy. *Cell Res* **27**, 96-108, doi:10.1038/cr.2016.149 (2017).

9 Nirschl, C. J. & Drake, C. G. Molecular Pathways: Co-Expression of Immune Checkpoint Molecules: Signaling Pathways and Implications for Cancer Immunotherapy. *Clinical cancer research : an official journal of the American Association for Cancer Research* **19**, 4917-4924, doi:10.1158/1078-0432.CCR-12-1972 (2013).

10 Sharma, P., Hu-Lieskovan, S., Wargo, J. A. & Ribas, A. Primary, Adaptive, and Acquired Resistance to Cancer Immunotherapy. *Cell* **168**, 707-723, doi:10.1016/j.cell.2017.01.017 (2017).

11 Topalian, Suzanne L., Drake, Charles G. & Pardoll, Drew M. Immune Checkpoint Blockade: A Common Denominator Approach to Cancer Therapy. *Cancer cell* **27**, 450-461, doi:10.1016/j.ccell.2015.03.001 (2015).

12 Pardoll, D. M. The blockade of immune checkpoints in cancer immunotherapy. *Nature reviews. Cancer* **12**, 252-264 (2012).

13 Pardoll, D. M. Immunology beats cancer: a blueprint for successful translation. *Nature immunology* **13**, 1129-1132 (2012).

14 Alexander, W. The Checkpoint Immunotherapy Revolution: What Started as a Trickle Has

Become a Flood, Despite Some Daunting Adverse Effects; New Drugs, Indications, and Combinations Continue to Emerge. *Pharmacy and Therapeutics* **41**, 185-191 (2016).

15 Schumacher, T. N. & Schreiber, R. D. Neoantigens in cancer immunotherapy. *Science (New York, N.Y.)* **348**, 69-74, doi:10.1126/science.aaa4971 (2015).

16 Takahashi, T. *et al.* Immunologic self-tolerance maintained by CD25+CD4+ naturally anergic and suppressive T cells: induction of autoimmune disease by breaking their anergic/suppressive state. *International immunology* **10**, 1969-1980, doi:10.1093/intimm/10.12.1969 (1998).

17 Arvey, A. *et al.* Inflammation-induced repression of chromatin bound by the transcription factor Foxp3 in regulatory T cells. *Nature immunology* **15**, 580-587, doi:10.1038/ni.2868 http://www.nature.com/ni/journal/v15/n6/abs/ni.2868.html#supplementary-information (2014).

18 Sakaguchi, S., Yamaguchi, T., Nomura, T. & Ono, M. Regulatory T Cells and Immune Tolerance. *Cell* **133**, 775-787, doi:http://dx.doi.org/10.1016/j.cell.2008.05.009 (2008).

19 Kim, J. M., Rasmussen, J. P. & Rudensky, A. Y. Regulatory T cells prevent catastrophic autoimmunity throughout the lifespan of mice. *Nature immunology* **8**, 191-197, doi:http://www.nature.com/ni/journal/v8/n2/suppinfo/ni1428_S1.html (2007).

20 Nishikawa, H. & Sakaguchi, S. Regulatory T cells in cancer immunotherapy. *Current Opinion in Immunology* **27**, 1-7, doi:http://dx.doi.org/10.1016/j.coi.2013.12.005 (2014).

21 Vignali, D. A. A., Collison, L. W. & Workman, C. J. How regulatory T cells work. *Nature reviews. Immunology* **8**, 523-532 (2008).

22 Tai, X. *et al.* Basis of CTLA-4 function in regulatory and conventional CD4<sup>+</sup> T cells. *Blood* **119**, 5155-5163, doi:10.1182/blood-2011-11-388918 (2012).

23 Maynard, C. L., Elson, C. O., Hatton, R. D. & Weaver, C. T. Reciprocal interactions of the intestinal microbiota and immune system. *Nature* **489**, 231-241 (2012).

24 Bluestone, J. A. *et al.* Type 1 diabetes immunotherapy using polyclonal regulatory T cells. *Science translational medicine* **7**, 315ra189-315ra189, doi:10.1126/scitranslmed.aad4134 (2015).

25 Shimizu, J., Yamazaki, S. & Sakaguchi, S. Induction of Tumor Immunity by Removing CD25+CD4+ T Cells: A Common Basis Between Tumor Immunity and Autoimmunity. *The Journal of Immunology* **163**, 5211-5218 (1999).

26 Bos, P. D., Plitas, G., Rudra, D., Lee, S. Y. & Rudensky, A. Y. Transient regulatory T cell ablation deters oncogene-driven breast cancer and enhances radiotherapy. *The Journal of experimental medicine* **210**, 2435-2466, doi:10.1084/jem.20130762 (2013).

27 Teng, M. W. L. *et al.* Conditional Regulatory T-Cell Depletion Releases Adaptive

Immunity Preventing Carcinogenesis and Suppressing Established Tumor Growth. *Cancer Research* **70**, 7800-7809, doi:10.1158/0008-5472.can-10-1681 (2010).

28 Roychoudhuri, R., Eil, R. L. & Restifo, N. P. The interplay of effector and regulatory T cells in cancer. *Current Opinion in Immunology* **33**, 101-111, doi:http://dx.doi.org/10.1016/j.coi.2015.02.003 (2015).

29 Baras, A. S. *et al.* The ratio of CD8 to Treg tumor-infiltrating lymphocytes is associated with response to cisplatin-based neoadjuvant chemotherapy in patients with muscle invasive urothelial carcinoma of the bladder. *Oncoimmunology* **5**, e1134412, doi:10.1080/2162402X.2015.1134412 (2016).

30 Motoyoshi, Y. *et al.* Different mechanisms for anti-tumor effects of low- and high-dose cyclophosphamide. *Oncology reports* **16**, 141-146 (2006).

31 Ghiringhelli, F. *et al.* CD4+CD25+ regulatory T cells suppress tumor immunity but are sensitive to cyclophosphamide which allows immunotherapy of established tumors to be curative. *European journal of immunology* **34**, 336-344, doi:10.1002/eji.200324181 (2004).

32 Hodi, F. S. *et al.* Improved Survival with Ipilimumab in Patients with Metastatic Melanoma. *The New England journal of medicine* **363**, 711-723, doi:10.1056/NEJMoa1003466 (2010).

33 Robert , C. *et al.* Ipilimumab plus Dacarbazine for Previously Untreated Metastatic Melanoma. *New England Journal of Medicine* **364**, 2517-2526, doi:10.1056/NEJMoa1104621 (2011).

34 Sharabi, A. B. *et al.* Stereotactic Radiation Therapy Augments Antigen-Specific PD-1-Mediated Antitumor Immune Responses via Cross-Presentation of Tumor Antigen. *Cancer Immunol Res* **3**, 345-355, doi:10.1158/2326-6066.cir-14-0196 (2015).

35 Wong, J. *et al.* High-Resolution, Small Animal Radiation Research Platform With X-Ray Tomographic Guidance Capabilities. *International Journal of Radiation Oncology*Biology*Physics* **71**, 1591-1599, doi:http://dx.doi.org/10.1016/j.ijrobp.2008.04.025 (2008).

36 Turnis, Meghan E. *et al.* Interleukin-35 Limits Anti-Tumor Immunity. *Immunity*, doi:http://dx.doi.org/10.1016/j.immuni.2016.01.013 (2016).

37 Monticelli, L. A. *et al.* Innate lymphoid cells promote lung-tissue homeostasis after infection with influenza virus. *Nature immunology* **12**, 1045-1054, doi:10.1031/ni.2131 (2011).

38 Spranger, S. *et al.* Mechanism of tumor rejection with doublets of CTLA-4, PD-1/PD-L1, or IDO blockade involves restored IL-2 production and proliferation of CD8(+) T cells directly within the tumor microenvironment. *Journal for Immunotherapy of Cancer* **2**, 3-

3, doi:10.1186/2051-1426-2-3 (2014).

39 Harrington, K. J. *et al.* Guidelines for preclinical and early phase clinical assessment of novel radiosensitisers. *Br J Cancer* **105**, 628-639 (2011).

40 Liauw, S. L., Connell, P. P. & Weichselbaum, R. R. New Paradigms and Future Challenges in Radiation Oncology: An Update of Biological Targets and Technology. *Science translational medicine* **5**, 173sr172-173sr172, doi:10.1126/scitranslmed.3005148 (2013).

41 Demaria, S., Golden, E. B. & Formenti, S. C. Role of Local Radiation Therapy in Cancer Immunotherapy. *JAMA oncology* **1**, 1325-1332, doi:10.1001/jamaoncol.2015.2756 (2015).

42 Sharabi, A. B., Lim, M., DeWeese, T. L. & Drake, C. G. Radiation and checkpoint blockade immunotherapy: radiosensitisation and potential mechanisms of synergy. *The Lancet Oncology* **16**, e498-e509, doi:http://dx.doi.org/10.1016/S1470-2045(15)00007-8 (2015).

43 Postow, M. A. *et al.* Immunologic correlates of the abscopal effect in a patient with melanoma. *The New England journal of medicine* **366**, doi:10.1056/NEJMoa1112824 (2012).

44 Drake, C. in *Molecular Determinants of Radiation Response Current Cancer Research* (eds Theodore L. DeWeese & Marikki Laiho) Ch. 12, 251-263 (Springer New York, 2011).

45 Apetoh, L. *et al.* Toll-like receptor 4-dependent contribution of the immune system to anticancer chemotherapy and radiotherapy. *Nature medicine* **13**, doi:10.1038/nm1622 (2007).

46 Reits, E. A. *et al.* Radiation modulates the peptide repertoire, enhances MHC class I expression, and induces successful antitumor immunotherapy. *The Journal of experimental medicine* **203**, 1259-1271, doi:10.1084/jem.20052494 (2006).

47 Deng, L. *et al.* STING-Dependent Cytosolic DNA Sensing Promotes Radiation-Induced Type I Interferon-Dependent Antitumor Immunity in Immunogenic Tumors. *Immunity* **41**, 843-852, doi:http://dx.doi.org/10.1016/j.immuni.2014.10.019 (2014).

48 van der Burg, S. H., Arens, R., Ossendorp, F., van Hall, T. & Melief, C. J. M. Vaccines for established cancer: overcoming the challenges posed by immune evasion. *Nature reviews. Cancer* **16**, 219-233, doi:10.1038/nrc.2016.16
http://www.nature.com/nrc/journal/v16/n4/abs/nrc.2016.16.html#supplementary-information (2016).

49 Martin, M., Lefaix, J.-L. & Delanian, S. TGF-$\beta$1 and radiation fibrosis: a master switch and a specific therapeutic target? *International Journal of Radiation Oncology*Biology*Physics* **47**, 277-290, doi:http://dx.doi.org/10.1016/S0360-3016(00)00435-1 (2000).

50 Thomas, D. A. & Massagué, J. TGF-$\beta$ directly targets cytotoxic T cell functions during tumor evasion of immune surveillance. *Cancer cell* **8**, 369-380, doi:http://dx.doi.org/10.1016/j.ccr.2005.10.012 (2005).

51 Hodi , F. S. *et al.* Improved Survival with Ipilimumab in Patients with Metastatic Melanoma. *New England Journal of Medicine* **363**, 711-723, doi:doi:10.1056/NEJMoa1003466 (2010).

52 Kachikwu, E. L. *et al.* Radiation Enhances Regulatory T Cell Representation. *International Journal of Radiation Oncology*Biology*Physics* **81**, 1128-1135, doi:http://dx.doi.org/10.1016/j.ijrobp.2010.09.034 (2011).

53 Price, J. G. *et al.* CDKN1A regulates Langerhans cell survival and promotes Treg cell generation upon exposure to ionizing irradiation. *Nature immunology* **advance online publication**, doi:10.1038/ni.3270 http://www.nature.com/ni/journal/vaop/ncurrent/abs/ni.3270.html#supplementary-information (2015).

54 Schuler, P. J. *et al.* Effects of Adjuvant Chemoradiotherapy on the Frequency and Function of Regulatory T Cells in Patients with Head and Neck Cancer. *Clinical Cancer Research* **19**, 6585-6596, doi:10.1158/1078-0432.ccr-13-0900 (2013).

55 Wirsdorfer, F. *et al.* Thorax irradiation triggers a local and systemic accumulation of immunosuppressive CD4+ FoxP3+ regulatory T cells. *Radiat Oncol* **9**, 98, doi:10.1186/1748-717x-9-98 (2014).

56 Chang, D.-K. *et al.* Anti-CCR4 monoclonal antibody enhances antitumor immunity by modulating tumor-infiltrating Tregs in an ovarian cancer xenograft humanized mouse model. *Oncoimmunology* **5**, e1090075, doi:10.1080/2162402X.2015.1090075 (2016).

57 Wing, K. *et al.* CTLA-4 control over Foxp3+ regulatory T cell function. *Science (New York, N.Y.)* **322**, 271-275, doi:10.1126/science.1160062 (2008).

58 Akimova, T., Beier, U. H., Wang, L., Levine, M. H. & Hancock, W. W. Helios Expression Is a Marker of T Cell Activation and Proliferation. *PloS one* **6**, e24226, doi:10.1371/journal.pone.0024226 (2011).

59 Zabransky, D. J. *et al.* Phenotypic and functional properties of Helios+ regulatory T cells. *PloS one* **7**, e34547, doi:10.1371/journal.pone.0034547 (2012).

60 Fuhrman, C. A. *et al.* Divergent Phenotypes of Human Regulatory T Cells Expressing the Receptors TIGIT and CD226. *The Journal of Immunology* **195**, 145-155, doi:10.4049/jimmunol.1402381 (2015).

61 So, T., Lee, S. W. & Croft, M. Immune regulation and control of regulatory T cells by OX40 and 4-1BB. *Cytokine & growth factor reviews* **19**, 253-262, doi:10.1016/j.cytogfr.2008.04.003 (2008).

62 Flavell, R. A., Sanjabi, S., Wrzesinski, S. H. & Licona-Limón, P. The polarization of immune cells in the tumour environment by TGF$\beta$. *Nature reviews. Immunology* **10**, 554-567 (2010).

63 Bueno, L. *et al.* Semi-mechanistic modelling of the tumour growth inhibitory effects of LY2157299, a new type I receptor TGF-$\beta$ kinase antagonist, in mice. *European Journal of Cancer* **44**, 142-150, doi:http://dx.doi.org/10.1016/j.ejca.2007.10.008 (2008).

64 Herbertz, S. *et al.* Clinical development of galunisertib (LY2157299 monohydrate), a small molecule inhibitor of transforming growth factor-beta signaling pathway. *Drug Design, Development and Therapy* **9**, 4479-4499, doi:10.2147/DDDT.S86621 (2015).

65 Serova, M. *et al.* Effects of TGF-beta signalling inhibition with galunisertib (LY2157299) in hepatocellular carcinoma models and in ex vivo whole tumor tissue samples from patients. *Oncotarget* **6** (2015).

66 Lee, E.-J. *et al.* Single high-dose irradiation aggravates eosinophil-mediated fibrosis through IL-33 secreted from impaired vessels in the skin compared to fractionated irradiation. *Biochemical and biophysical research communications* **464**, 20-26, doi:http://dx.doi.org/10.1016/j.bbrc.2015.05.081 (2015).

67 Halin, C. *et al.* The S1P-analog FTY720 differentially modulates T-cell homing via HEV: T-cell-expressed S1P1 amplifies integrin activation in peripheral lymph nodes but not in Peyer patches. *Blood* **106**, 1314-1322, doi:10.1182/blood-2004-09-3687 (2005).

68 Deloch, L. *et al.* Modern Radiotherapy Concepts and the Impact of Radiation on Immune Activation. *Frontiers in Oncology* **6**, 141, doi:10.3389/fonc.2016.00141 (2016).

69 Demaria, S. & Formenti, S. C. Radiation as an immunological adjuvant: current evidence on dose and fractionation. *Front Oncol* **2** (2012).

70 Burnette, B. & Weichselbaum, R. R. The Immunology of Ablative Radiation. *Seminars in Radiation Oncology* **25**, 40-45, doi:http://dx.doi.org/10.1016/j.semradonc.2014.07.009 (2015).

71 Gough, M. J. & Crittenden, M. R. Combination approaches to immunotherapy: the radiotherapy example. *Immunotherapy* **1**, 1025-1037, doi:10.2217/imt.09.64 (2009).

72 Hori, S., Nomura, T. & Sakaguchi, S. Control of Regulatory T Cell Development by the Transcription Factor Foxp3. *Science (New York, N.Y.)* **299**, 1057-1061, doi:10.1126/science.1079490 (2003).

73 Chen, W. *et al.* Conversion of peripheral CD4+CD25- naive T cells to CD4+CD25+ regulatory T cells by TGF-beta induction of transcription factor Foxp3. *The Journal of experimental medicine* **198**, 1875-1886, doi:10.1084/jem.20030152 (2003).

74 Vanpouille-Box, C. *et al.* TGFbeta is a master regulator of radiation therapy-induced antitumor immunity. *Cancer Res* **75**, doi:10.1158/0008-5472.can-14-3511 (2015).

75 Hardee, M. E. *et al.* Resistance of Glioblastoma-Initiating Cells to Radiation Mediated by the Tumor Microenvironment Can Be Abolished by Inhibiting Transforming Growth Factor-β. *Cancer Research* **72**, 4119-4129, doi:10.1158/0008-5472.can-12-0546 (2012).

76 Young, K. H. *et al.* TGFbeta inhibition prior to hypofractionated radiation enhances efficacy in preclinical models. *Cancer Immunol Res* **2**, 1011-1022, doi:10.1158/2326-6066.CIR-13-0207 (2014).

77 Wu, C.-T., Hsieh, C.-C., Yen, T.-C., Chen, W.-C. & Chen, M.-F. TGF-β1 mediates the radiation response of prostate cancer. *Journal of Molecular Medicine* **93**, 73-82, doi:10.1007/s00109-014-1206-6 (2015).

78 Turnquist, H. R. *et al.* IL-33 Expands Suppressive CD11b+ Gr-1int and Regulatory T Cells, including ST2L+ Foxp3+ Cells, and Mediates Regulatory T Cell-Dependent Promotion of Cardiac Allograft Survival. *The Journal of Immunology* **187**, 4598-4610, doi:10.4049/jimmunol.1100519 (2011).

79 Matta, B. M. *et al.* IL-33 is an unconventional Alarmin that stimulates IL-2 secretion by dendritic cells to selectively expand IL-33R/ST2+ regulatory T cells. *Journal of immunology (Baltimore, Md. : 1950)* **193**, 4010-4020, doi:10.4049/jimmunol.1400481 (2014).

80 Matta, B. M. *et al.* Peri-alloHCT IL-33 administration expands recipient T-regulatory cells that protect mice against acute GVHD. *Blood* **128**, 427-439, doi:10.1182/blood-2015-12-684142 (2016).

81 Burnette, B. & Weichselbaum, R. R. Radiation as an Immune Modulator. *Seminars in Radiation Oncology* **23**, 273-280, doi:http://dx.doi.org/10.1016/j.semradonc.2013.05.009 (2013).

82 Tanaka, A. & Sakaguchi, S. Regulatory T cells in cancer immunotherapy. *Cell Res*, doi:10.1038/cr.2016.151 (2016).

83 Chinen, T. *et al.* An essential role for the IL-2 receptor in Treg cell function. *Nature immunology* **17**, 1322-1333, doi:10.1038/ni.3540 http://www.nature.com/ni/journal/v17/n11/abs/ni.3540.html#supplementary-information (2016).

84 Turley, S. J., Cremasco, V. & Astarita, J. L. Immunological hallmarks of stromal cells in the tumour microenvironment. *Nature reviews. Immunology* **15**, 669, doi:10.1038/nri3902 (2015).

85 Plaza-Sirvent, C. *et al.* c-FLIP Expression in Foxp3-Expressing Cells Is Essential for Survival of Regulatory T Cells and Prevention of Autoimmunity. *Cell Reports* **18**, 12-22, doi:http://doi.org/10.1016/j.celrep.2016.12.022 (2017).

86 Vatner, R. E. & Formenti, S. C. Myeloid-Derived Cells in Tumors: Effects of Radiation.

*Seminars in Radiation Oncology* **25**, 18-27, doi:http://dx.doi.org/10.1016/j.semradonc.2014.07.008 (2015).

87 Muroyama, Y. *et al.* Stereotactic radiotherapy increases functionally suppressive regulatory T cells in the tumor microenvironment. *The Journal of Immunology* **198**, 204.219-204.219 (2017).

88 Schaue, D. & McBride, W. T lymphocytes and normal tissue responses to radiation. *Frontiers in Oncology* **2**, doi:10.3389/fonc.2012.00119 (2012).

89 Rubtsov, Y. P. *et al.* Stability of the Regulatory T Cell Lineage in Vivo. *Science (New York, N.Y.)* **329**, 1667-1671, doi:10.1126/science.1191996 (2010).

90 Overacre-Delgoffe, A. E. *et al.* Interferon-γ Drives Treg Fragility to Promote Anti-tumor Immunity. *Cell* **169**, 1130-1141.e1111, doi:https://doi.org/10.1016/j.cell.2017.05.005 (2017).

91 DuPage, M. *et al.* The Chromatin-Modifying Enzyme Ezh2 Is Critical for the Maintenance of Regulatory T Cell Identity after Activation. *Immunity* **42**, 227-238, doi:http://doi.org/10.1016/j.immuni.2015.01.007 (2015).

92 Muroyama, Y. *et al.* Stereotactic Radiotherapy Increases Functionally Suppressive Regulatory T Cells in the Tumor Microenvironment. *Cancer Immunology Research* **5**, 992-1004, doi:10.1158/2326-6066.cir-17-0040 (2017).

93 Vanpouille-Box, C. *et al.* DNA exonuclease Trex1 regulates radiotherapy-induced tumour immunogenicity. *Nature communications* **8**, 15618, doi:10.1038/ncomms15618 http://dharmasastra.live.cf.private.springer.com/articles/ncomms15618#supplementary-information (2017).

94 Chaudhary, B. & Elkord, E. Regulatory T Cells in the Tumor Microenvironment and Cancer Progression: Role and Therapeutic Targeting. *Vaccines* **4**, 28, doi:10.3390/vaccines4030028 (2016).

95 Sugiyama, D. *et al.* Anti-CCR4 mAb selectively depletes effector-type FoxP3+CD4+ regulatory T cells, evoking antitumor immune responses in humans. *Proceedings of the National Academy of Sciences* **110**, 17945-17950, doi:10.1073/pnas.1316796110 (2013).

96 Arvey, A. *et al.* Genetic and epigenetic variation in the lineage specification of regulatory T cells. *eLife* **4**, doi:10.7554/eLife.07571 (2015).

97 Plitas, G. *et al.* Regulatory T Cells Exhibit Distinct Features in Human Breast Cancer. *Immunity* **45**, 1122-1134, doi:http://dx.doi.org/10.1016/j.immuni.2016.10.032 (2016).

98 De Simone, M. *et al.* Transcriptional Landscape of Human Tissue Lymphocytes Unveils Uniqueness of Tumor-Infiltrating T Regulatory Cells. *Immunity* **45**, 1135-1147, doi:http://doi.org/10.1016/j.immuni.2016.10.021 (2016).

99 Rao, Rajesh R. *et al.* Meteorin-like Is a Hormone that Regulates Immune-Adipose

Interactions to Increase Beige Fat Thermogenesis. *Cell* **157**, 1279-1291, doi:http://dx.doi.org/10.1016/j.cell.2014.03.065 (2014).

100 Ushach, I. *et al.* METEORIN-LIKE is a cytokine associated with barrier tissues and alternatively activated macrophages. *Clin Immunol* **156**, 119-127, doi:10.1016/j.clim.2014.11.006 (2015).

101 Jorgensen, J. R. *et al.* Cometin is a novel neurotrophic factor that promotes neurite outgrowth and neuroblast migration in vitro and supports survival of spiral ganglion neurons in vivo. *Exp Neurol* **233**, 172-181, doi:10.1016/j.expneurol.2011.09.027 (2012).

102 Li, Z. Y. *et al.* Subfatin is a novel adipokine and unlike Meteorin in adipose and brain expression. *CNS Neurosci Ther* **20**, 344-354, doi:10.1111/cns.12219 (2014).

103 Miyara, M. *et al.* Sialyl Lewis x (CD15s) identifies highly differentiated and most suppressive FOXP3high regulatory T cells in humans. *Proceedings of the National Academy of Sciences* **112**, 7225-7230, doi:10.1073/pnas.1508224112 (2015).

104 Kochl, R. *et al.* WNK1 kinase balances T cell adhesion versus migration in vivo. *Nature immunology* **advance online publication**, doi:10.1038/ni.3495 http://www.nature.com/ni/journal/vaop/ncurrent/abs/ni.3495.html#supplementary-information (2016).

105 Chan, C. W. Y. *et al.* Soluble Fibrinogen-Like Protein 2/Fibroleukin Exhibits Immunosuppressive Properties: Suppressing T Cell Proliferation and Inhibiting Maturation of Bone Marrow-Derived Dendritic Cells. *The Journal of Immunology* **170**, 4036-4044, doi:10.4049/jimmunol.170.8.4036 (2003).

106 Joller, N. *et al.* Treg Cells Expressing the Coinhibitory Molecule TIGIT Selectively Inhibit Proinflammatory Th1 and Th17 Cell Responses. *Immunity* **40**, 569-581, doi:http://dx.doi.org/10.1016/j.immuni.2014.02.012 (2014).

107 Hollinger, S. & Hepler, J. R. Cellular Regulation of RGS Proteins: Modulators and Integrators of G Protein Signaling. *Pharmacological Reviews* **54**, 527-559 (2002).

108 Gibbons, D. L. *et al.* Cutting Edge: Regulator of G Protein Signaling-1 Selectively Regulates Gut T Cell Trafficking and Colitic Potential. *The Journal of Immunology* **187**, 2067-2071, doi:10.4049/jimmunol.1100833 (2011).

109 Huang, C.-Y. & Tan, T.-H. DUSPs, to MAP kinases and beyond. *Cell & Bioscience* **2**, 24-24, doi:10.1186/2045-3701-2-24 (2012).

110 Lang, R., Hammer, M. & Mages, J. DUSP Meet Immunology: Dual Specificity MAPK Phosphatases in Control of the Inflammatory Response. *The Journal of Immunology* **177**, 7497-7504, doi:10.4049/jimmunol.177.11.7497 (2006).

111 Wancket, L. M., Frazier, W. J. & Liu, Y. Mitogen-activated protein kinase phosphatase (MKP)-1 in immunology, physiology, and disease. *Life Sciences* **90**, 237-248,

doi:http://dx.doi.org/10.1016/j.lfs.2011.11.017 (2012).

112 Zhao, Q. *et al.* MAP kinase phosphatase 1 controls innate immune responses and suppresses endotoxic shock. *The Journal of experimental medicine* **203**, 131-140, doi:10.1084/jem.20051794 (2006).

113 Chi, H. *et al.* Dynamic regulation of pro- and anti-inflammatory cytokines by MAPK phosphatase 1 (MKP-1) in innate immune responses. *Proceedings of the National Academy of Sciences of the United States of America* **103**, 2274-2279, doi:10.1073/pnas.0510965103 (2006).

114 Salojin, K. & Oravecz, T. Regulation of innate immunity by MAPK dual-specificity phosphatases: knockout models reveal new tricks of old genes. *Journal of leukocyte biology* **81**, 860-869, doi:10.1189/jlb.1006639 (2007).

115 Huang, G., Wang, Y., Shi, L. Z., Kanneganti, T.-D. & Chi, H. Signaling by the Phosphatase MKP-1 in Dendritic Cells Imprints Distinct Effector and Regulatory T Cell Fates. *Immunity* **35**, 45-58, doi:10.1016/j.immuni.2011.05.014 (2011).

116 Lazo, J. S. *et al.* Novel benzofuran inhibitors of human mitogen-activated protein kinase phosphatase-1. *Bioorganic & Medicinal Chemistry* **14**, 5643-5650, doi:http://dx.doi.org/10.1016/j.bmc.2006.04.036 (2006).

117 Lazo, J. S. *et al.* Structurally Unique Inhibitors of Human Mitogen-Activated Protein Kinase Phosphatase-1 Identified in a Pyrrole Carboxamide Library. *Journal of Pharmacology and Experimental Therapeutics* **322**, 940-947, doi:10.1124/jpet.107.122242 (2007).

118 Vogt, A. *et al.* The Benzo[c]phenanthridine Alkaloid, Sanguinarine, Is a Selective, Cell-active Inhibitor of Mitogen-activated Protein Kinase Phosphatase-1. *Journal of Biological Chemistry* **280**, 19078-19086, doi:10.1074/jbc.M501467200 (2005).

119 Ephrem, A. *et al.* Modulation of Treg cells/T effector function by GITR signaling is context–dependent. *European journal of immunology* **43**, 2421-2429, doi:10.1002/eji.201343451 (2013).

120 Yan, D., Farache, J., Mathis, D. & Benoist, C. Imbalanced signal transduction in regulatory T cells expressing the transcription factor FoxP3. *Proceedings of the National Academy of Sciences*, doi:10.1073/pnas.1520393112 (2015).

121 Arthur, J. S. C. & Ley, S. C. Mitogen-activated protein kinases in innate immunity. *Nature reviews. Immunology* **13**, 679-692, doi:10.1038/nri3495 (2013).

122 Cornell, T. T., Rodenhouse, P., Cai, Q., Sun, L. & Shanley, T. P. Mitogen-Activated Protein Kinase Phosphatase 2 Regulates the Inflammatory Response in Sepsis. *Infection and Immunity* **78**, 2868-2876, doi:10.1128/iai.00018-10 (2010).

123 Sethakorn, N. & Dulin, N. O. RGS expression in cancer: oncomining the cancer

microarray data. *Journal of Receptors and Signal Transduction* **33**, 166-171, doi:doi:10.3109/10799893.2013.773450 (2013).

124 Moratz, C., Hayman, J. R., Gu, H. & Kehrl, J. H. Abnormal B-Cell Responses to Chemokines, Disturbed Plasma Cell Localization, and Distorted Immune Tissue Architecture in Rgs1−/− Mice. *Molecular and Cellular Biology* **24**, 5767-5775, doi:10.1128/mcb.24.13.5767-5775.2004 (2004).

# FIGURES

## FIGURE LEGENDS FOR CHAPTER I

**Figure I-1: Balance between anti-tumor immunity and immuno-suppression in the tumor microenvironment (TME)**

**Figure I-2: Timeline for basic and clinical development of PD-1/PD-L1 targeted cancer immunotherapy**

Upper timeline: Pre-clinical studies, Lower / magnified timeline: FDA approvals

# FIGURES FOR CHAPTER I

# Figure I-1: Balance between anti-tumor immunity and immuno-suppression in the tumor microenvironment (TME)

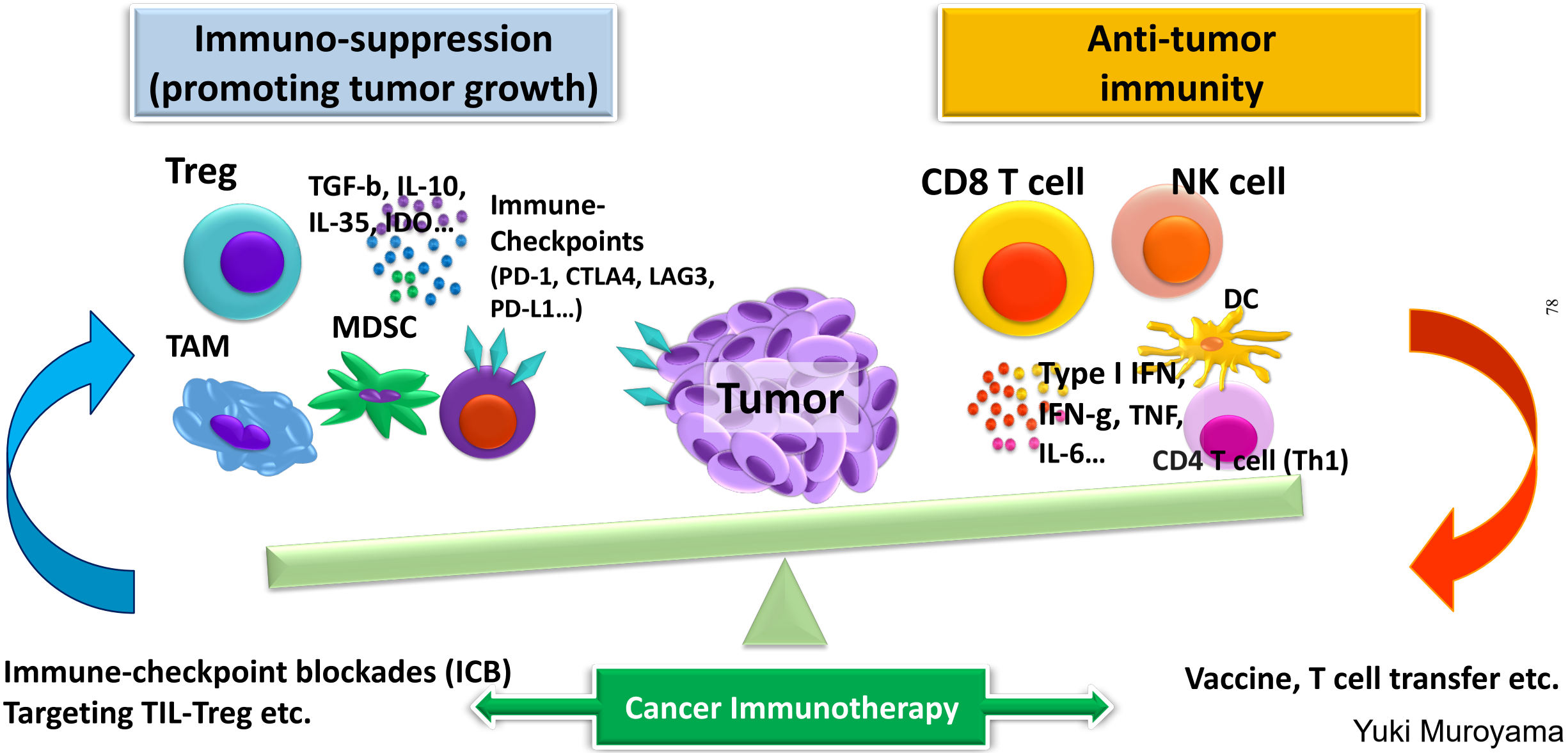


Yuki Muroyama

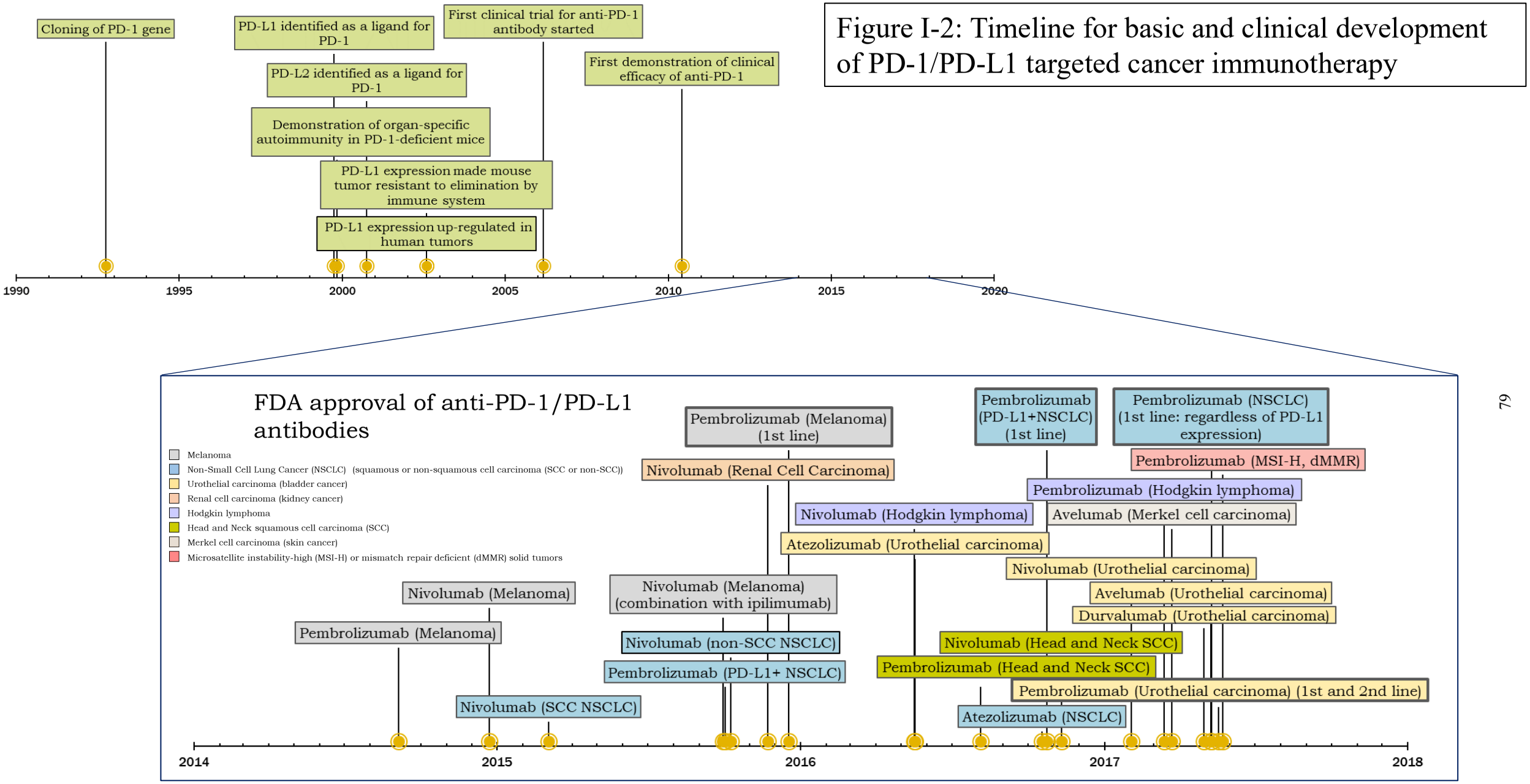


Figure I-2: Timeline for basic and clinical development of PD-1/PD-L1 targeted cancer immunotherapy



Yuki Muroyama

## FIGURE LEGENDS FOR CHAPTER III

**Figure III-1: Stereotactic radiotherapy increases Treg in tumors.**

(A) Experimental design. $5x10^5$ B16/F10, $1.5x10^6$ MC38 or $3x10^5$ RENCA cells were implanted subcutaneously (s.c.) to the flank of wild-type C57BL/6J mice (in B16/F10 or MC38 experiments) or Balb/c mice (in RENCA experiment), respectively on day 0. Mice received 10 Gy of stereotactic radiotherapy (RT) via SARRP on day 7 (B16/F10), day 16 (RENCA), day 10 (MC38), respectively. Tumors, draining lymph nodes (DLN), and spleens were harvested 7 days after the radiation. (B) Tumor growth curves of B16/F10-bearing mice as in (A). Non-irradiated tumors (control) in black line and irradiated tumors (RT) in red line, respectively. (C) The absolute number of TIL-Treg per gram tumor weight in B16/F10 model. (D-F) Representative flow plots (D) and quantitative bar graph of % $Foxp3^+$ cells (E) and MFI of Foxp3 (F) in $CD4^+$ cells from TILs. N = 7-15 per group, repeated at least 4x. (G) Immunohistochemistry of Foxp3 in tumors (B16/F10, RENCA, MC38), 20X and 40X magnification as indicated. $Foxp3^+$ cells are stained red in B16/F10 (due to the brown pigment in melanoma), and brown in RENCA and MC38 tumors. Error bars represent SEM, ***: $p < 0.001$, **: $p < 0.01$, *: $p < 0.05$, determined by two-way ANOVA (B) or unpaired Student's t-test (C, E and F).

**Figure III-2: Stereotactic radiotherapy increases the activation/suppression markers of tumor-infiltrating Treg (TIL-Treg).**

(A, B) Representative flow plots (A) and quantitative scatterplot (B) depicting of the percentages of $CCR4^+$, $CTLA4^+$, $4\text{-}1BB^+$ or $Helios^+$ TIL-Treg, from day 14 B16/F10 tumor-bearing mice. N= 8 per group, repeated 3x. Error bars represent SEM, ***: p <

0.001, **: $p < 0.01$, *: $p < 0.05$, determined by unpaired Student's t-test (B).

**Figure III-3**: **Radiated tumor-infiltrating Treg (TIL-Treg) are functionally suppressive.**

(A) Representative figure of the *in vitro* suppression assay. Tresponder cells were gated based on the CD45.1 congenically marked and their proliferation was analyzed based on the dilution of CTV dye. Solid lines show the conditions with Spleen Treg (black line), non-irradiated Control TIL-Treg (blue line), and RT TIL-Treg (red line); filled green histograms shows the Tresponder only condition. (B) Quantitative plots represent percent suppression at the indicated Treg:T responder ratio. A representative experiment of a total of three independent replicates is shown. (N = 2-3 per group, repeated 3x.)

**Figure III-4: The effect of TGF-β on post-RT increase of Treg in tumor.**

(A) Experimental design. C57BL/6 mice were injected subcutaneously with $5x10^5$ B16/F10 cells on day 0. Mice received 10 Gy of RT on day 7. Mice received a dose of 300 mg/kg/day Galunisertib (LY2157299) or vehicle via oral gavage every 12 hours, starting a day before RT. Tumors, DLNs and spleens were harvested on day 14. (B) Tumor growth curves of vehicle versus Galunisertib treated mice (dashed lines versus real line respectively), with or without radiation (black line or red line, respectively). (C) Representative flow plot of TIL-Treg. (D, E) Quantitative scatter plots of the % $Foxp3^+$ cells of tumor-infiltrating $CD4^+$ cells (D) and the absolute number of TIL-Treg per gram tumor weight (E) in Galunisertib treated versus vehicle treated group. (B) N = 5-6 per group, repeated x2. (D, E) show pooled data from two experiments. Error bars represent SEM, ***: $p < 0.001$, **: $p < 0.01$, *: $p < 0.05$, determined by two-way ANOVA (B), and

unpaired Student's t-test (D, E).

**Figure III- 5: The effect of IL-33 on post-RT increase of Treg in tumor.**

(A) The time course of IL-33 level in tumor lysates from different time points (1, 6, 24, 48, 72 hours and 7 days post RT) measured by ELISA. N = 5 per group. (B) Experimental design. C57BL/6 mice were injected subcutaneously with $5x10^5$ B16/F10 cells on day 0. Mice received 10 Gy of RT on day 7. Mice received a dose of 200 μg/mouse anti-ST2 antibody (Anti-ST2 Ab) or vehicle intraperitoneally (i.p.) every 3 days, starting one day before RT. Tumors, DLNs and spleens were harvested on day 14. (C) Tumor growth curves of vehicle control (dashed-line) versus anti-ST2 Ab-treated mice (solid line), with or without radiation (black or red, respectively). (D) Representative flow plot of TIL-Treg. (E, F) Quantitative scatter plots of % $Foxp3^+$ cells of tumor-infiltrating $CD4^+$ cells (E), and the absolute number of TIL-Treg per gram tumor weight (F) in anti-ST2 Ab-treated versus vehicle-treated group. N = 5 per group, repeated x2. Error bars represent SEM, ***: $p < 0.001$, **: $p < 0.01$, *: $p < 0.05$, determined by two-way ANOVA (A, C), and unpaired Student's t-test (E, F).

**Figure III- 6: Stereotactic radiation enhances preferential Treg proliferation in the tumor microenvironment (TME).**

(A) Experimental design. C57BL/6 mice were injected subcutaneously with $5x10^5$ B16/F10 cells on day 0. Mice received 10 Gy of RT on day 7. Mice received a dose of 25 μg Fingolimod (FTY720) or PBS containing DMSO as control via oral gavage on day 6, 9, 12. Peripheral blood was collected for monitoring lymphocyte counts. Tumors, DLNs

and spleens were harvested on day 14. (B) Tumor growth curves of vehicle versus FTY720-treated mice (dashed line versus solid line respectively), with or without radiation (black or red line respectively). (C) Representative flow plot of TIL-Treg ($CD4^+$ $Foxp3^+$). (D) Absolute number Treg per gram tumor weight in FTY720-treated versus vehicle treated group. (E, F) Representative flow plot (E) and quantitative scatter plot (F) of tumor-infiltrating Ki-$67^+$ Treg ($CD4^+$ $Foxp3^+$ cells). (G) Quantitative scatter plot of Ki-67 expression in tumor-infiltrating $CD3^+$, $CD4^+$, $CD8^+$ T cells and Treg. (H) Fold change of Ki-67 expression of irradiated TIL to compared with that of non-irradiated TIL. (I) Quantitative scatter plot of Ki-67 expression in tumor-infiltrating CD3+, CD4+, CD8+ T cells and Treg from non-irradiated tumors. N = 9-10 per group, repeated x2. (D) shows pooled data from two experiments. Error bars represent SEM, ***: $p < 0.001$, **: $p < 0.01$, *: $p < 0.05$, determined by Two-way ANOVA (B), unpaired Student's t-test (D, F-I).

**Supplementary Figure Legends:**

**Supplementary Figure III- 1: Radiotherapy suppresses tumor growth.**

(A, B) Tumor volume curves of RENCA (A) and MC38 (B) bearing mice. Non-irradiated tumors in black line and irradiated tumors in red line, respectively. N = 5-15 per group,

repeated at least 4x. Error bars represent SEM, ***: $p < 0.001$, **: $p < 0.01$, *: $p < 0.05$, determined by unpaired t-test at the day of harvest (A, B).

**Supplementary Figure III- 2**: **Characterization of the TME of B16/F10 tumors post-RT.**

Heatmaps of RNA expression of genes associated with immune cell subsets by NanoString assay. RNAs were extracted from the tumors on day 14 B16/F10 tumor-bearing mice (7 days post RT). N= 4-5 per group.

**Supplementary Figure III- 3: Stereotactic radiation does not change Treg in draining lymph nodes nor in spleens of treated mice.**

(A, C) Representative flow plots of Treg from DLN (A) and spleen (C) from B16/F10, RENCA, or MC38 bearing mice. (B, D) Bar graph of % $Foxp3^+$ cells in $CD4^+$ cells from DLN (B) and spleen (D). N = 7 - 14 per group, repeated at least 4x. Error bars represent SEM, ***: $p < 0.001$, **: $p < 0.01$, *: $p < 0.05$.

**Supplementary Figure III- 4: Persistently Increased Treg Post-RT.**

Representative flow plots (A) and quantitative scatterplot (B) depicting of the percentages of $Foxp3^+$ cells in $CD4^+$ cells from TILs, from day 21 (14 days post-RT) B16/F10 tumor-bearing mice. N= 7-9 per group, repeated 2x. Error bars represent SEM, *: $p < 0.05$, determined by unpaired Student's t-test (B).

**Supplementary Figure III- 5: Stereotactic radiation increases the suppressive markers of Treg in the RENCA tumor model.**

(A, B) Representative flow plots (A) and quantitative scatterplot (B) depicting the percentages of $CCR4^+$, $CTLA\text{-}4^+$, $4\text{-}1BB^+$ or $Helios^+$ TIL-Treg, from day 23 RENCA-bearing mice. N = 7 per group, repeated 3x. Error bars represent SEM, ***: $p < 0.001$, **: $p < 0.01$, *: $p < 0.05$, determined by unpaired Student's t-test (B).

**Supplementary Figure III- 6: Stereotactic radiation increases the suppressive markers of Treg in the MC38 tumor model.**

(A, B) Representative flow plots (A) and quantitative scatterplot (B) depicting the percentages of $CCR4^+$, $CTLA4^+$, $4\text{-}1BB^+$ or $Helios^+$ TIL-Treg, from day 17 MC38-bearing mice. N = 14 per group, repeated x2. Error bars represent SEM, ***: $p < 0.001$, **: $p < 0.01$, *: $p < 0.05$, determined by unpaired Student's t-test (B).

**Supplementary Figure III- 7: Stereotactic radiation does not change the expression of the suppressive markers of Treg in DLNs.**

(A, B) Representative flow plots (A) and quantitative scatterplot (B) depicting the percentages of $CCR4^+$, $CTLA4^+$, $4\text{-}1BB^+$ or $Helios^+$ Treg, from DLNs of day 14 B16/F10-bearing mice. N = 8 per group, repeated 3x. Error bars represent SEM, ***: $p < 0.001$, **: $p < 0.01$, *: $p < 0.05$, determined by unpaired Student's t-test (B).

**Supplementary Figure III- 8: Stereotactic radiation does not change the expression of the suppressive markers of Treg in spleens.**

(A, B) Representative flow plots (A) and quantitative scatterplot (B) depicting of the percentages of $CCR4^+$, $CTLA4^+$, $4\text{-}1BB^+$ or $Helios^+$ Treg, from spleens of day 14

B16/F10-bearing mice. N = 8 per group, repeated 3x. Error bars represent SEM, ***: $p < 0.001$, **: $p < 0.01$, *: $p < 0.05$, determined by unpaired Student's t-test (B).

**Supplementary Figure III- 9: Expression of the selected markers of TIL-CD4$^+$Foxp3$^-$ cells (Tconv) in the B16/F10 model.**

(A, B) Representative flow plots (A) and quantitative scatterplot (B) depicting the percentages of CCR4$^+$, CTLA-4$^+$, 4-1BB$^+$ or Helios$^+$ TIL-CD4$^+$Foxp3$^-$ cells, from day 14 B16/F10-bearing mice. N = 8 per group, repeated 3x. Error bars represent SEM, ***: $p < 0.001$, **: $p < 0.01$, *: $p < 0.05$, determined by unpaired Student's t-test (B).

**Supplementary Figure III- 10: Expression of the selected markers of TIL-CD4$^+$Foxp3$^-$ cells (Tconv) in the RENCA model.**

(A, B) Representative flow plots (A) and quantitative scatterplot (B) depicting the percentages of CCR4$^+$, CTLA-4$^+$, 4-1BB$^+$ or Helios$^+$ TIL-CD4$^+$Foxp3$^-$ cells, from day 23 RENCA-bearing mice. N = 9 per group, repeated 3x. Error bars represent SEM, ***: $p < 0.001$, **: $p < 0.01$, *: $p < 0.05$, determined by unpaired Student's t-test (B).

**Supplementary Figure III- 11: Expression of the selected markers of TIL-CD4$^+$Foxp3$^-$ cells (Tconv) in the MC38 model.**

(A, B) Representative flow plots (A) and quantitative scatterplot (B) depicting the percentages of CCR4$^+$, CTLA-4$^+$, 4-1BB$^+$ or Helios$^+$ TIL-CD4$^+$Foxp3$^-$ cells, from day 17 MC38-bearing mice. N = 14 per group, repeated 2x. Error bars represent SEM, ***: $p < 0.001$, **: $p < 0.01$, *: $p < 0.05$, determined by unpaired Student's t-test (B).

**Supplementary Figure III- 12: Expression of 4-1BB on TIL-CD8$^+$ cells.**

(A, B) Representative flow plots (A) and quantitative scatterplot (B) depicting the percentages of 4-1BB$^+$TIL-CD8$^+$ cells, from day 14 B16/F10-bearing mice, day 23 RENCA-bearing mice and day 17 MC38-bearing mice. N = 8-14 per group, repeated 2-3x. Error bars represent SEM, ***: $p < 0.001$, **: $p < 0.01$, *: $p < 0.05$, determined by unpaired Student's t-test (B).

**Supplementary Figure III- 13: The effect of TGF-β blockade on different T cell subsets.**

(A-C) The absolute numbers of tumor-infiltrating CD3$^+$ (A), CD4$^+$ (B) and CD8$^+$ (C) cells per gram tumor weight from vehicle treated and Galunisertib treated groups, with or without radiation, from day 14 B16/F10-bearing mice are shown. N = 5 per group, repeated x2. Error bars represent SEM, ***: $p < 0.001$, **: $p < 0.01$, *: $p < 0.05$, determined by unpaired Student's t-test (A-C).

**Supplementary Figure III- 14: TGF-β expression in the tumor microenvironment.**

(A-C) Female Balb/c mice were subcutaneously implanted with $3x10^5$ RENCA cells and received 10 Gy RT as previously described. Tumor lysates were collected at different time points post RT and the intratumoral levels of TGF-β1 and TGF-β2 were analyzed by Luminex assay. N = 4 - 5 per group. (A) Heatmap of $\log_2$ (fold change of radiated tumor chemokine levels compared to those of non-radiated control tumors). (B, C) Time courses of TGF-β1 and TGF-β2. TGF-β levels were normalized to tumor protein concentration. N = 4 - 5 per group. Error bars represent SEM, ***: $p < 0.001$, **: $p < 0.01$, *: $p < 0.05$, determined two-way ANOVA (B, C).

**Supplementary Figure III- 15: ST2 expression on splenic and tumor infiltrating Treg.**

(A) Representative flow plots depicting the percentages of $ST2^+$ Treg from spleen and tumor of day 14 B16/F10-bearing mice, repeated x2.

**Supplementary Figure III- 16: The effect of Fingolimod (FTY720) on peripheral blood lymphocytes counts.**

Peripheral blood samples were collected from tail veins on day 5, 7, 11, and 13. Sequestration of peripheral lymphocytes was monitored using Hemavet whole blood cell counter. Time course of the concentration of lymphocytes (A) and ratio to the baseline lymphocyte counts (B), vehicle versus FTY720-treated mice (dashed line versus solid line respectively), with or without radiation (black or red line respectively).

**Supplementary Figure III- 17**: **Chemokine/cytokine expression of a selected panel in the tumor microenvironment post-radiation.**

(A, B) Female Balb/c mice were subcutaneously implanted with $3x10^5$ RENCA cells and received 10 Gy RT as previously described. Tumor lysates were collected at different time points post RT and chemokine/cytokine (IL-2) levels were analyzed by Luminex assay. (A) Heatmap of $\log_2$ (fold change of radiated tumor chemokine levels compared to those of non-radiated control tumors). (B) Time courses of selected chemokines/cytokines. Chemokine/cytokine level were normalized to tumor protein concentration. Non-irradiated tumors are represented by a black line, and irradiated tumors are represented by a red line, respectively. N = 4 - 5 per group. Error bars represent SEM, ***: $p < 0.001$, **: $p < 0.01$, *: $p < 0.05$, determined two-way ANOVA (B).

**Supplementary Figure III- 18: RT does not increase the cell death of TIL-Treg.**

Quantitative scatterplot depicting the percentages of Live/Dead negative ("alive") TIL-Treg (A), as well as other T cell subsets (B) from day 14 B16/F10-bearing mice. N = 7 per group, repeated 3x. Error bars represent SEM, p-value determined by unpaired Student's t-test (A, B).

**Supplementary Figure III- 19**: **Differentially expressed molecules post-RT TME of B16/F10 tumors.**

(A) PCA analysis and (B) Volcano plot of RNA expression of genes associated with RT by NanoString assay. RNAs were extracted from the tumors on day 14 B16/F10 tumor-bearing mice (7 days post RT). N= 4-5 per group.

**Supplementary Figure III- 20: RT decreased G-MDSC (PMN-MDSC) population in B16/F10 tumor.**

(A, B) Representative flow plots (gated on $LD^{-}CD45^{+}$ cells) (A) and quantitative scatterplot (B) depicting of the percentages of $Ly6C^{+}Ly6G^{+}$ ("G-MDSC") cells, $Ly6C^{+}Ly6G^{+}$ ("M-MDSC") cells, and ratio of M/G-MDSC cells, from day 14 B16/F10 tumor-bearing mice. N= 7-8 per group. Error bars represent SEM, ***: $p < 0.001$, **: $p < 0.01$, *: $p < 0.05$, determined by unpaired Student's t-test

# FIGURES FOR CHAPTER III

# Figures

Yuki Muroyama
Thesis
RT-Treg part

**Figure III- 1**

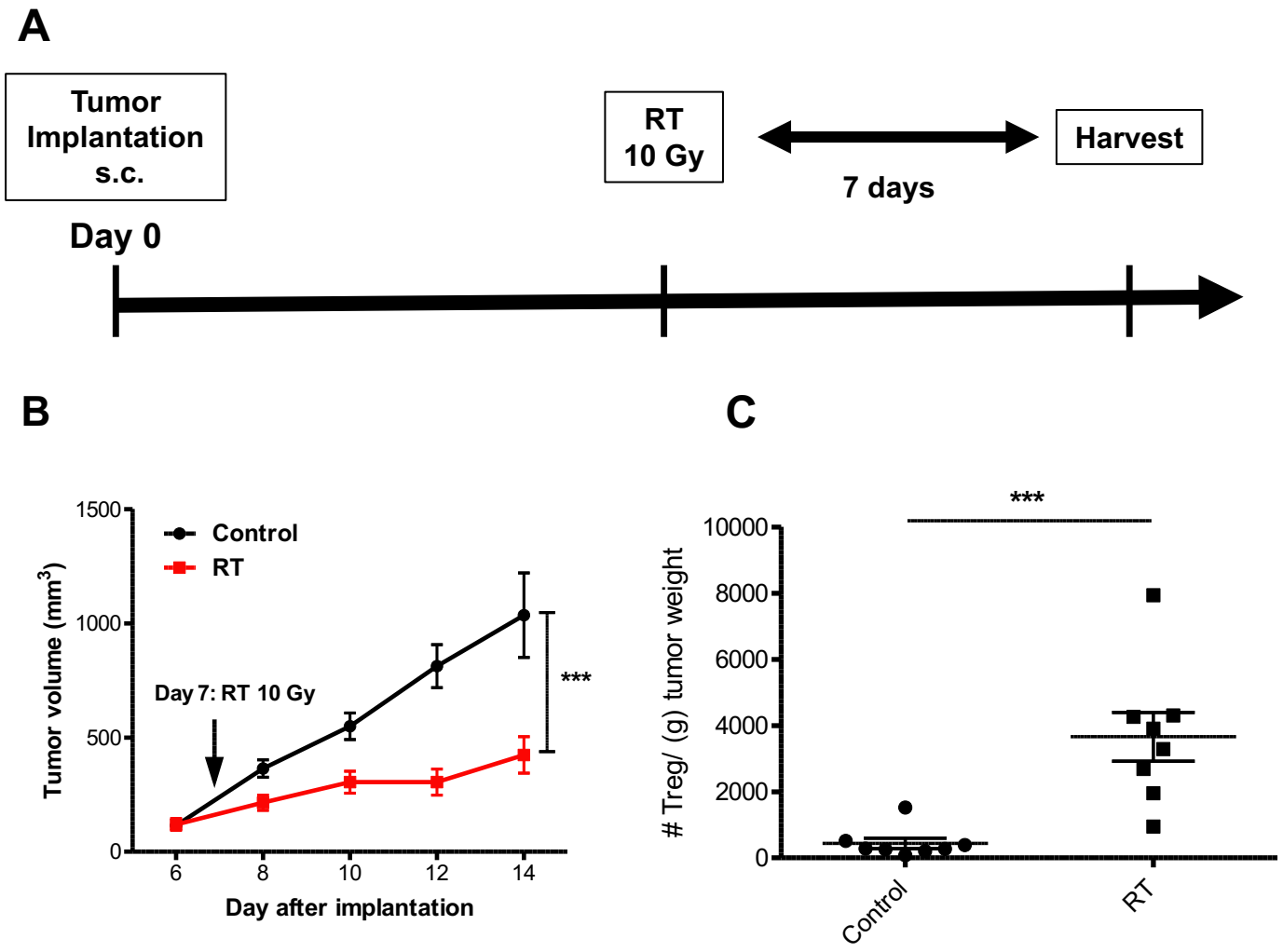
A
Tumor Implantation s.c.
Day 0
RT 10 Gy
7 days
Harvest
B
Control
RT
Tumor volume (mm3)
Day 7: RT 10 Gy
***
Day after implantation
C
***
# Treg/ (g) tumor weight
Control
RT

**Figure III- 1 Continued**

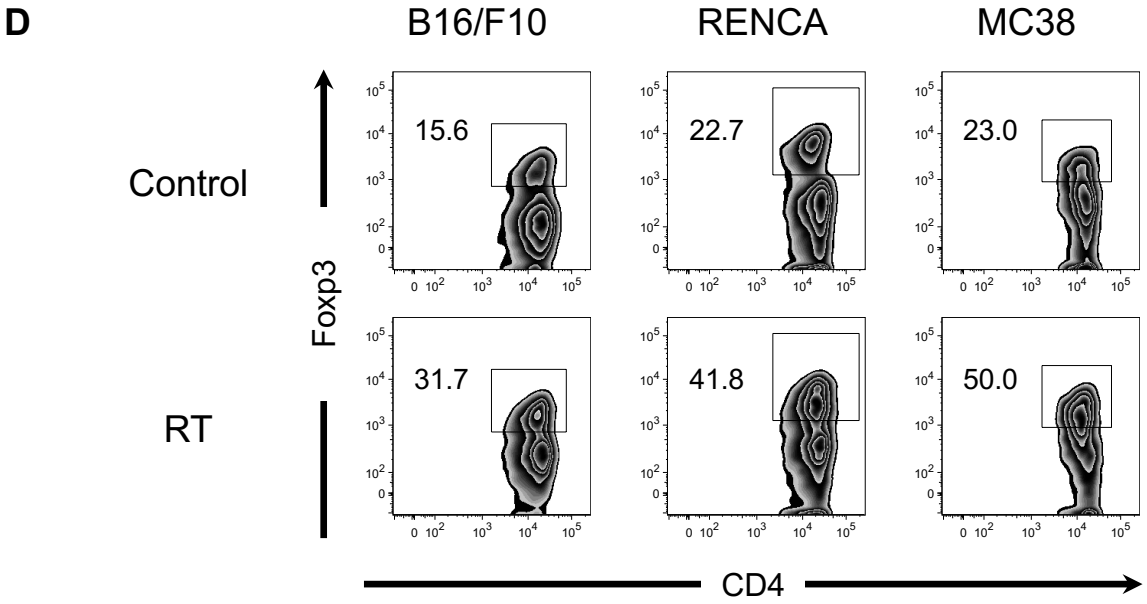


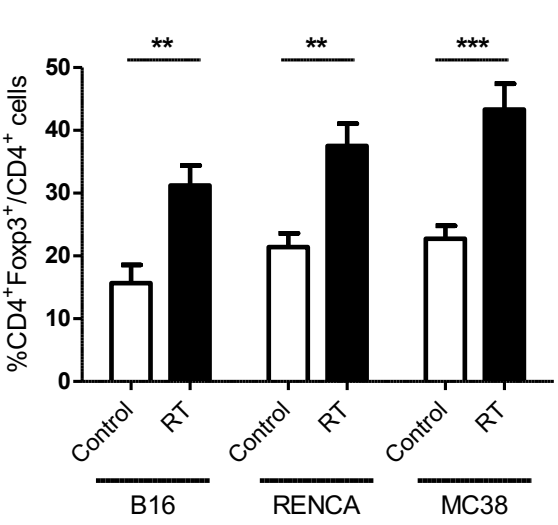


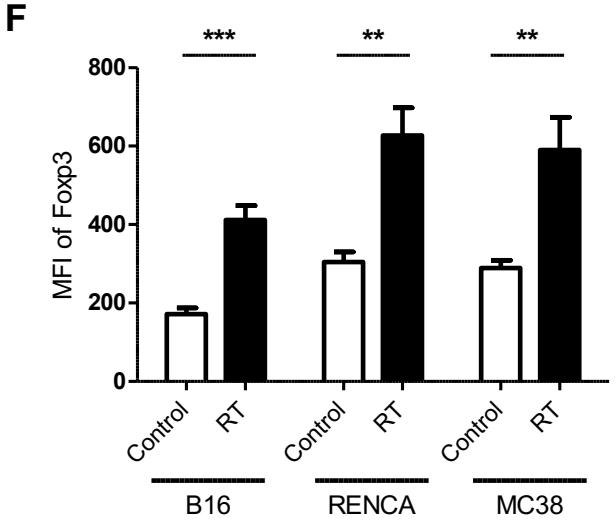


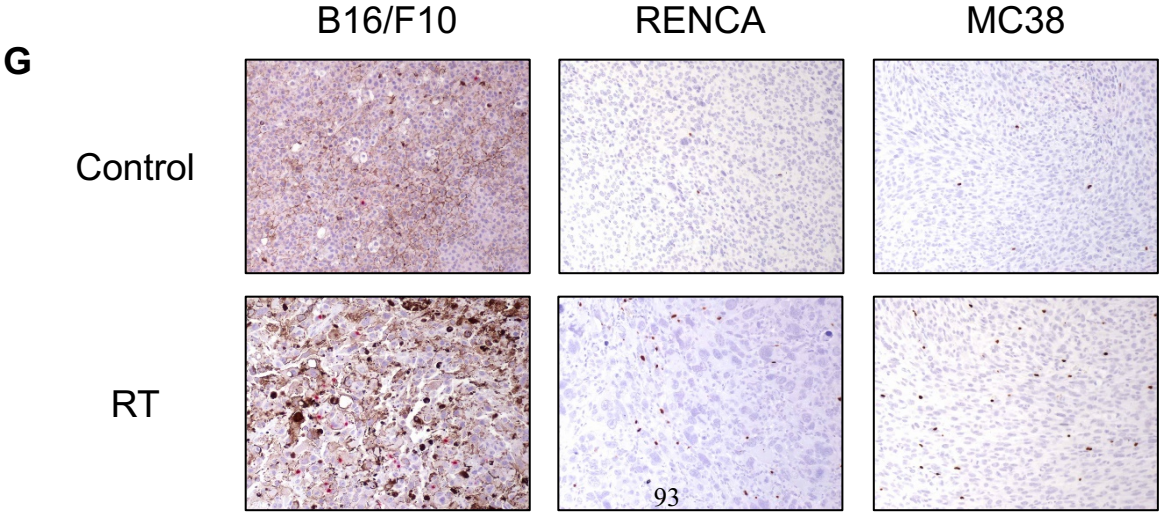

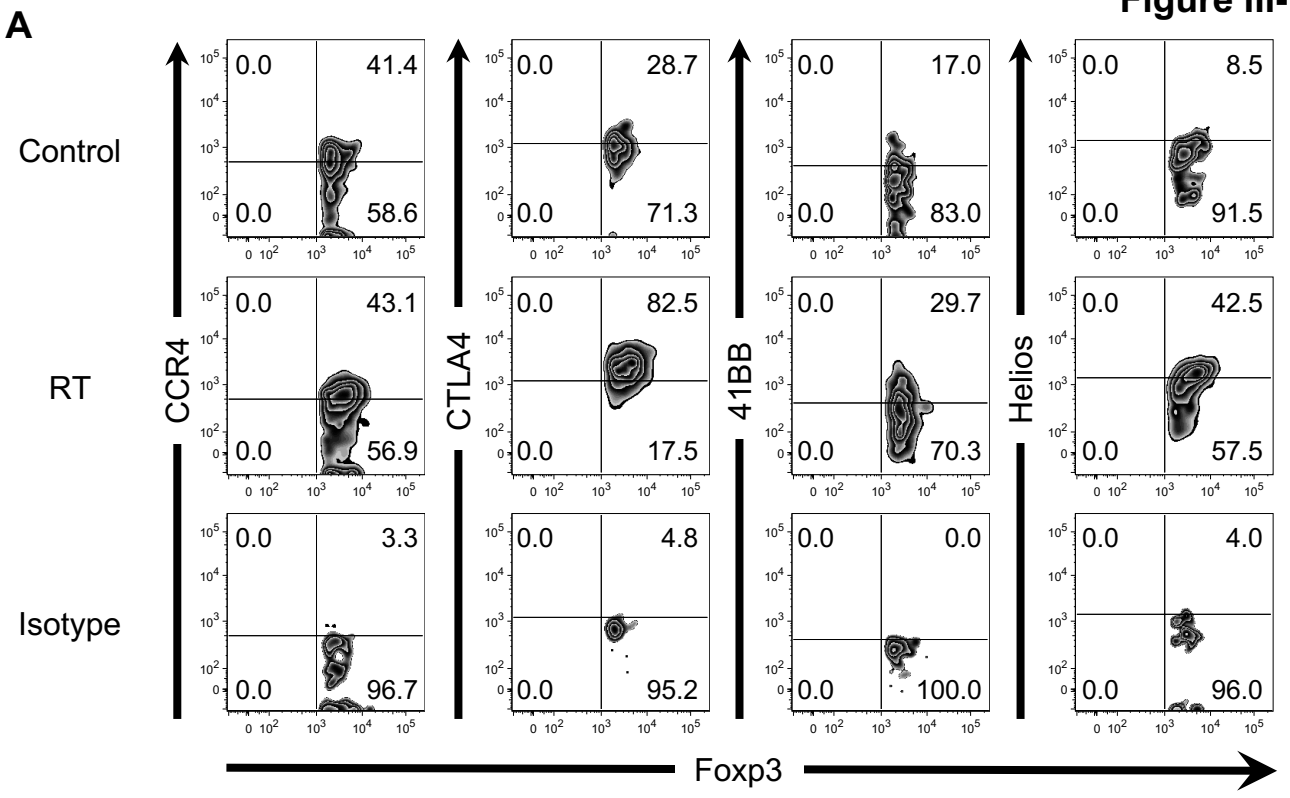
A
Control
RT
Isotype
CCR4
CTLA4
41BB
Helios
Foxp3
0.0
41.4
58.6
28.7
71.3
17.0
83.0
8.5
91.5
43.1
56.9
82.5
17.5
29.7
70.3
42.5
57.5
3.3
96.7
4.8
95.2
0.0
100.0
4.0
96.0

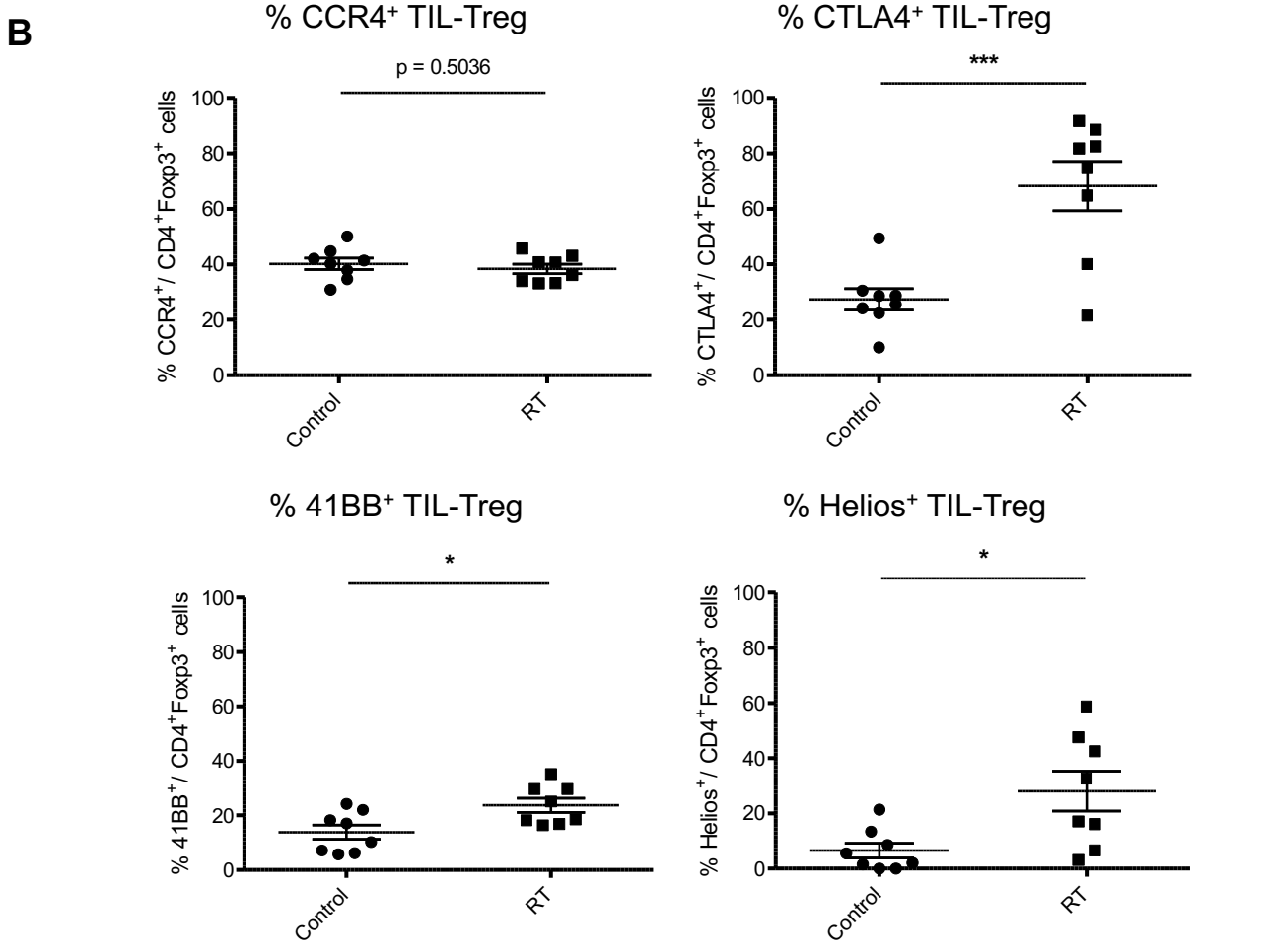
B
% CCR4⁺ TIL-Treg
p = 0.5036
% CCR4⁺ / CD4⁺Foxp3⁺ cells
% CTLA4⁺ TIL-Treg
***
% CTLA4⁺ / CD4⁺Foxp3⁺ cells
% 41BB⁺ TIL-Treg
*
% 41BB⁺ / CD4⁺Foxp3⁺ cells
% Helios⁺ TIL-Treg
*
% Helios⁺ / CD4⁺Foxp3⁺ cells
Control
RT

A

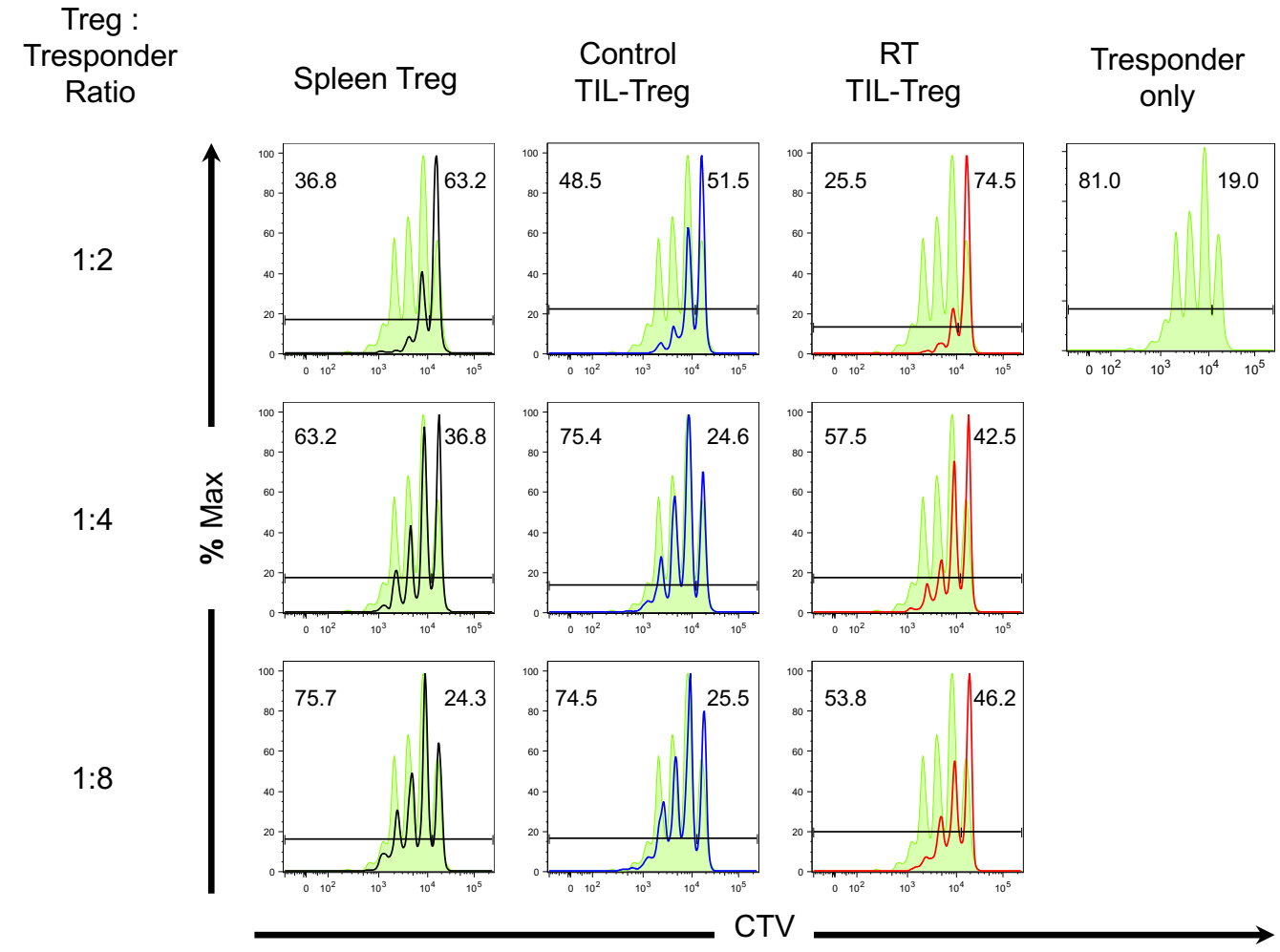


B

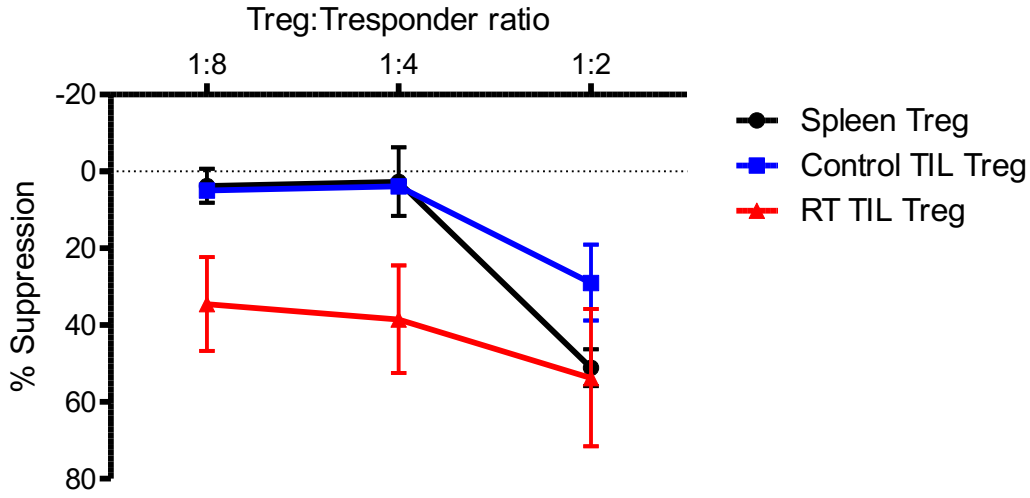


**Figure 3: Radiated tumor-infiltrating Tregs (TIL-Treg) are functionally suppressive.**

Figure III- 4

A

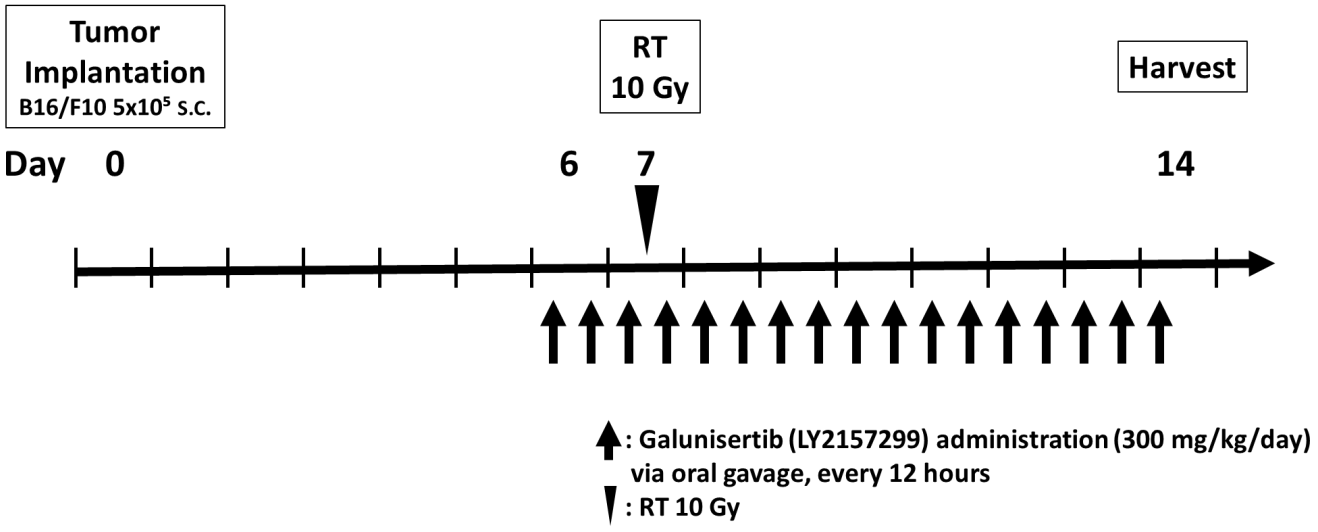


B

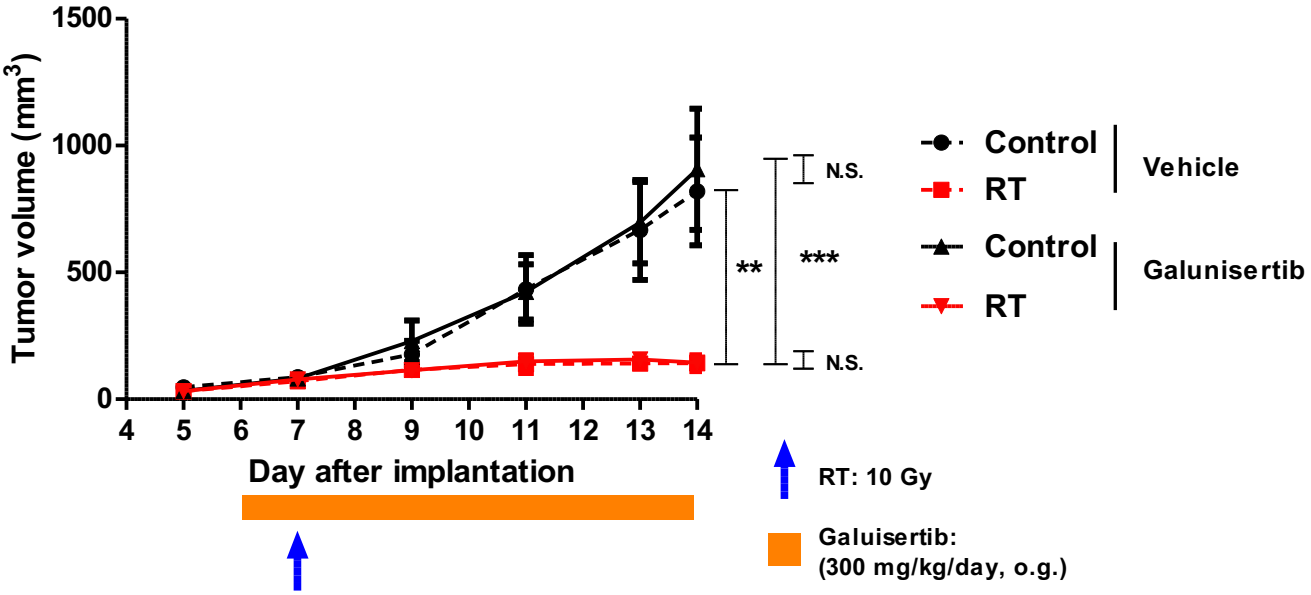

## Figure III- 4 Continued

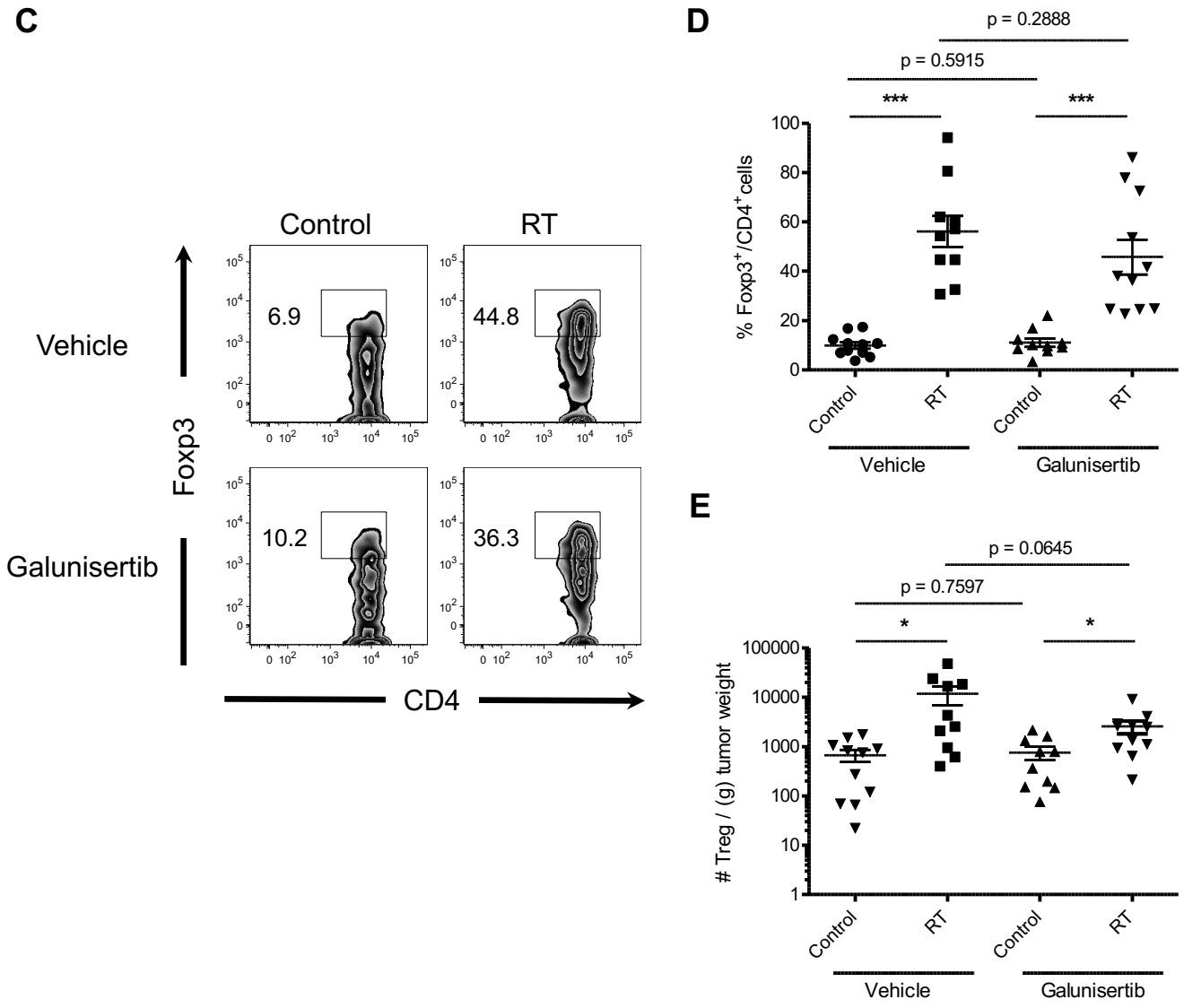

# Figure III- 5

A

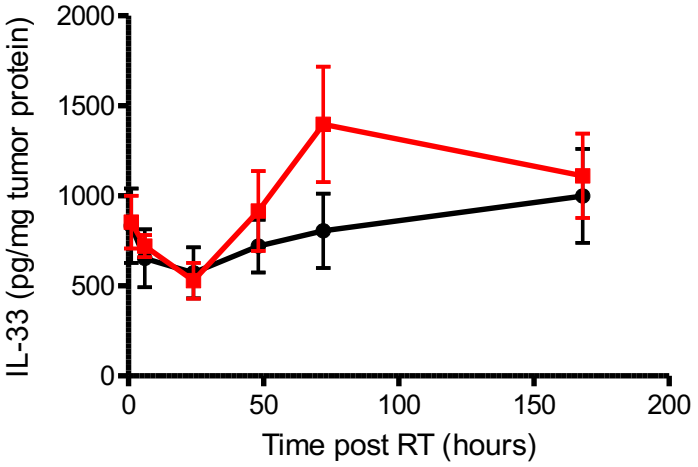


B

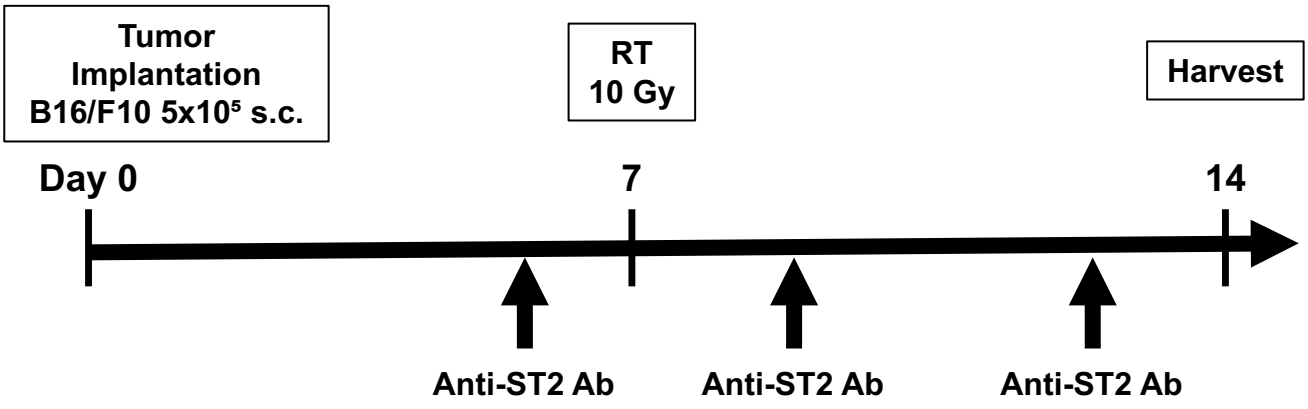


**Anti-ST2-Ab: Administration of anti-ST2/IL-33R monoclonal antibody (200 ug) intraperitoneally (i.p.) every 3 days (Day 6, 9, 12)**

C

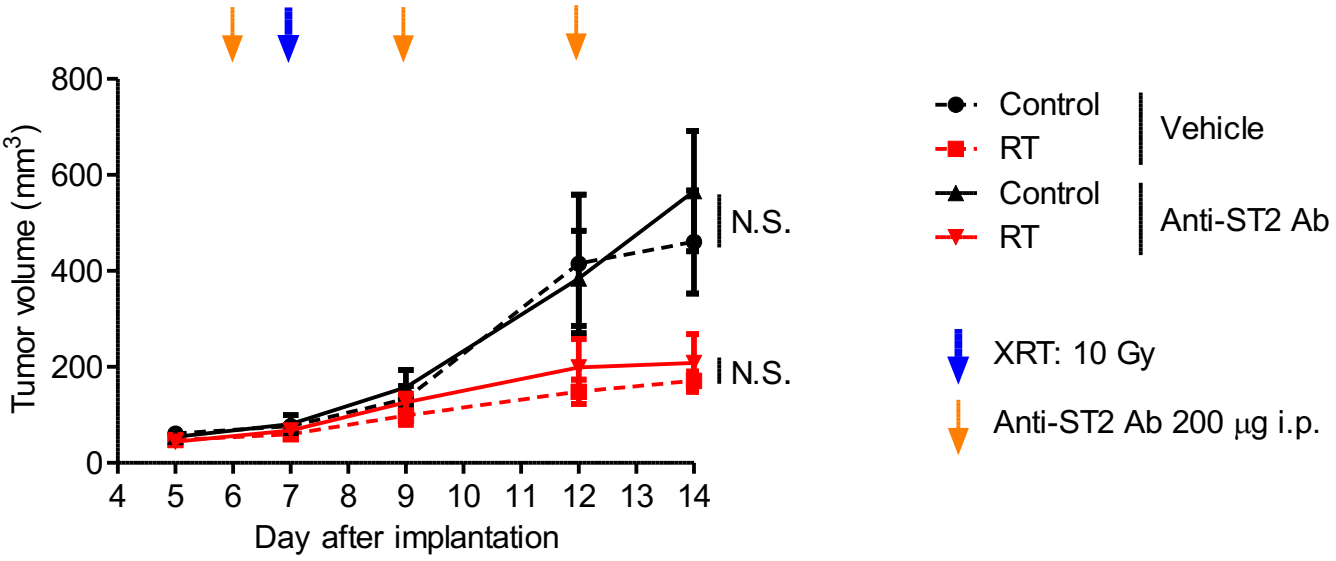

# Figure III- 5 continued

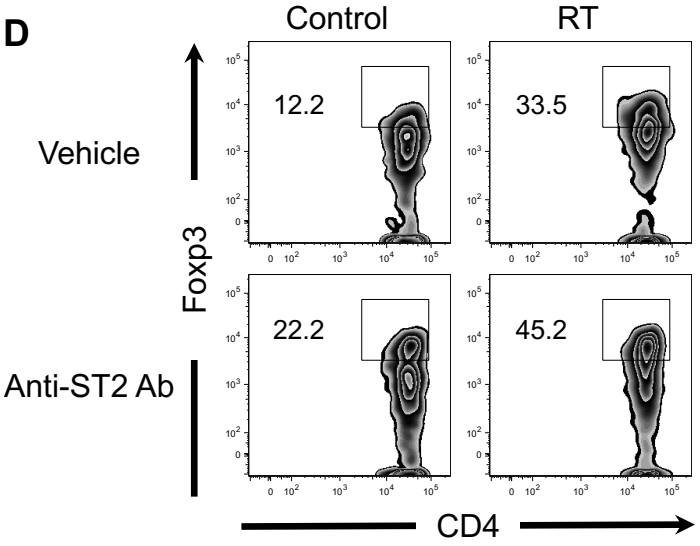


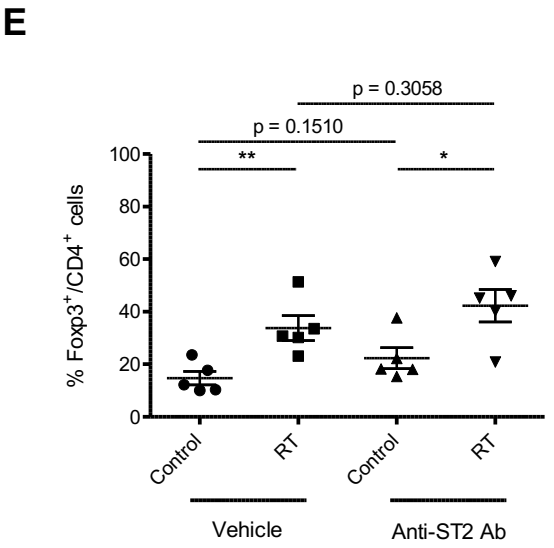


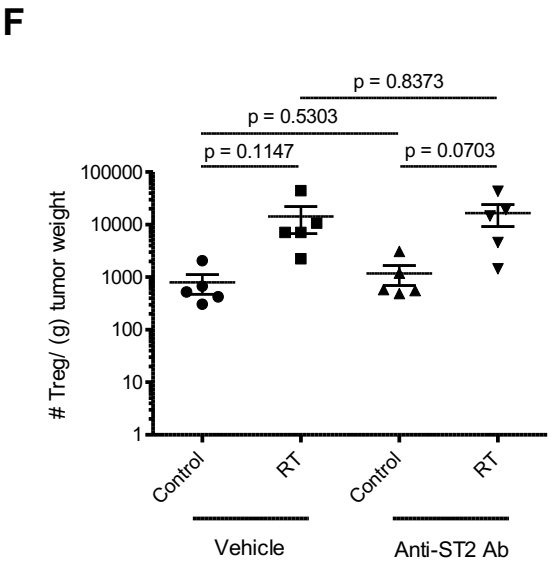

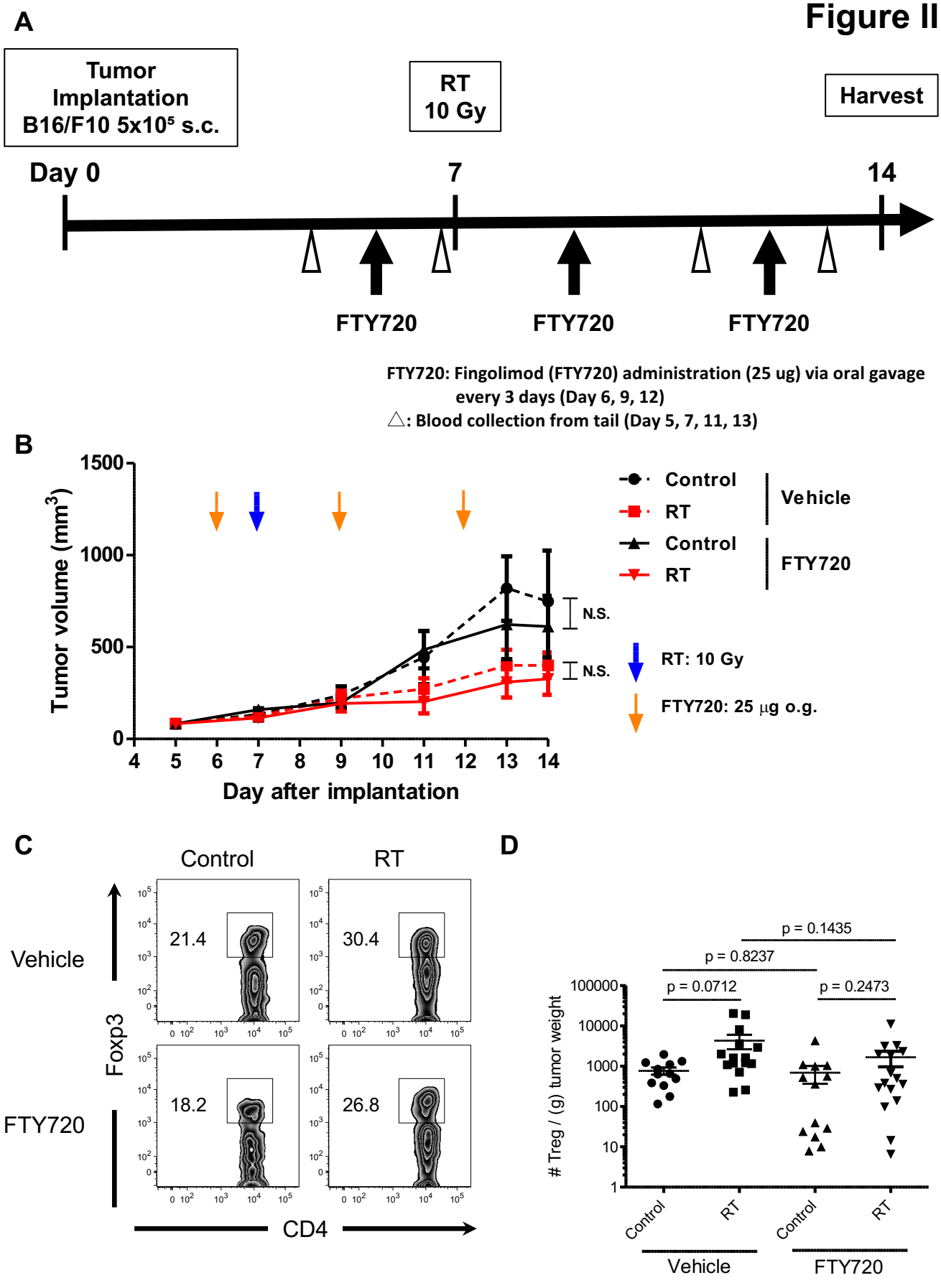
A
Tumor Implantation B16/F10 5x10⁵ s.c.
RT 10 Gy
Harvest
Day 0
7
14
FTY720
FTY720
FTY720
FTY720: Fingolimod (FTY720) administration (25 ug) via oral gavage every 3 days (Day 6, 9, 12)
△: Blood collection from tail (Day 5, 7, 11, 13)
B
Tumor volume (mm³)
Day after implantation
Control
RT
Control
RT
Vehicle
FTY720
N.S.
N.S.
RT: 10 Gy
FTY720: 25 μg o.g.
C
Control
RT
Vehicle
FTY720
Foxp3
CD4
21.4
30.4
18.2
26.8
D
# Treg / (g) tumor weight
p = 0.1435
p = 0.8237
p = 0.0712
p = 0.2473
Control
RT
Control
RT
Vehicle
FTY720

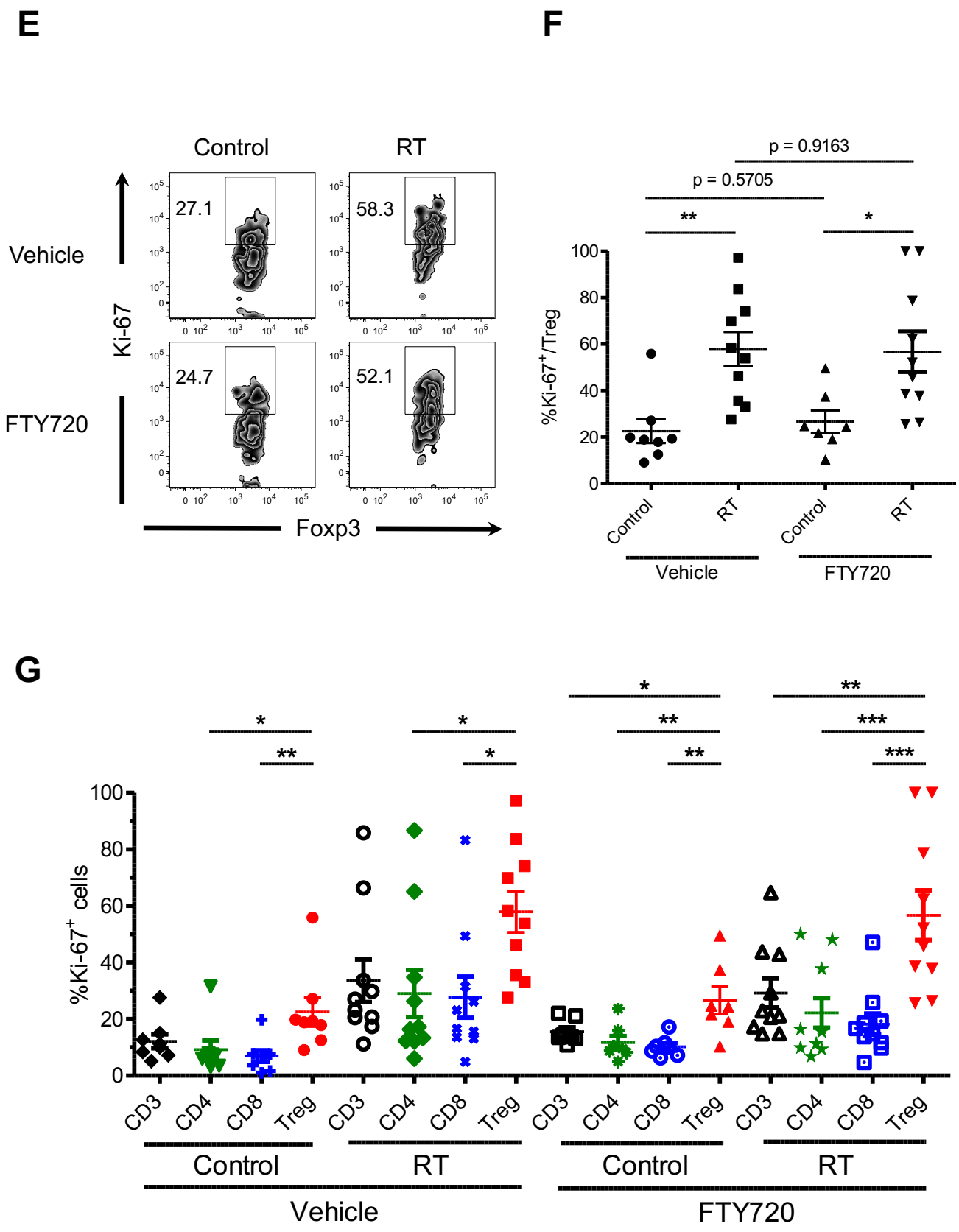
E
Control
RT
Vehicle
FTY720
Ki-67
Foxp3
27.1
58.3
24.7
52.1
F
p = 0.9163
p = 0.5705
**
*
%Ki-67+/Treg
Control
RT
Control
RT
Vehicle
FTY720
G
*
**
*
*
*
**
**
**
***
***
%Ki-67+ cells
CD3
CD4
CD8
Treg
Control
RT
Control
RT
Vehicle
FTY720

# Figure III- 6 continued

**H**

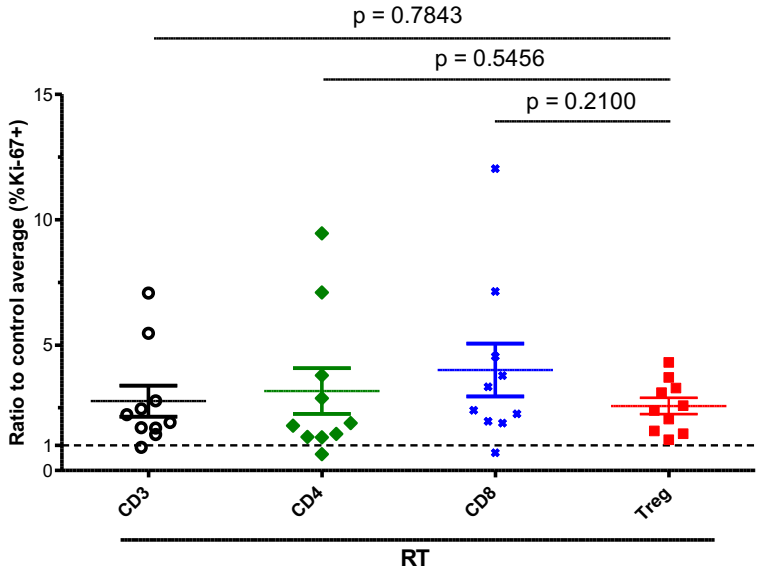


**I**

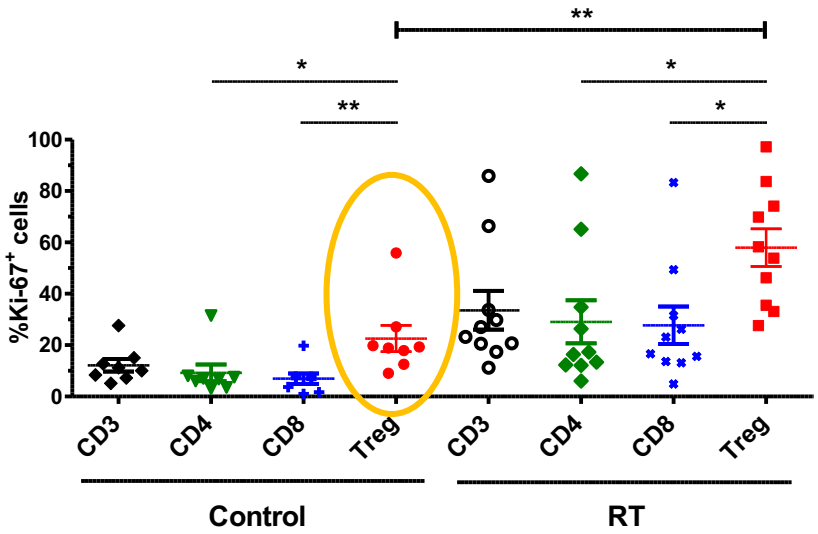

# Supplementary Data

# RT-Treg

**Supplementary Figure III- 1**

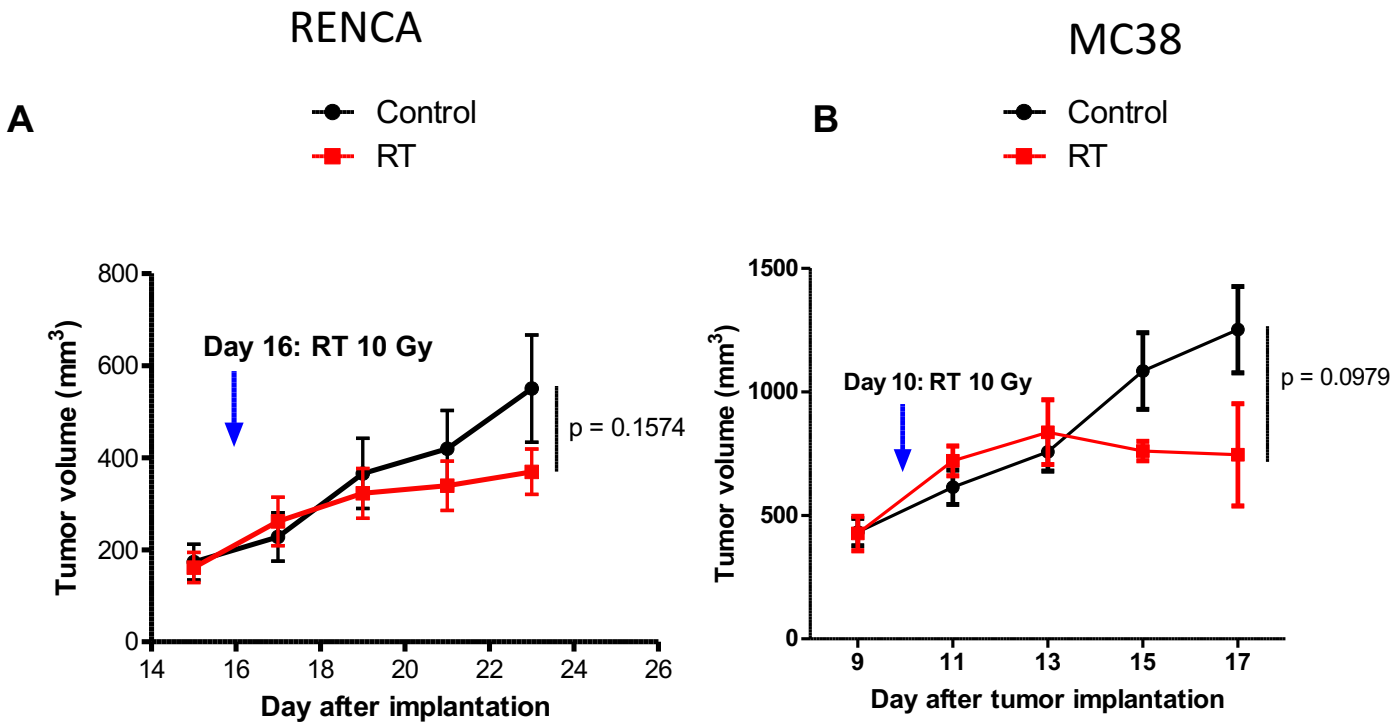

# Supplementary Figure III- 2

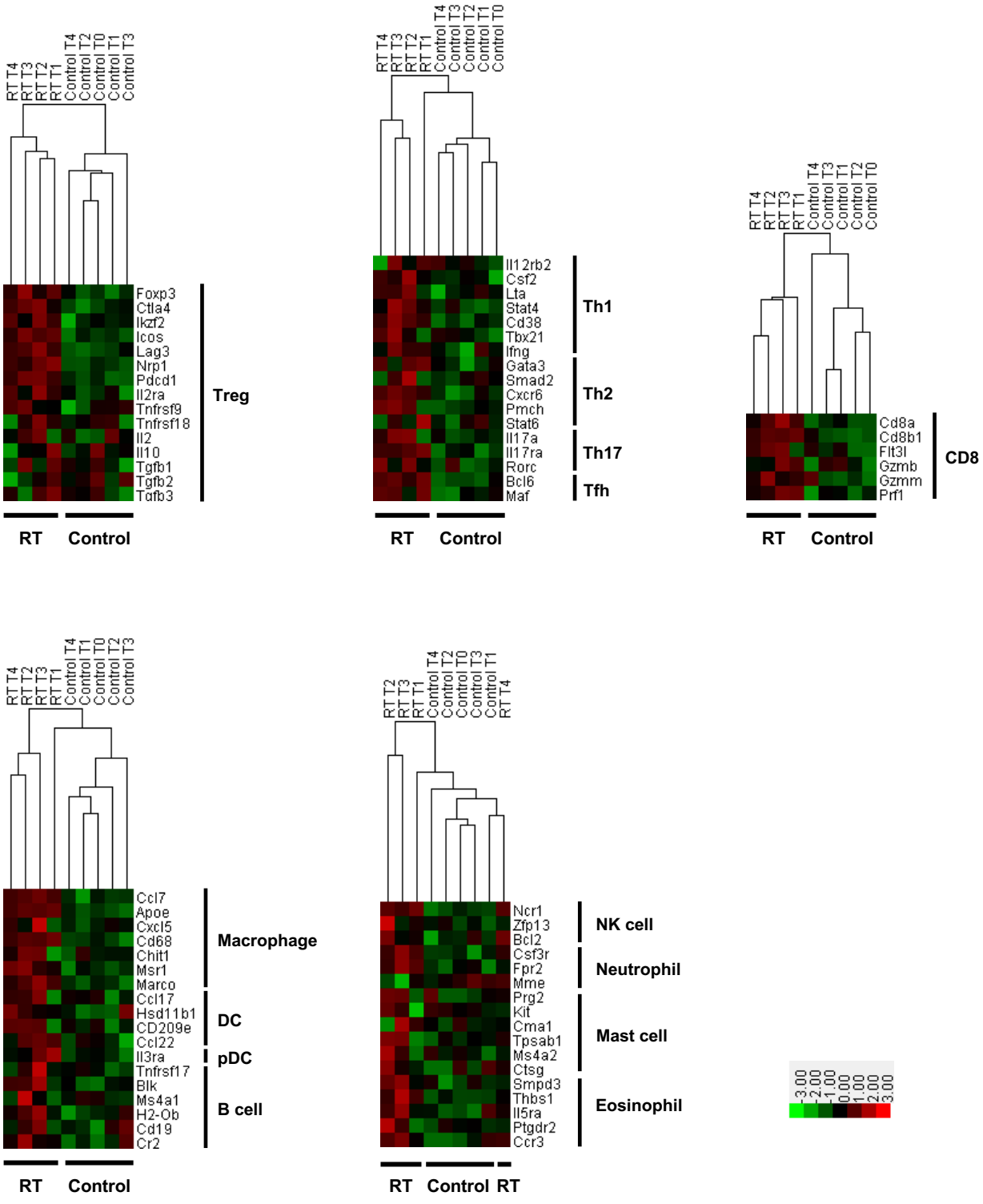

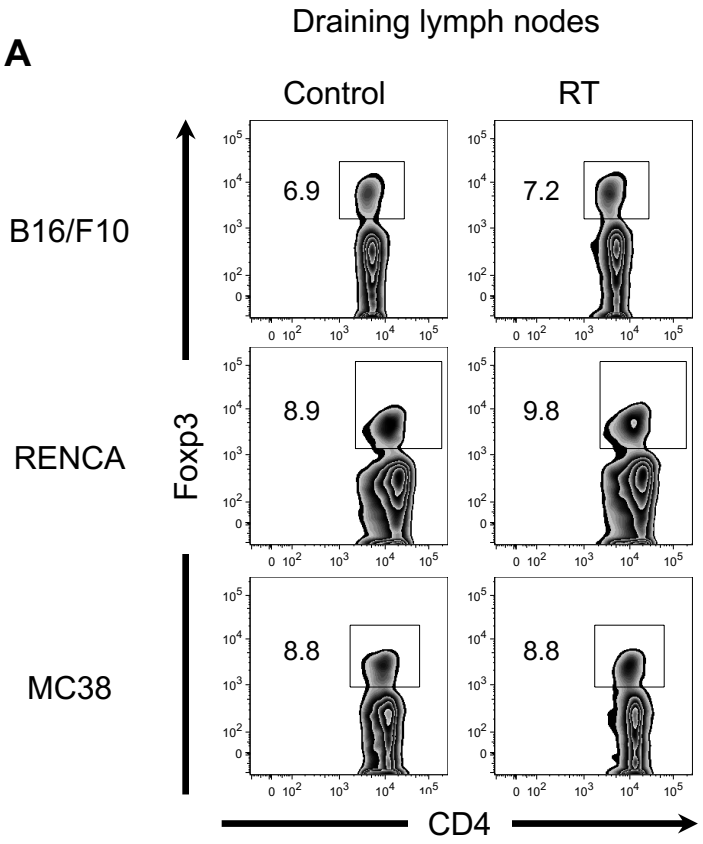
A
Draining lymph nodes
Control
RT
B16/F10
RENCA
MC38
Foxp3
CD4
6.9
7.2
8.9
9.8
8.8
8.8

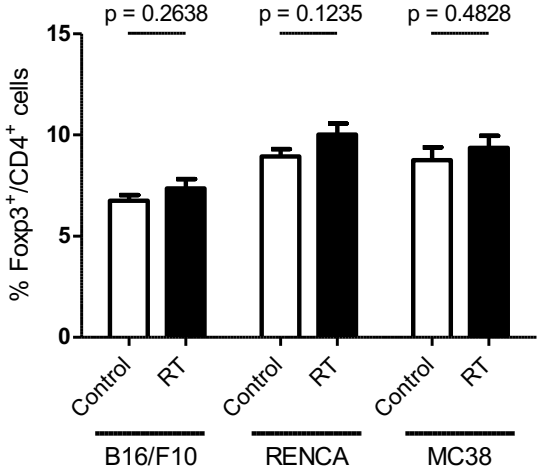
B
p = 0.2638
p = 0.1235
p = 0.4828
% Foxp3+/CD4+ cells
15
10
5
0
Control
RT
B16/F10
RENCA
MC38

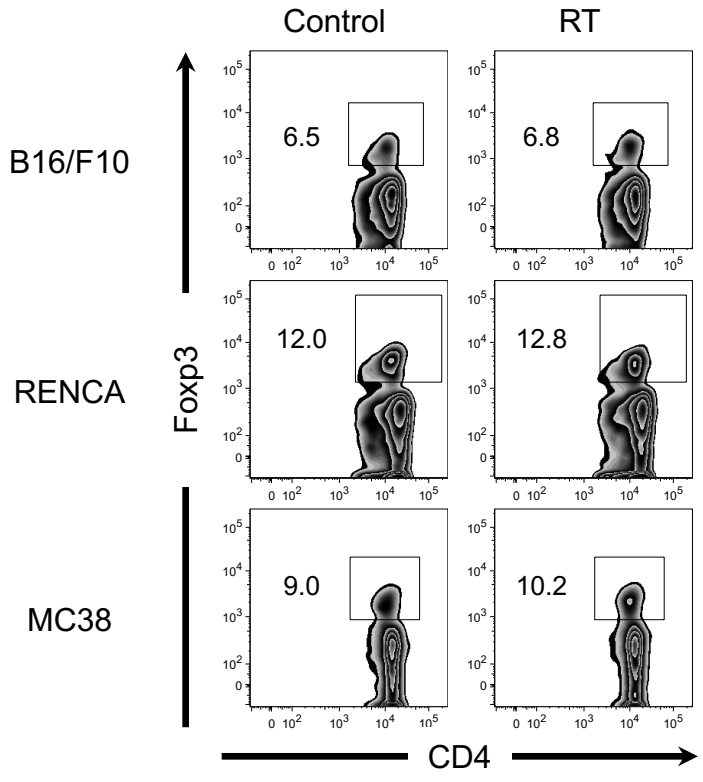
C
Spleen
Control
RT
B16/F10
RENCA
MC38
Foxp3
CD4
6.5
6.8
12.0
12.8
9.0
10.2

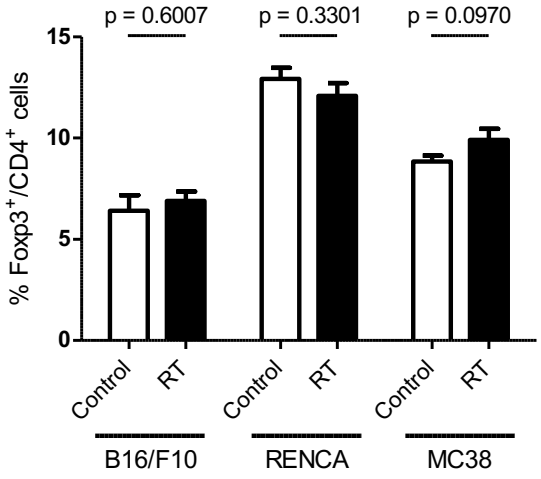
D
p = 0.6007
p = 0.3301
p = 0.0970
% Foxp3+/CD4+ cells
15
10
5
0
Control
RT
B16/F10
RENCA
MC38

Day 21 (14 days post-RT) B16/F10 TIL

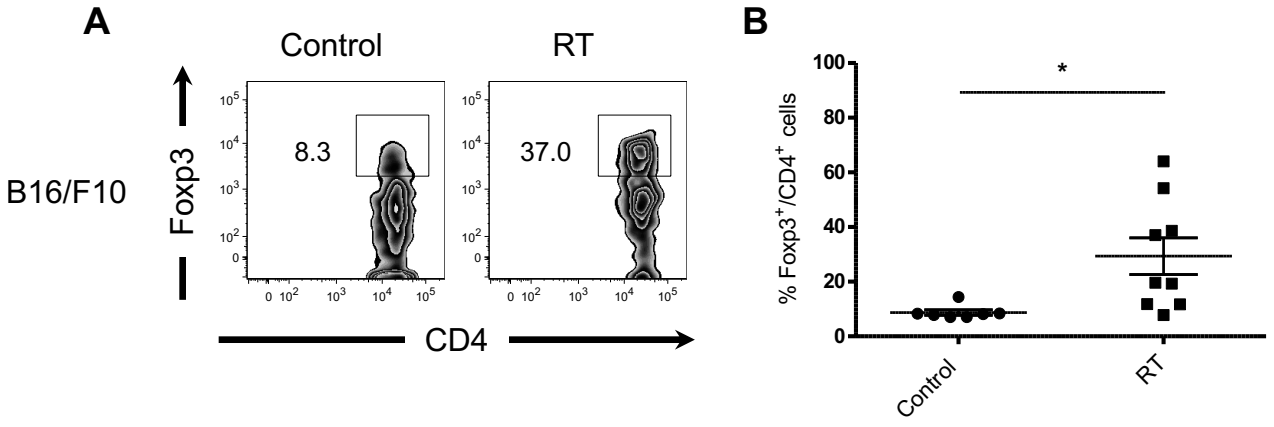

**Supplementary Figure III- 5**

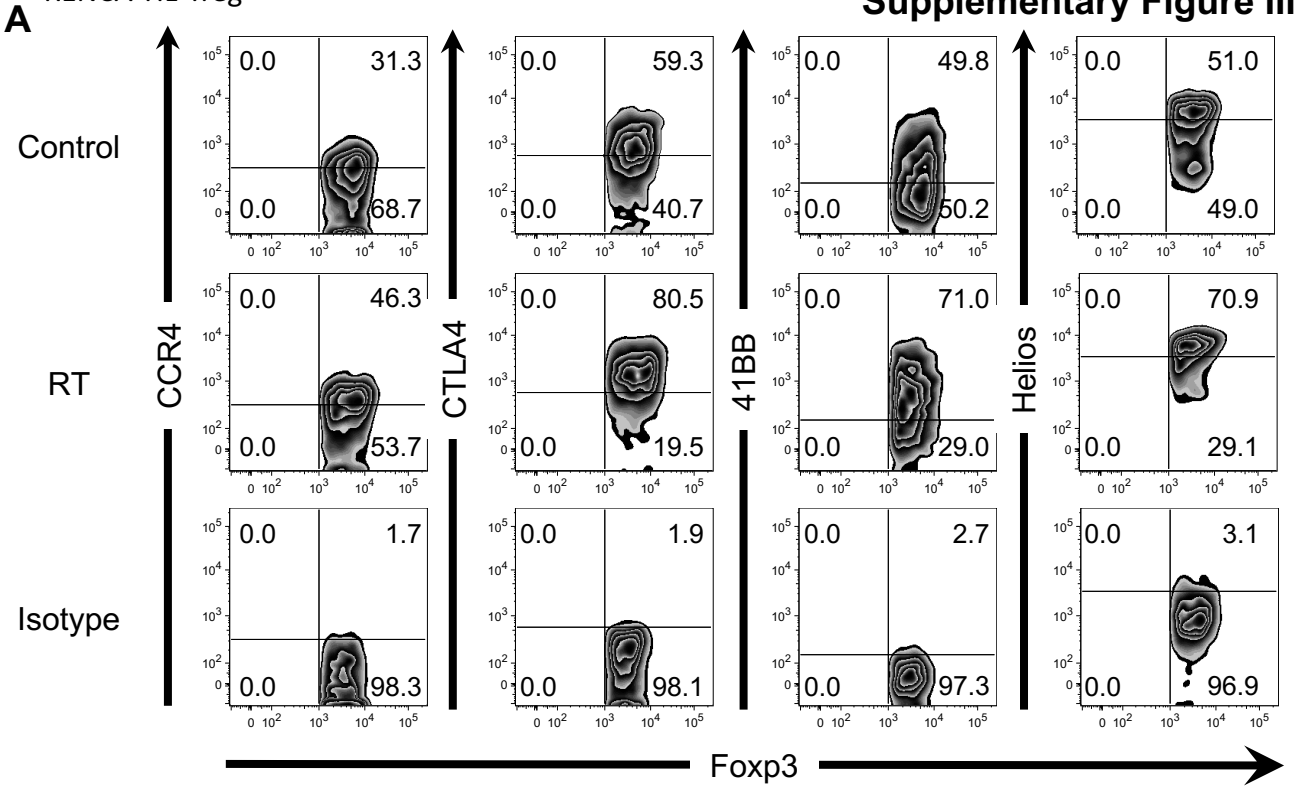


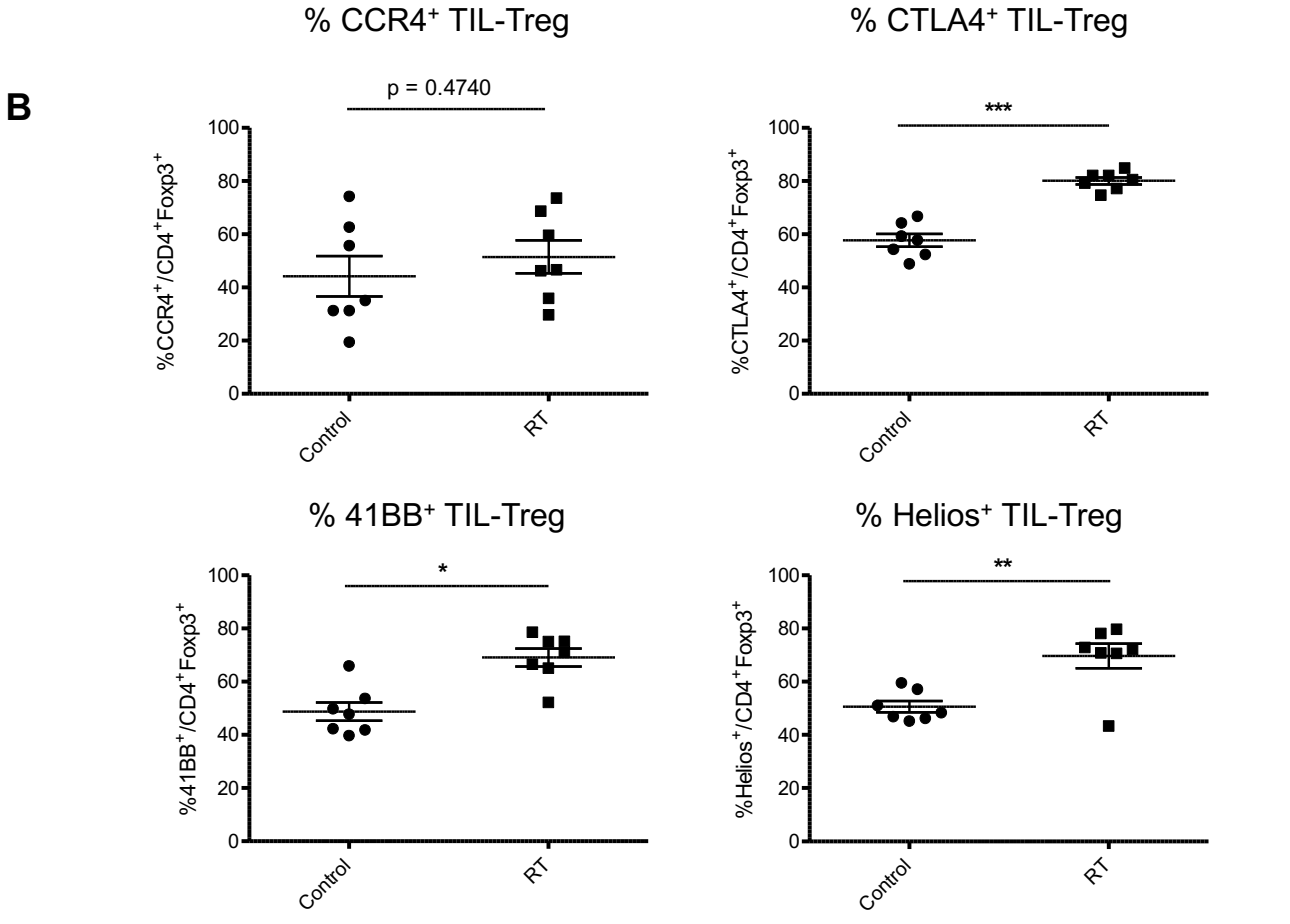

**Supplementary Figure III- 6**

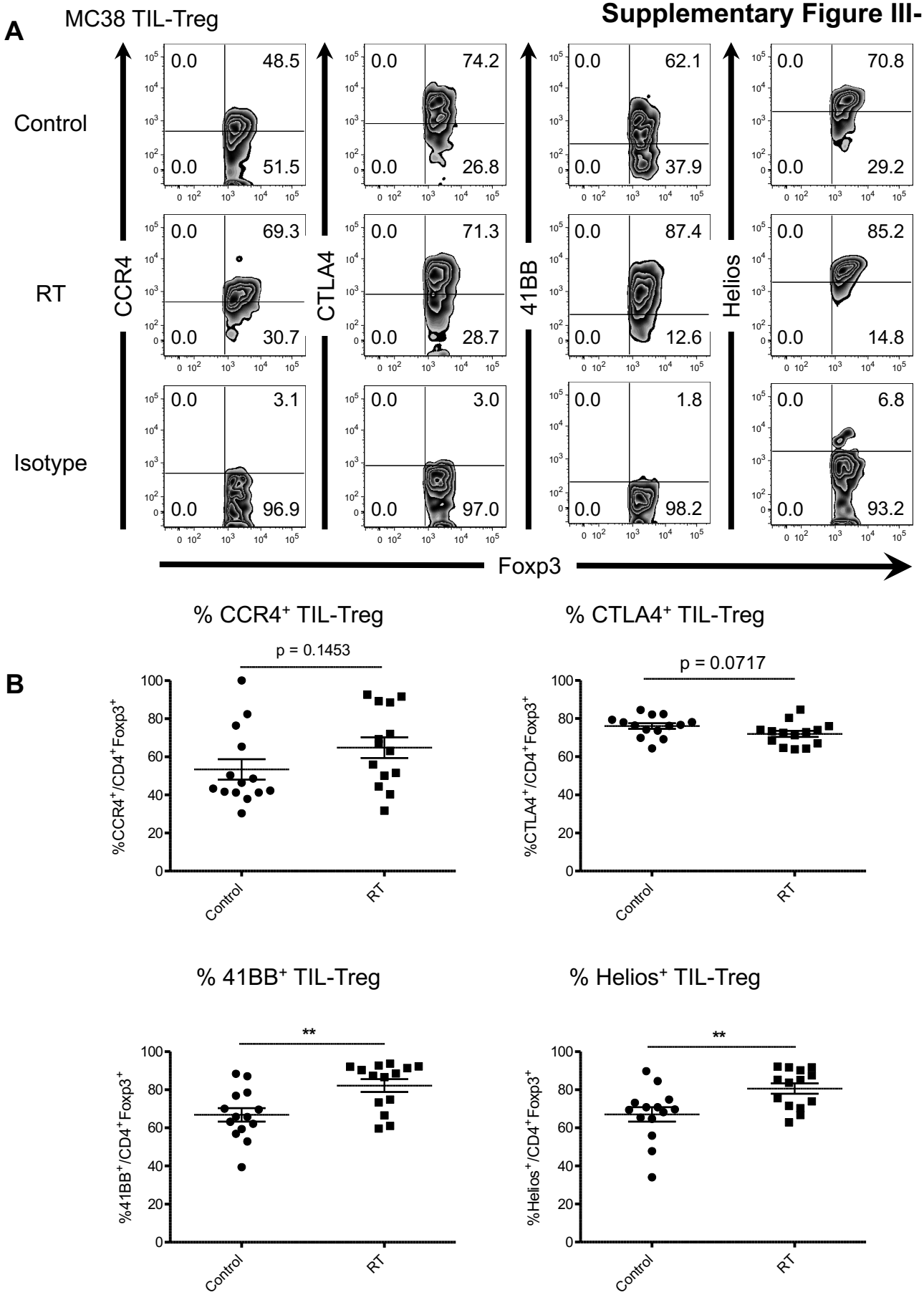

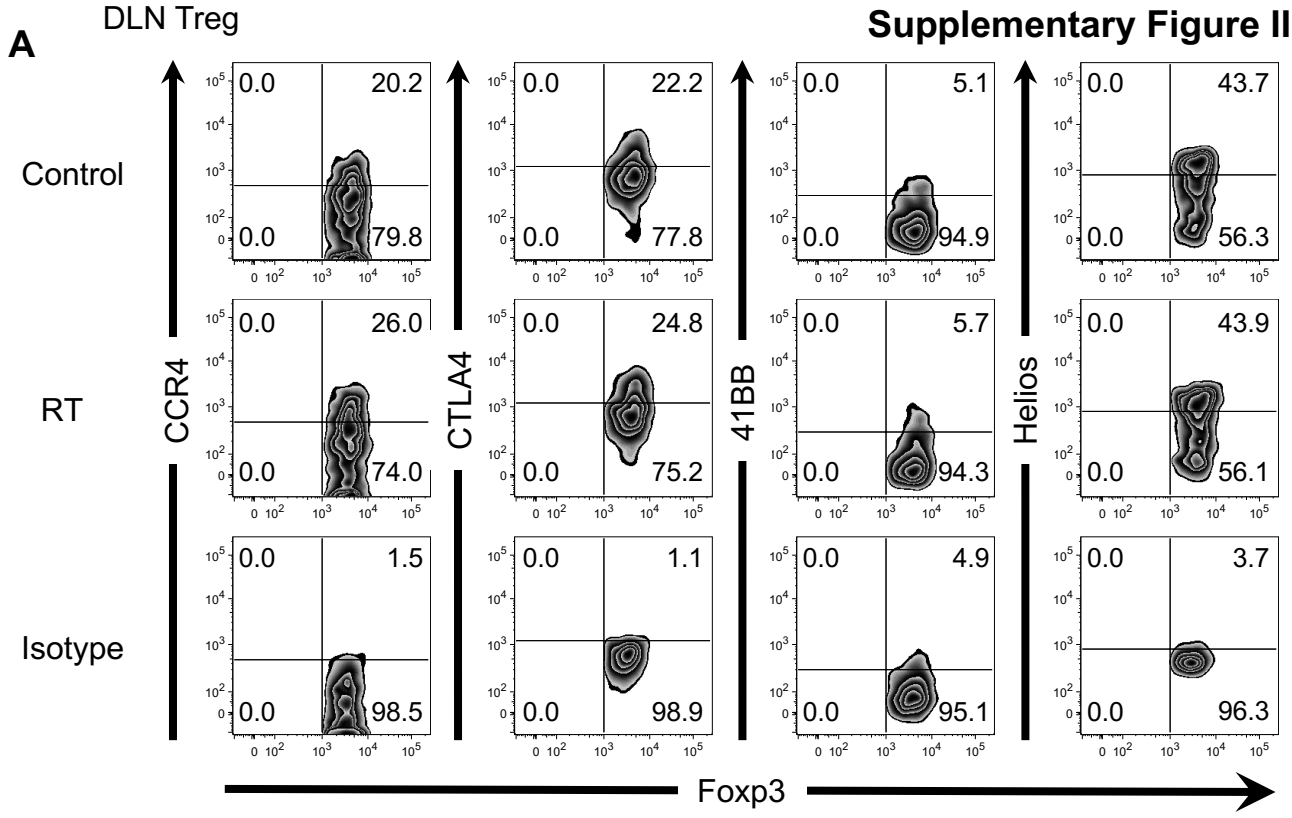
A
DLN Treg
Control
RT
Isotype
CCR4
CTLA4
41BB
Helios
Foxp3
0.0
20.2
79.8
22.2
77.8
5.1
94.9
43.7
56.3
26.0
74.0
24.8
75.2
5.7
94.3
43.9
56.1
1.5
98.5
1.1
98.9
4.9
95.1
3.7
96.3

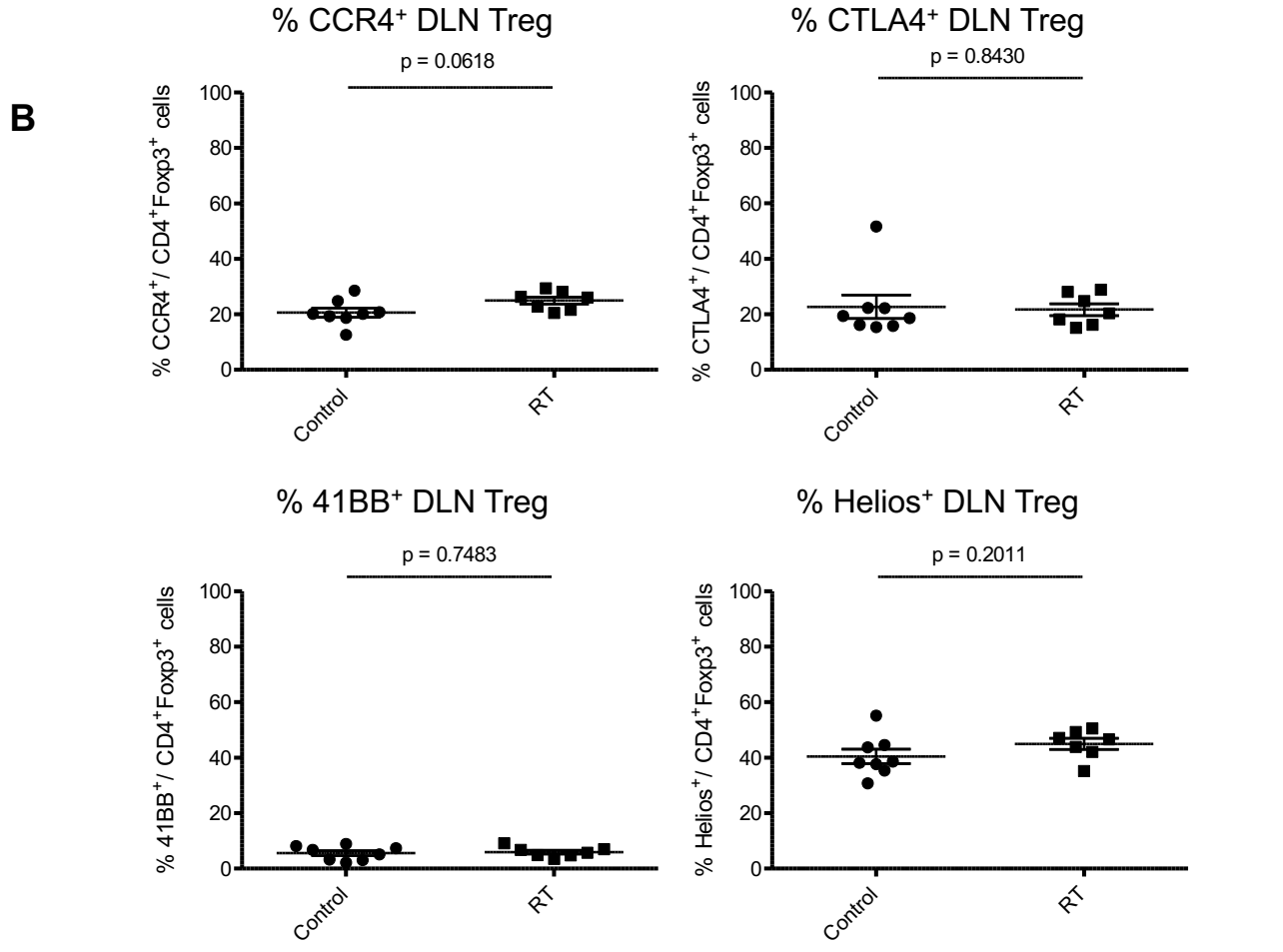
B
% CCR4⁺ DLN Treg
p = 0.0618
% CCR4⁺ / CD4⁺Foxp3⁺ cells
% CTLA4⁺ DLN Treg
p = 0.8430
% CTLA4⁺ / CD4⁺Foxp3⁺ cells
% 41BB⁺ DLN Treg
p = 0.7483
% 41BB⁺ / CD4⁺Foxp3⁺ cells
% Helios⁺ DLN Treg
p = 0.2011
% Helios⁺ / CD4⁺Foxp3⁺ cells
Control
RT

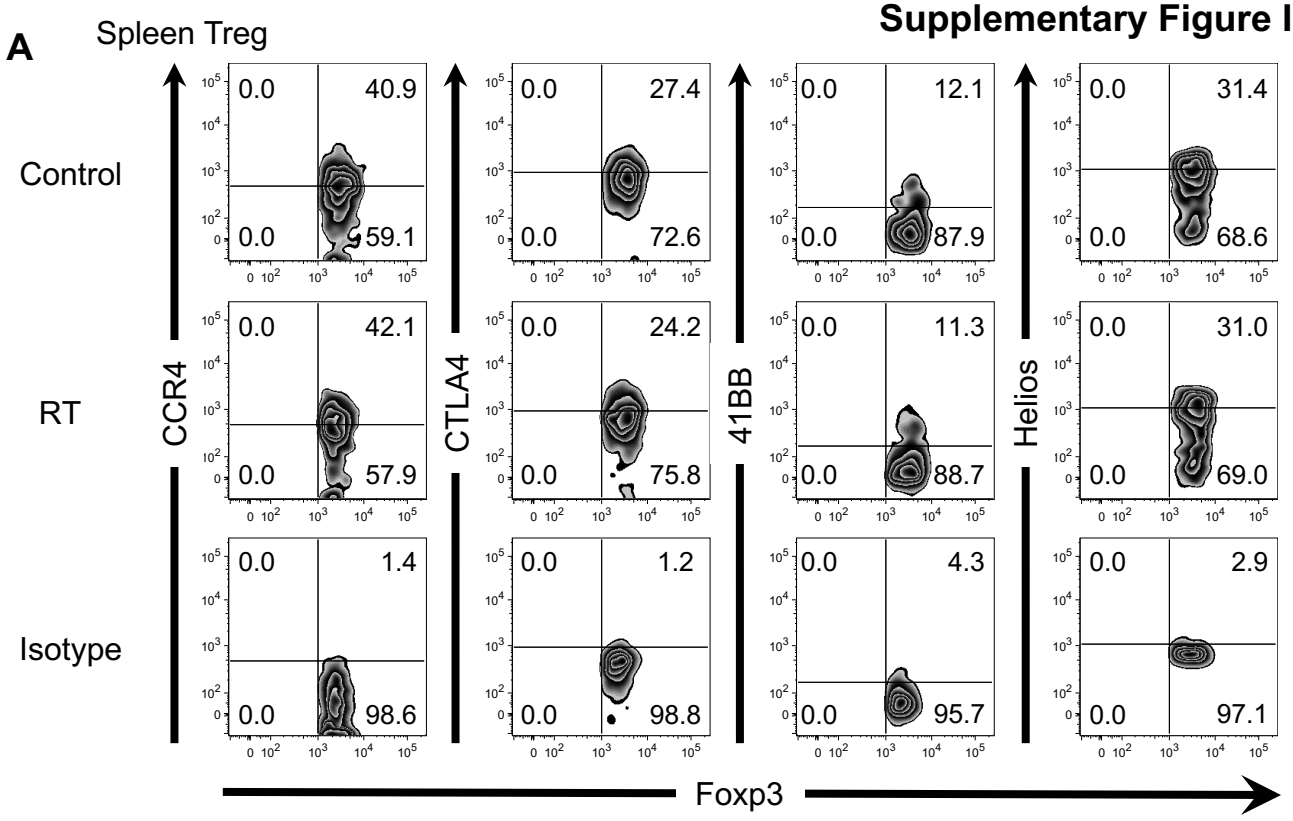
A
Spleen Treg
Control
RT
Isotype
CCR4
CTLA4
41BB
Helios
Foxp3
0.0
40.9
59.1
27.4
72.6
12.1
87.9
31.4
68.6
42.1
57.9
24.2
75.8
11.3
88.7
31.0
69.0
1.4
98.6
1.2
98.8
4.3
95.7
2.9
97.1

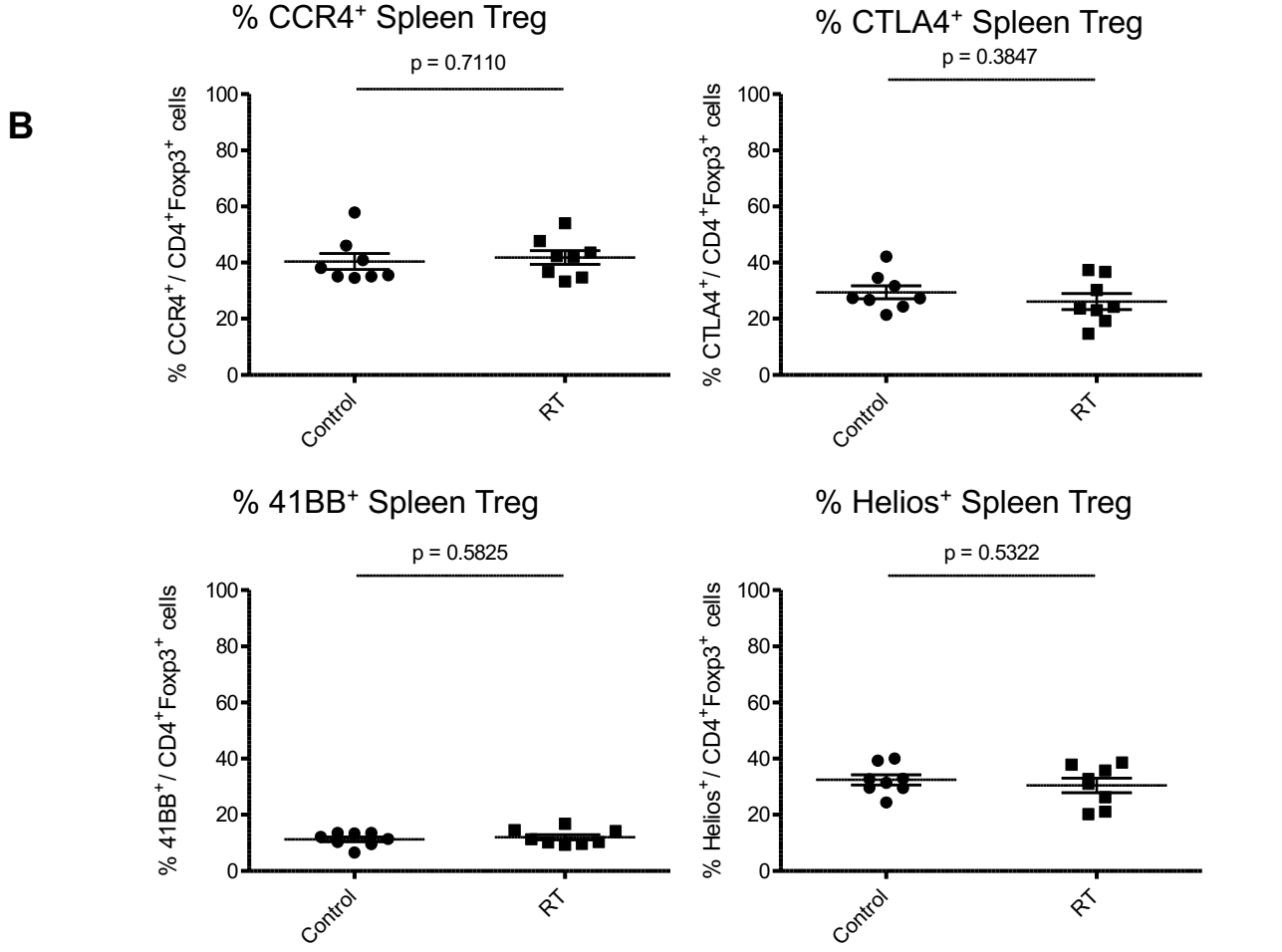
B
% CCR4⁺ Spleen Treg
p = 0.7110
% CCR4⁺ / CD4⁺Foxp3⁺ cells
% CTLA4⁺ Spleen Treg
p = 0.3847
% CTLA4⁺ / CD4⁺Foxp3⁺ cells
% 41BB⁺ Spleen Treg
p = 0.5825
% 41BB⁺ / CD4⁺Foxp3⁺ cells
% Helios⁺ Spleen Treg
p = 0.5322
% Helios⁺ / CD4⁺Foxp3⁺ cells
Control
RT

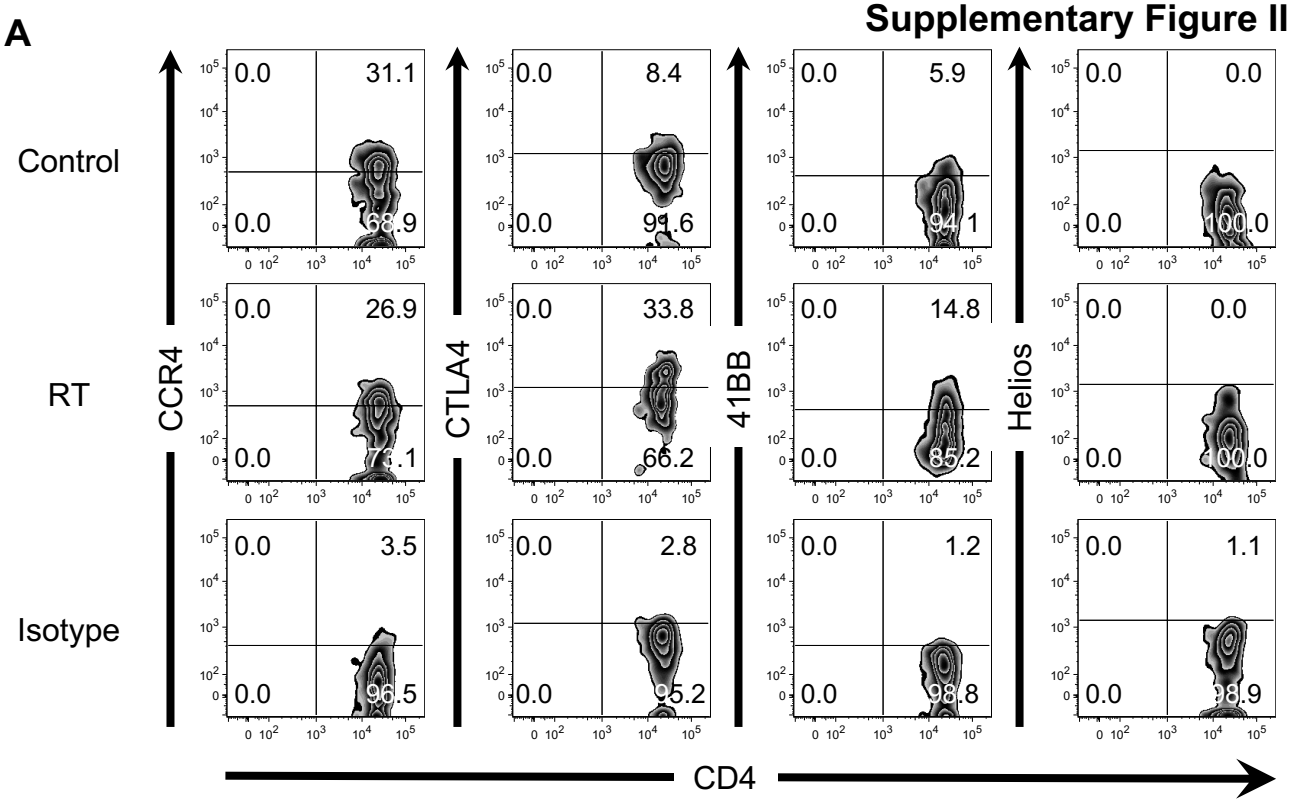
A
Control
RT
Isotype
CCR4
CTLA4
41BB
Helios
CD4
0.0
31.1
68.9
8.4
91.6
5.9
94.1
0.0
100.0
26.9
73.1
33.8
66.2
14.8
85.2
3.5
96.5
2.8
95.2
1.2
98.8
1.1
98.9

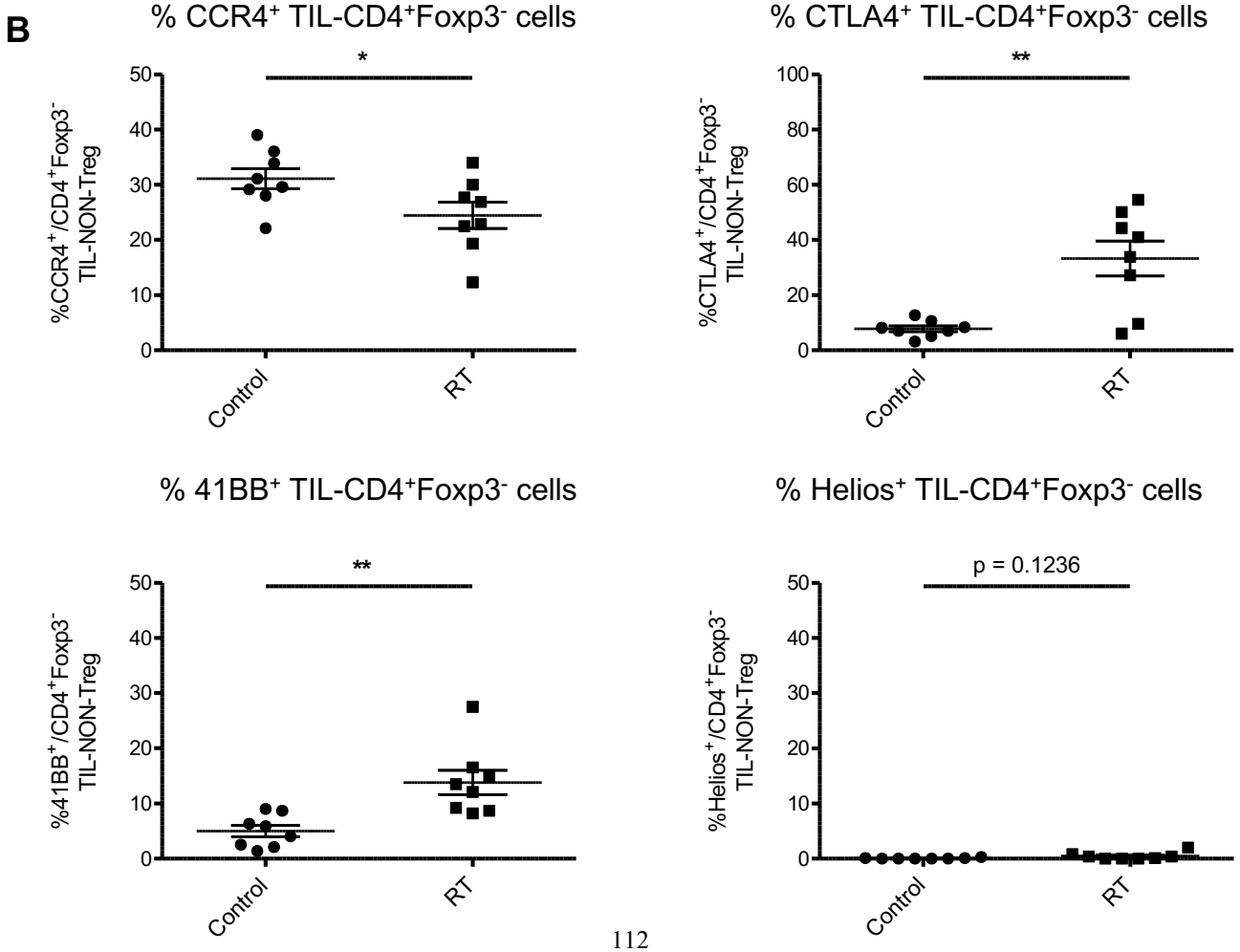
B
% CCR4+ TIL-CD4+Foxp3- cells
% CTLA4+ TIL-CD4+Foxp3- cells
% 41BB+ TIL-CD4+Foxp3- cells
% Helios+ TIL-CD4+Foxp3- cells
%CCR4+/CD4+Foxp3- TIL-NON-Treg
%CTLA4+/CD4+Foxp3- TIL-NON-Treg
%41BB+/CD4+Foxp3- TIL-NON-Treg
%Helios+/CD4+Foxp3- TIL-NON-Treg
*
**
**
p = 0.1236
Control
RT

**Supplementary Figure III- 10**

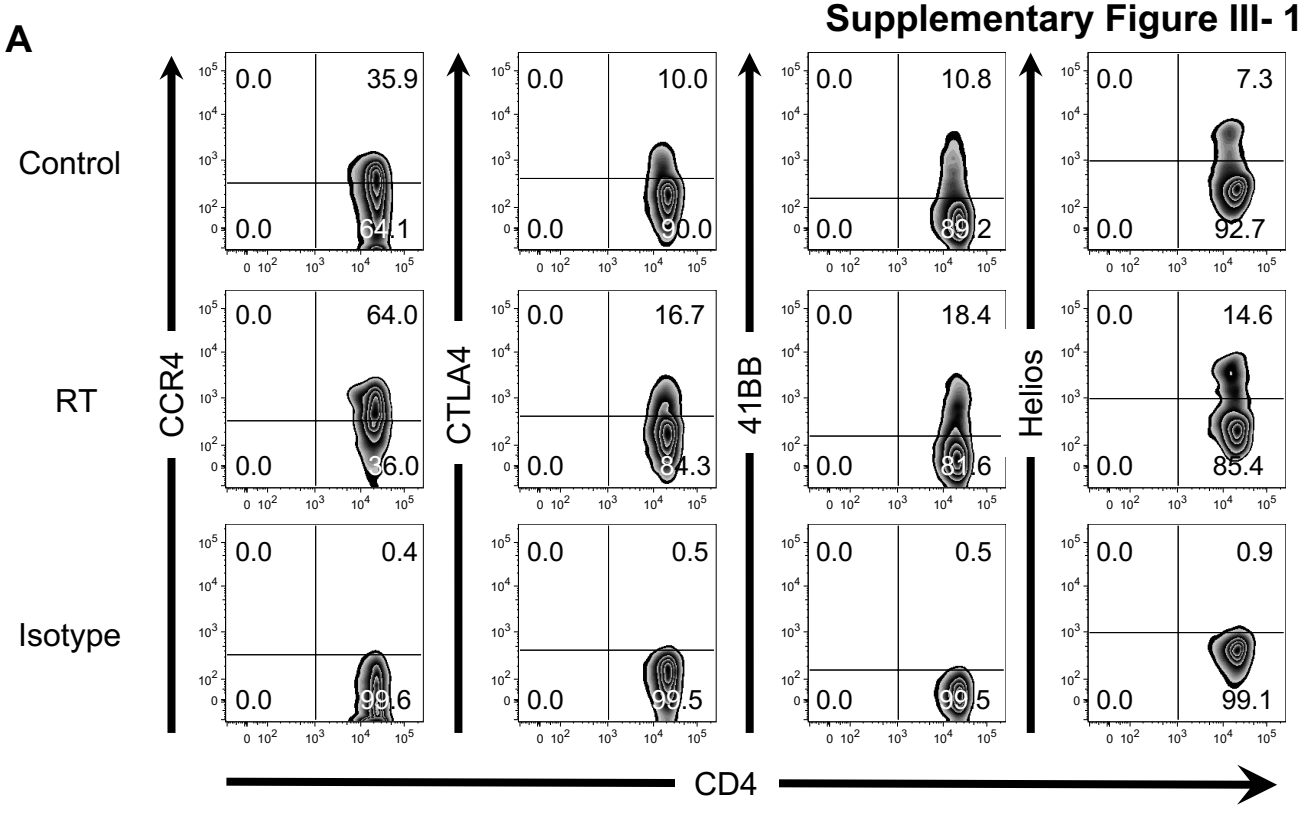


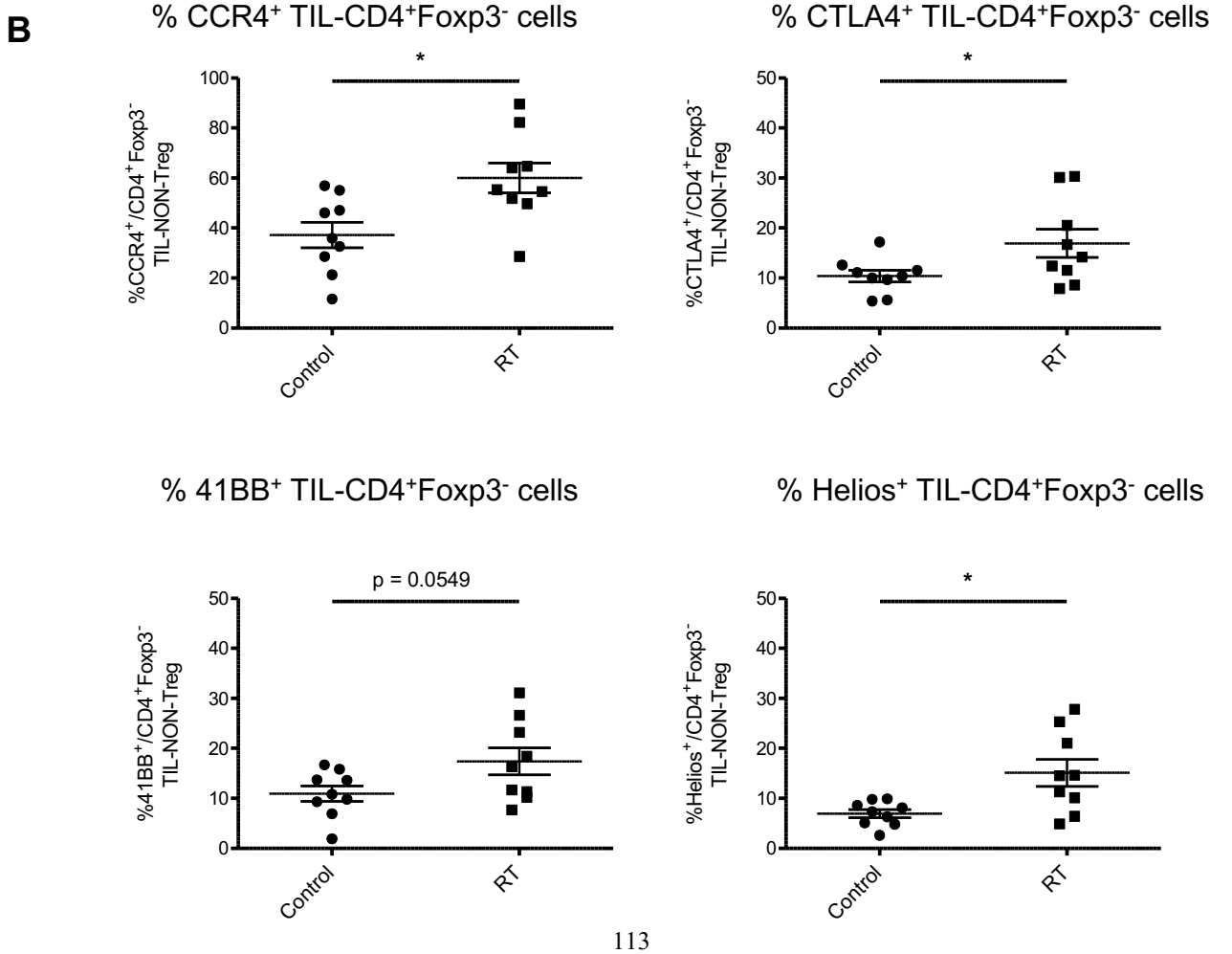

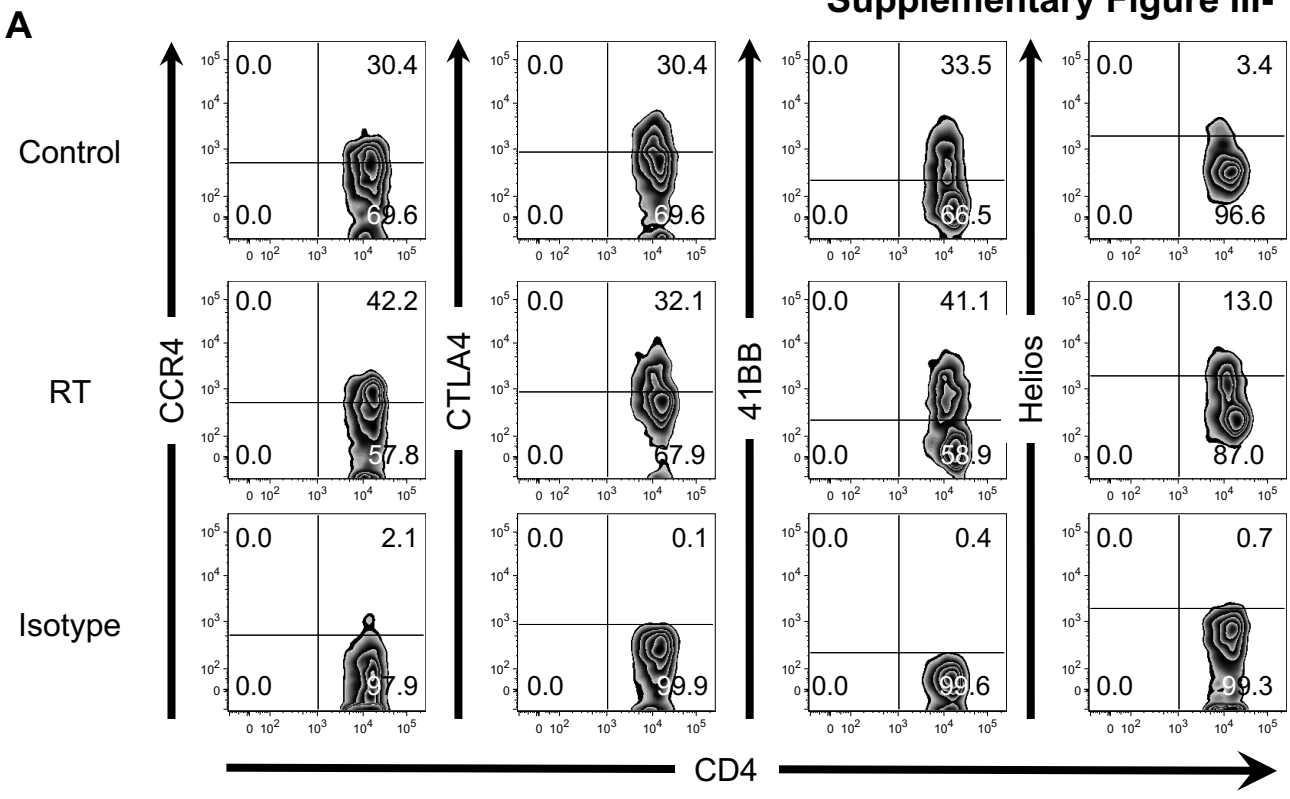
A
Control
RT
Isotype
CCR4
CTLA4
41BB
Helios
CD4
0.0
30.4
69.6
0.0
30.4
69.6
0.0
33.5
66.5
0.0
3.4
96.6
0.0
42.2
57.8
0.0
32.1
67.9
0.0
41.1
58.9
0.0
13.0
87.0
0.0
2.1
97.9
0.0
0.1
99.9
0.0
0.4
99.6
0.0
0.7
99.3

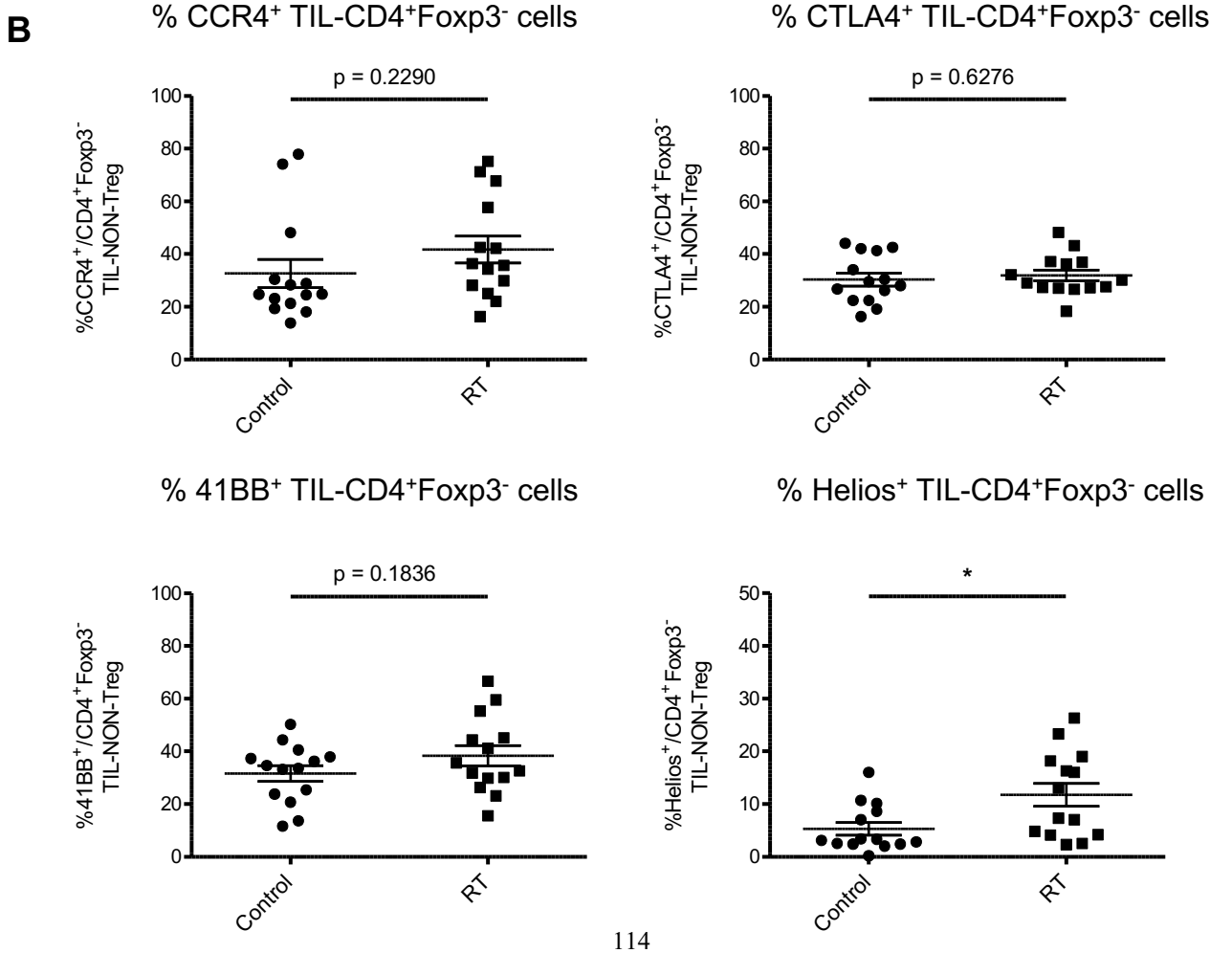
B
% CCR4+ TIL-CD4+Foxp3- cells
p = 0.2290
%CCR4+/CD4+Foxp3- TIL-NON-Treg
Control
RT
% CTLA4+ TIL-CD4+Foxp3- cells
p = 0.6276
%CTLA4+/CD4+Foxp3- TIL-NON-Treg
% 41BB+ TIL-CD4+Foxp3- cells
p = 0.1836
%41BB+/CD4+Foxp3- TIL-NON-Treg
% Helios+ TIL-CD4+Foxp3- cells
*
%Helios+/CD4+Foxp3- TIL-NON-Treg

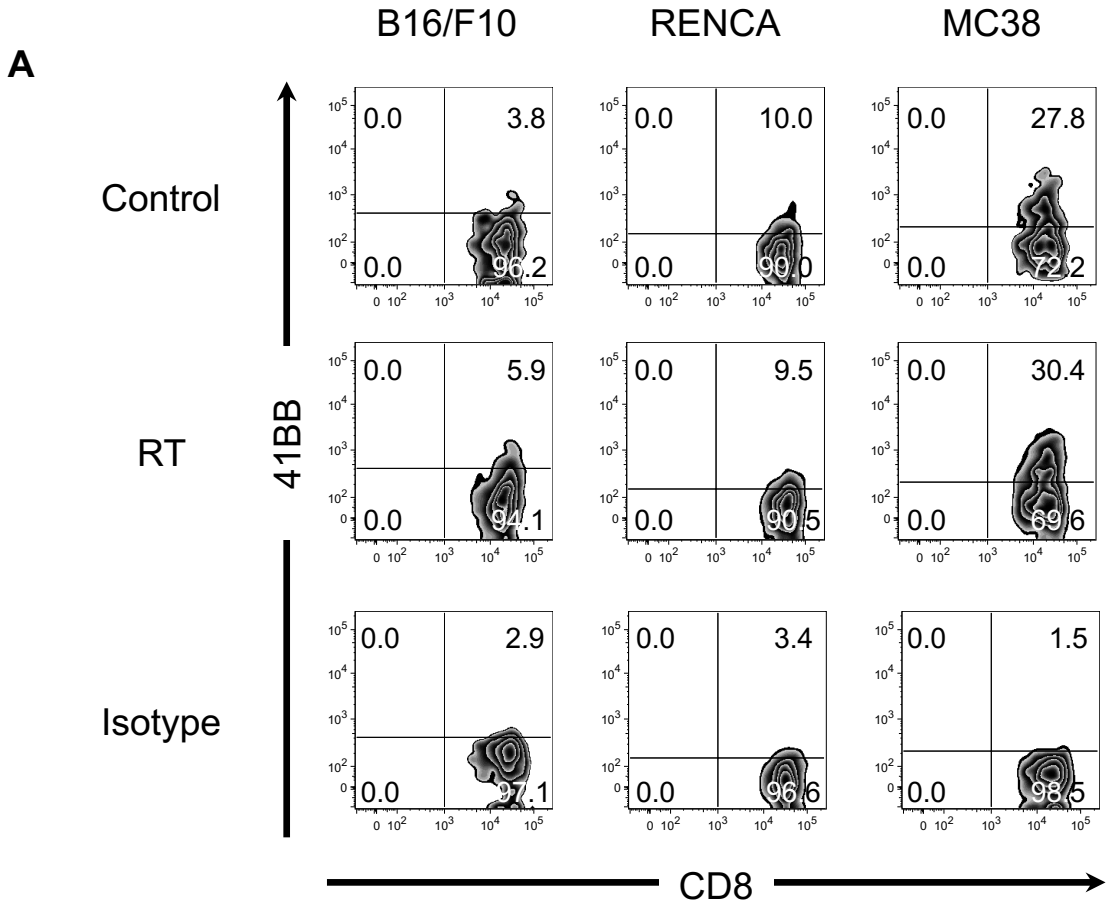
A
B16/F10
RENCA
MC38
Control
RT
Isotype
41BB
CD8
0.0
3.8
96.2
0.0
10.0
90.0
0.0
27.8
72.2
0.0
5.9
94.1
0.0
9.5
90.5
0.0
30.4
69.6
0.0
2.9
97.1
0.0
3.4
96.6
0.0
1.5
98.5

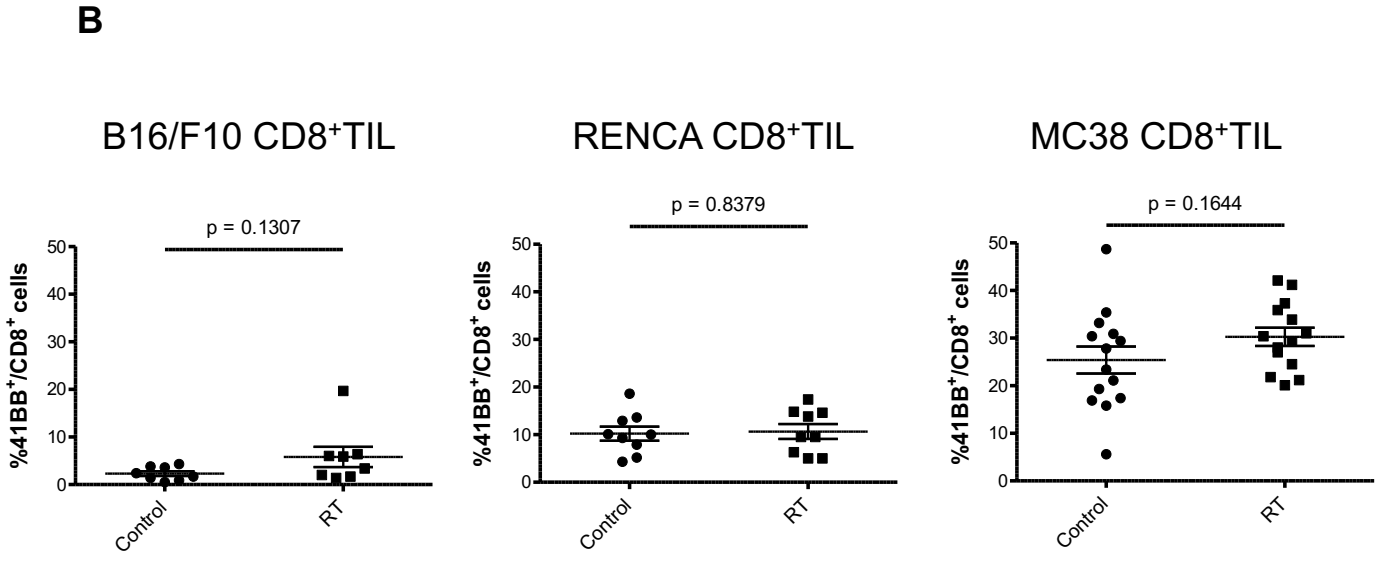
B
B16/F10 CD8+TIL
RENCA CD8+TIL
MC38 CD8+TIL
p = 0.1307
p = 0.8379
p = 0.1644
%41BB+/CD8+ cells
Control
RT

**Supplementary Figure III- 13**

A

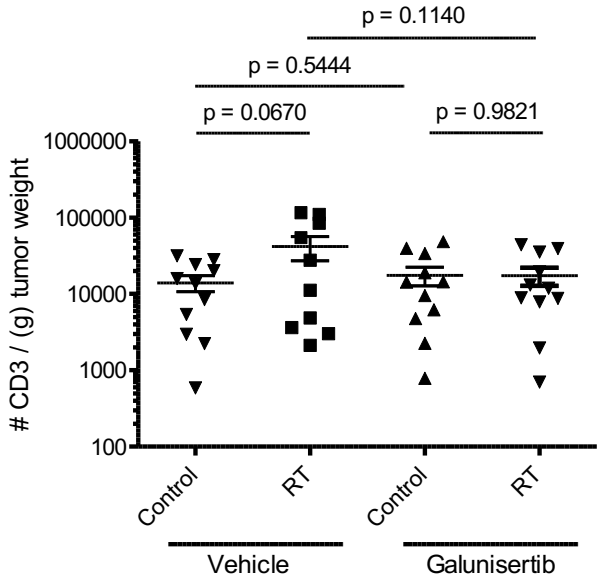


B

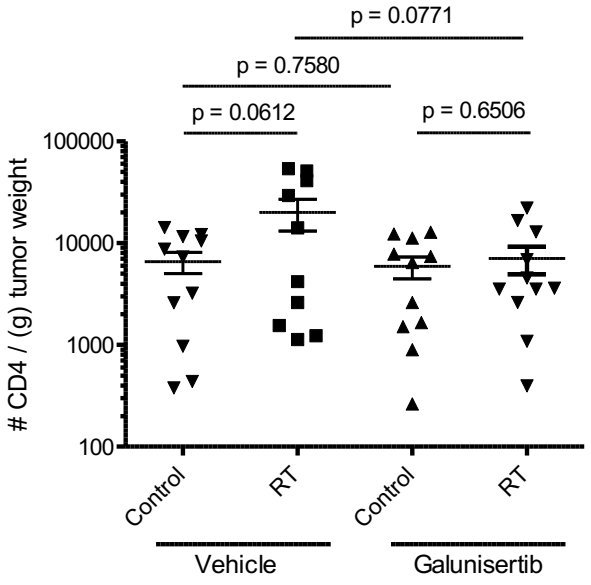


C

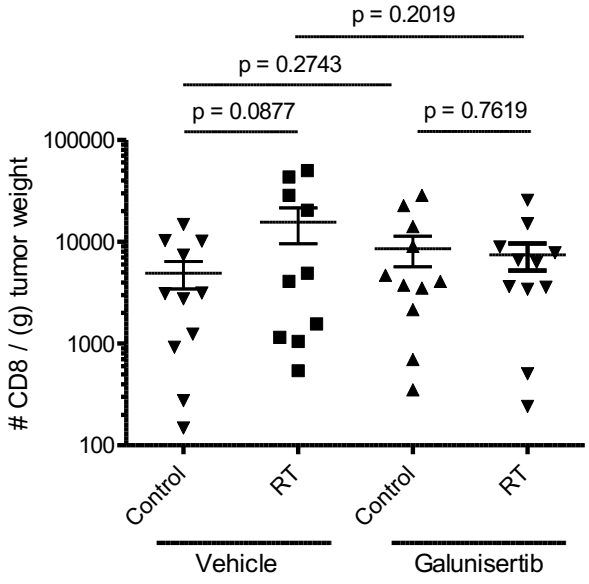

**A**

## Supplementary Figure III- 14

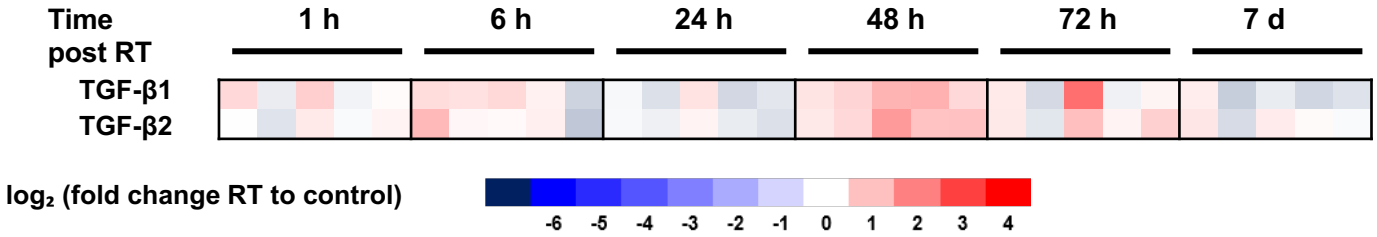


**B**

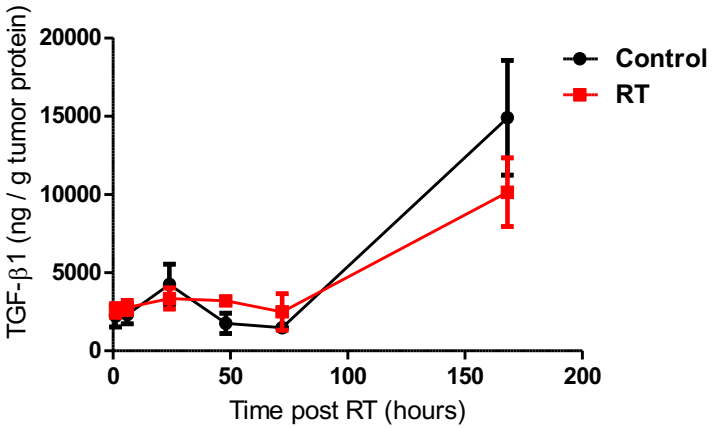


**C**

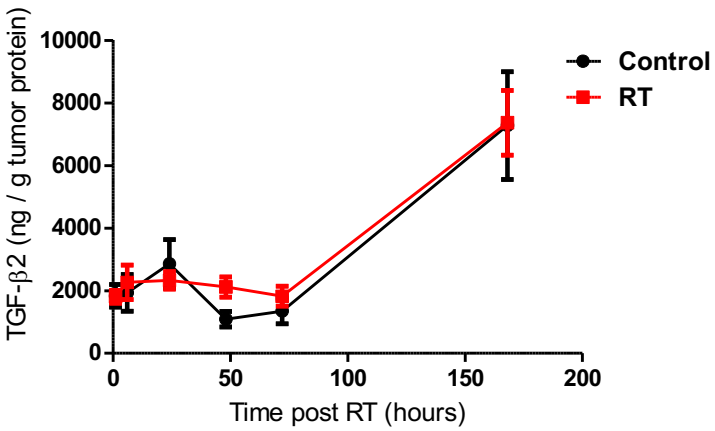

**A** Gated on LD$^-$CD3$^+$CD4$^+$Foxp3$^+$

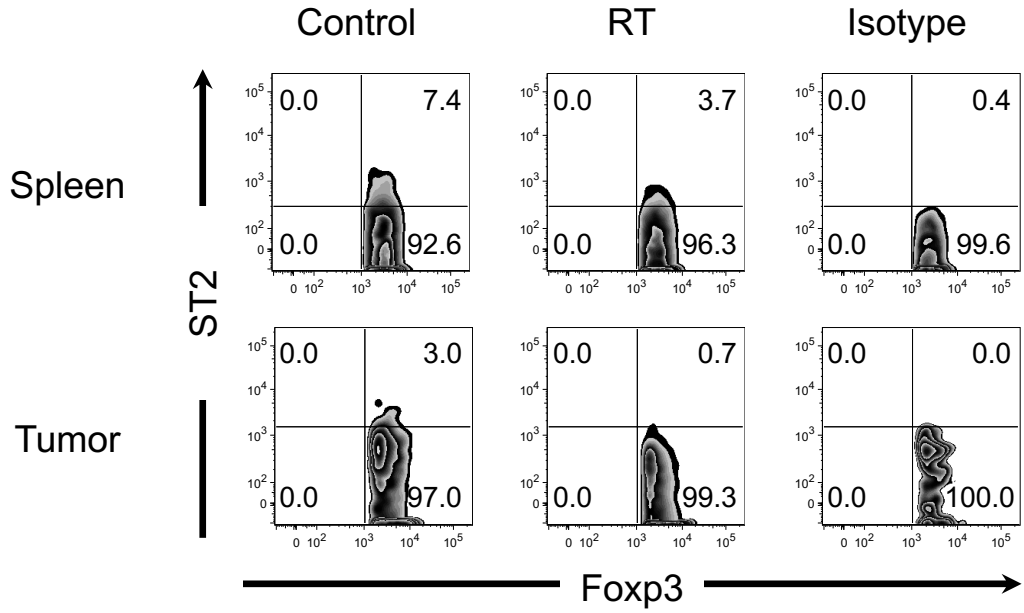


**Supplementary Figure III- III-15: ST2 expression on splenic and tumor infiltrating Treg**

A

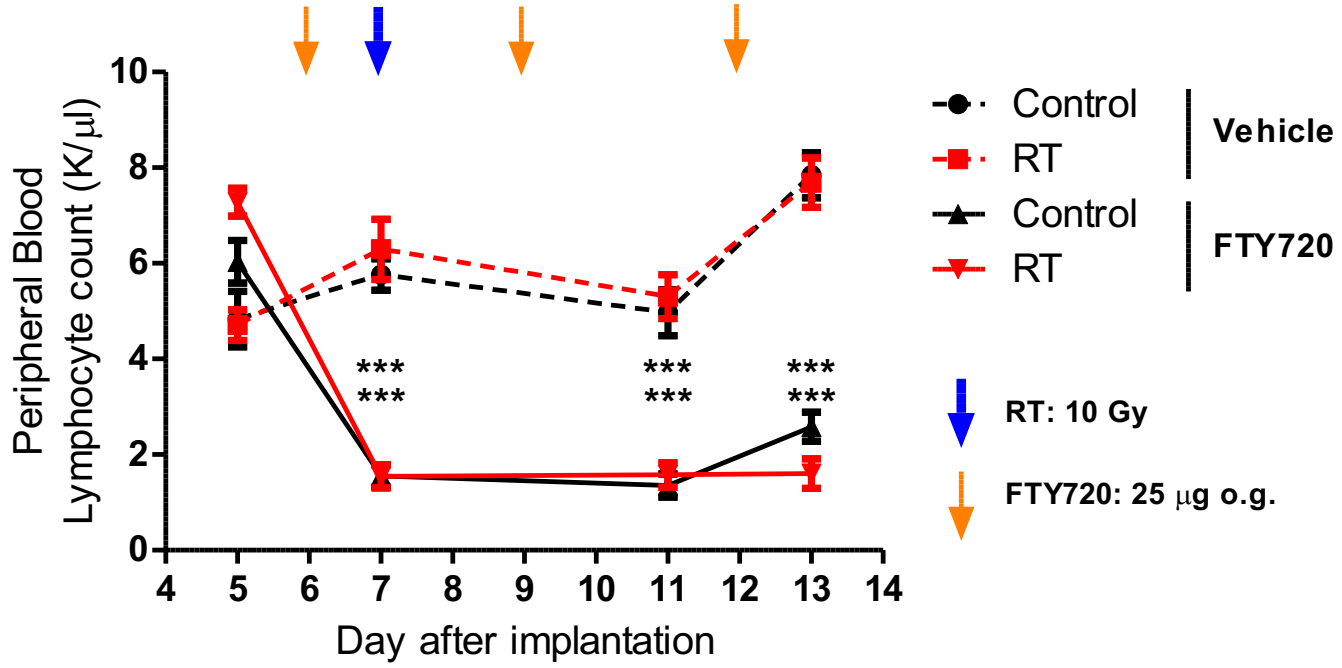
Peripheral Blood Lymphocyte count (K/µl)
10
8
6
4
2
0
4 5 6 7 8 9 10 11 12 13 14
Day after implantation
*** ***
*** ***
*** ***
Control
RT
Control
RT
Vehicle
FTY720
RT: 10 Gy
FTY720: 25 µg o.g.

B

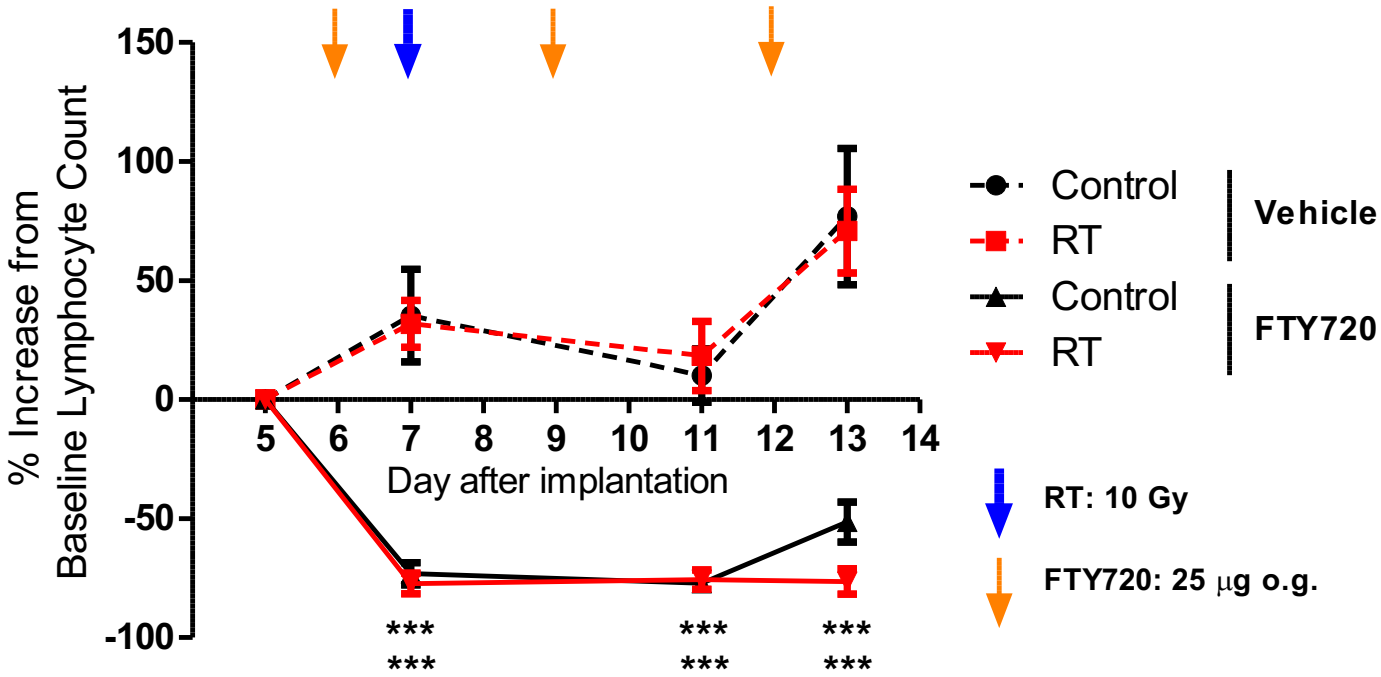
% Increase from Baseline Lymphocyte Count
150
100
50
0
-50
-100
5 6 7 8 9 10 11 12 13 14
Day after implantation
*** ***
*** ***
*** ***
Control
RT
Control
RT
Vehicle
FTY720
RT: 10 Gy
FTY720: 25 µg o.g.

# Supplementary Figure III- 17

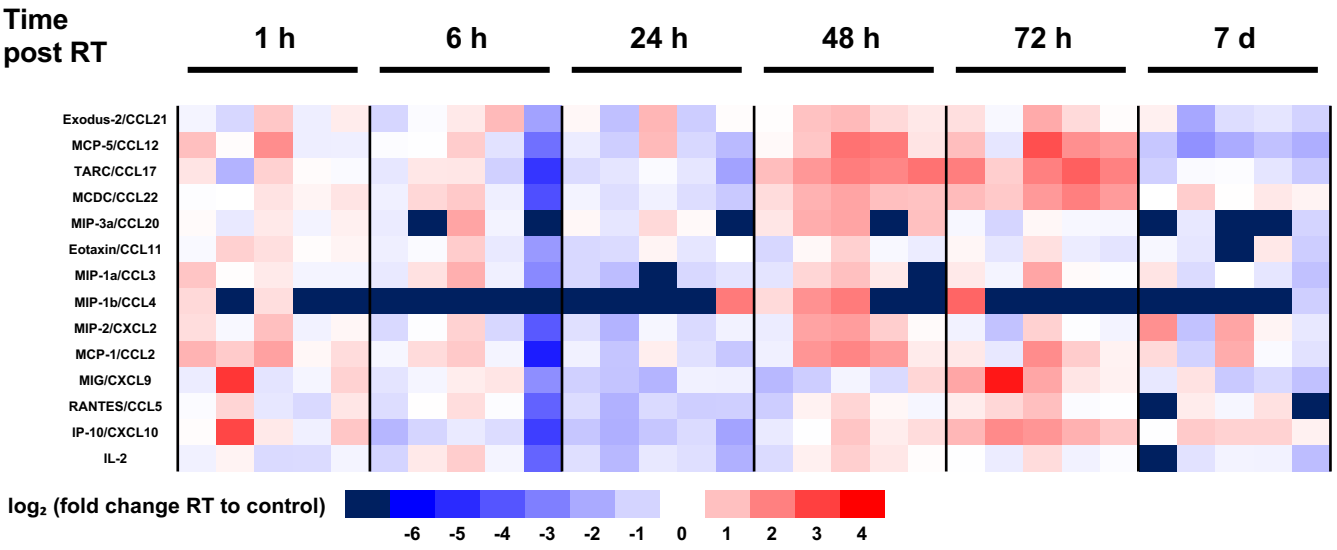


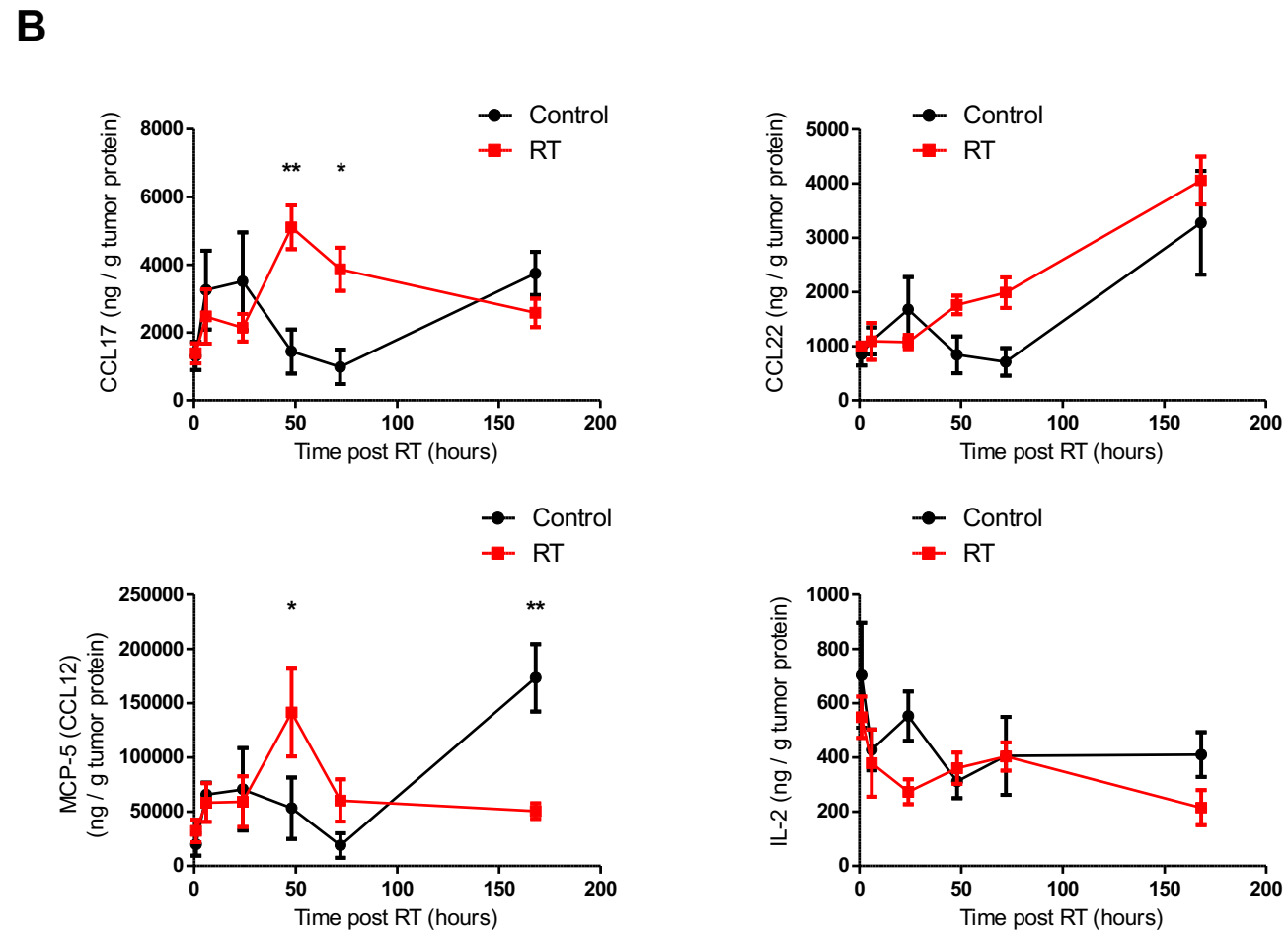

A

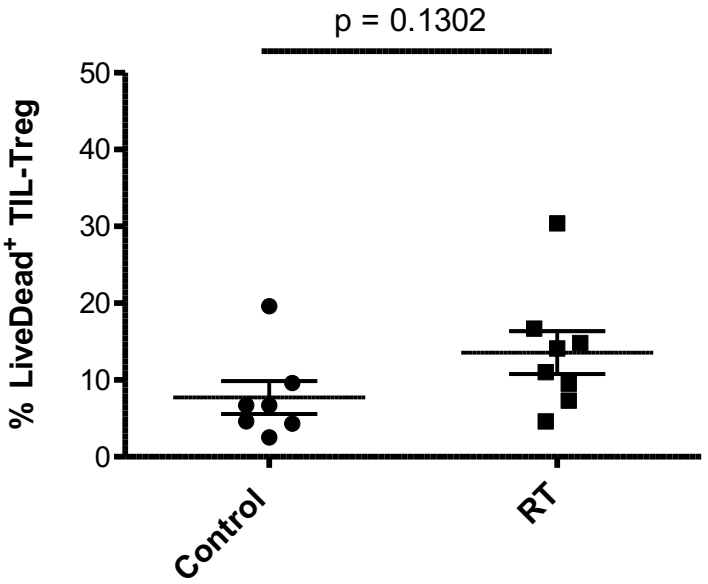


B

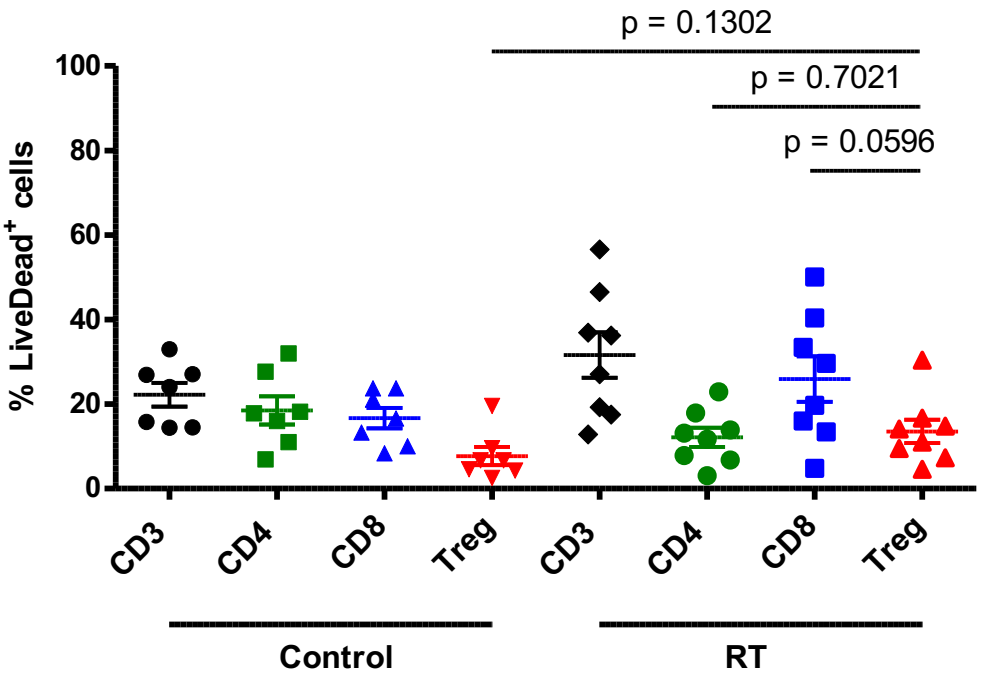


**Supplementary Figure III- III-18: RT does not increase the cell death of TIL-Treg.**

# Supplementary Figure III- 19

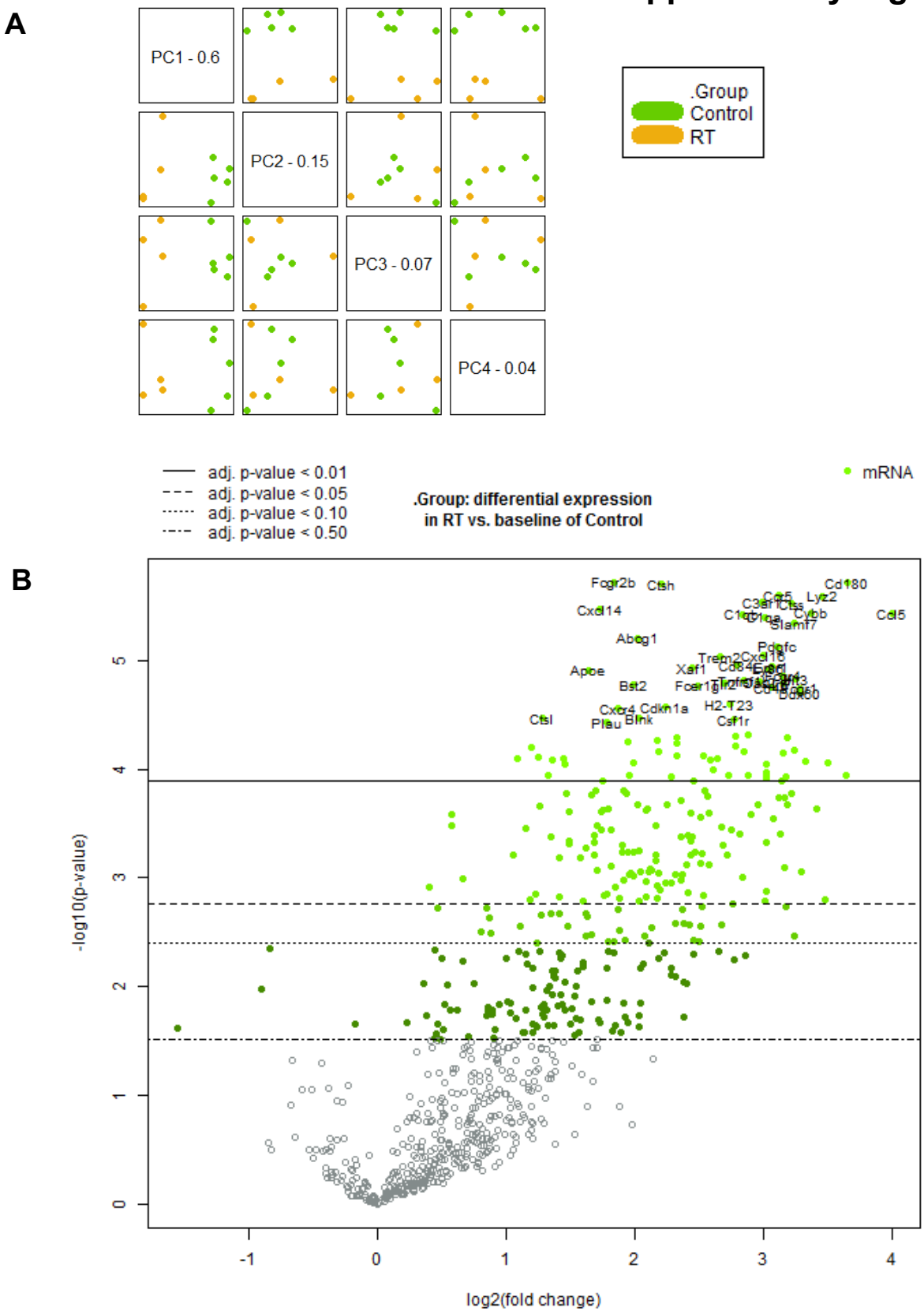


**Supplementary Figure III- 19: Differentially expressed molecules post-RT TME of B16/F10 tumors.**

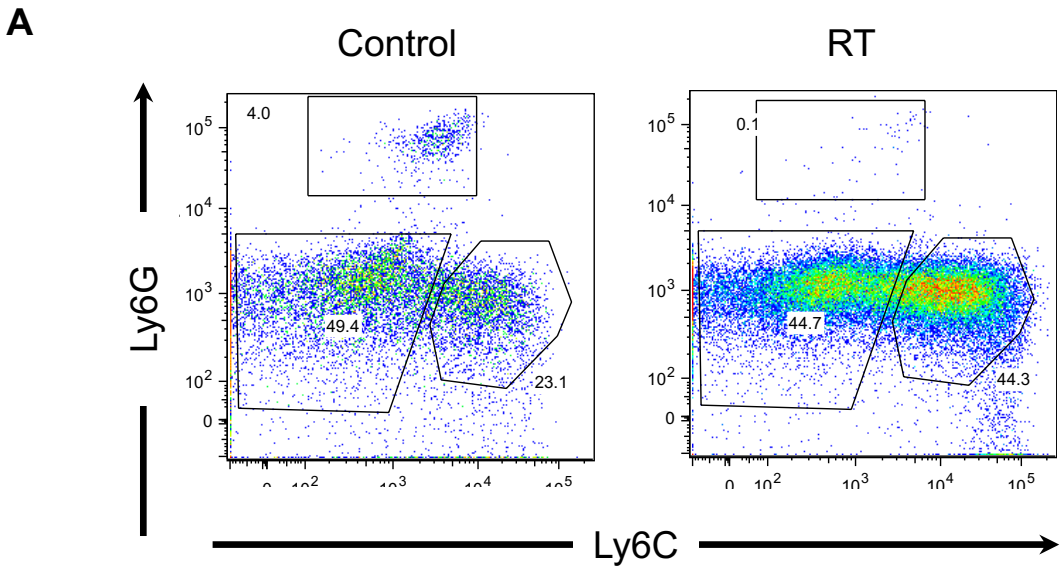


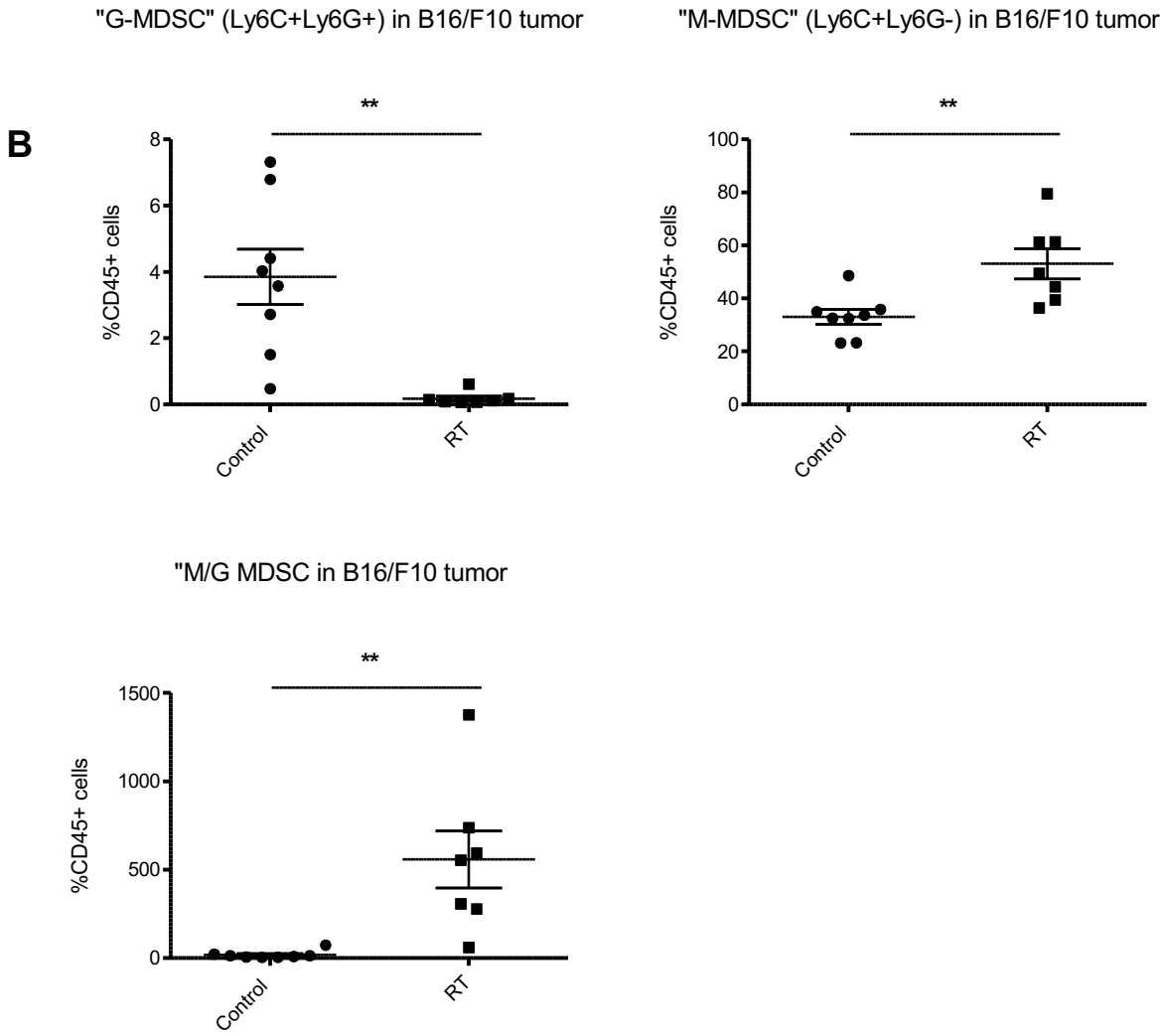


**Supplementary Figure III- 20: RT decreases G-MDSC (PMN-MDSC) population in B16/F10 tumor.**

## FIGURE LEGENDS FOR CHAPTER IV

**Figure IV-1: Volcano Plots for TIL Treg vs PBMC Controls.**

Volcano plot comparing the log odds versus log FC (fold-change) for genes from TIL-Treg relative to PBMC CD4 naïve cells (A), PBMC CD4 activated cells (B), and PBMC Treg.

**Figure IV-2: Genes differently expressed in TIL-Treg from prostate cancer patients RNAseq data**

Scatter plots of RNA expressions represented by FPKM for CCR4, CCR6, METRNL, RGS16, FUT7, FUT9, SLC1A2, FGL2 from RNAseq of prostate cancer patients. N = 12 (High Grade: Gleason Grade $\geq$ 4+3; N=6, Low Grade: Gleason Grade $\leq$ 4+3; N=6). ***: $p < 0.001$, **: $p < 0.01$, *: $p < 0.05$, determined by unpaired Student's t-test.

**Figure IV-3: Downregulation of DUSP1 upon activation despite its high expression in Treg, with the reciprocal expression pattern with DUSP4.**

(A-C) Scatter plots of RNA expressions represented by FPKM for DUSP1 and DUSP4 expression in CD4 T cells from RNAseq of multiple tumor types; (A) prostate cancer, (B) glioblastoma, and (C) renal cell carcinoma. N = 12, 8, 6, respectively. (D-E) Confirmation by qPCR for DUSP1 and DUSP4 in human and mouse; Fold change from Treg population. (D) qPCR of healthy donor PBMC (Leukopak) (D) qPCR of corresponding T cell populations from spleens of GFP-Foxp3 mouse. (D-E) qPCR were performed in triplicates, repeated X2-3. ***: $p < 0.001$, **: $p < 0.01$, *: $p < 0.05$, determined by one-way ANOVA, followed by Dunnett's test.

**Figure IV-4: Expression patterns of DUSP1 and DUSP4 in CD8 populations.**

(A-C) Scatter plots of RNA expressions represented by FPKM for DUSP1 and DUSP4 expression in CD8 T cells from RNAseq of multiple tumor types; (A) prostate cancer, (B) glioblastoma, and (C) renal cell carcinoma. N = 12, 8, 6, respectively. (D, E) Confirmation by qPCR for DUSP1 and DUSP4 in human and mouse; Fold change from naïve CD8 T cell. (D) qPCR of healthy donor PBMC (Leukopak). (E) qPCR of corresponding T cell populations from spleens of GFP-Foxp3 mouse. (D-E) qPCR were performed in triplicates, repeated X2-3. ***: $p < 0.001$, **: $p < 0.01$, *: $p < 0.05$, determined by one-way ANOVA, followed by Dunnett's test.

**Figure IV-5: Selectively higher expression of RGS1 in TIL.**

(A-C) Scatter plots of RNA expressions represented by FPKM for RGS1 expression in CD4 and CD8 T cells from RNAseq of multiple tumor types; (A) prostate cancer, (B) glioblastoma, and (C) renal cell carcinoma. N = 12, 8, 6, respectively. (D, E) Confirmation by qPCR for RGS1 in human and mouse; relative expression to house-keeping genes (18S). (E) qPCR of healthy donor PBMC (Leukopak). (D) qPCR of corresponding T cell populations from spleens of GFP-Foxp3 mouse. (D-E) qPCR were performed in triplicates, repeated X2-3. ***: $p < 0.001$, **: $p < 0.01$, *: $p < 0.05$, determined by one-way ANOVA, followed by Dunnett's test.

**Figure IV-6: Gene-targeting strategies for the generation of conditional DUSP1 or RGS1 knockout mice.**

(A) LoxP variant sites were introduced flanking exon 2 of *Dusp1* gene. Those mice were crossed to FlpE-expressing mice for neo removal. After making them homozygous for floxed alleles, those mice will be crossed to Cre-expressing mice to generate the knockout allele with a deletion of exon 2. (B) LoxP variant sites were introduced flanking exon 3 of *Rgs1* gene. Those mice were crossed to FlpE-expressing mice for neo removal. After making them homozygous for floxed alleles, those mice will be crossed to Cre-expressing mice to generate the knockout allele with a deletion of exon 3. (Ozgene)

**SUPPLEMENTARY FIGURE LEGENDS FOR CHAPTER IV:**

**Supplementary Figure IV-1: Gating strategies for the sorting for RNAseq and qPCR.**

Representative Gating strategies of human PBMC and TIL for CD4 populations (A) and CD8 populations (B). The following population were sorted out: PBMC CD4 naïve ($CD4^+CD25^{Low}CD127^{+/-}CCR7^+CD45RA^+CD27^+CD28^+$), PBMC CD4 regulatory T cell (Treg)($CD4^+CD25^{Hi}CD127^{Low}$), PBMC CD8 naïve ($CD8^+CD45RA^+CD45RO^-CD27^+CD28^+$), PBMC CD8 antigen experienced ($CD8^+$ $CD45RA^-CD45RO^+$), TIL CD4 regulatory T cell ($CD4^+CD25^{Hi}CD127^{Low}$) and TIL CD8 antigen experienced ($CD8^+CD45RA^-CD45RO^+$). PBMC CD4 naïve and PBMC CD8 naïve (both from fresh and frozen samples) were activated ex-vivo using anti-CD3/anti-CD28 activation beads for 72 hours.

(*Flow images for Supplementary Figure IV-1 were modified from Nirschl, Muroyama, Drake et al.)

**Supplementary Figure IV-2: qPCR for DUSP1 and DUSP4 in human with TIL-Treg.**

(D, E) qPCR of healthy donor PBMC (Leukopak) and of RNA extracted from renal cell carcinoma TIL-Treg. RNA expression, relative expression to house-keeping genes (18S) for DUSP1 (D) and DUSP4 (E), respectively. qPCR were performed in triplicates.

**Supplementary Figure IV-3: qPCR for DUSP1 and DUSP4 in B16/F10-bearing GFP-Foxp3 mice.**

(A) Gating strategies for the isolation of naïve CD4/8 T cells, antigen-experienced CD8 T cells and Treg from spleens and tumors of B16/F10-bearing GFP-Foxp3 mice. Representative images from tumor samples are shown. (B-M) q Confirmation by qPCR for DUSP1 (B-D), DUSP4 (E-G), RGS1 (H-J), and RGS16 (K-M). PCR of corresponding T cell populations from spleens and TIL of B16/F10-bearing GFP-Foxp3 mouse. (B, E, H, K) Overview, relative expression to house-keeping genes (18S), (C, F, I, L) Fold change expression from naïve CD4 T cells, (D, G, J, M) Fold change expression from naïve CD8 T cells. qPCR were performed in triplicates. ***: $p < 0.001$, **: $p < 0.01$, *: $p < 0.05$, determined by one-way ANOVA, followed by Dunnett's test. (Note: CT value for TIL-derived or DLN-derived samples were high (>34), which made the data preliminary.)

**Supplementary Figure IV-4: Investigating the roles of DUSP1/4 and RGS1 *in vitro*.**

(A) Experimental design (plan). Human PBMC (Leukopak) were transfected with siRNA oligos via electropolation, then Treg were isolated, followed by *in vitro* suppression assay. (B) Time course of Foxp3 knockdown for different siRNA oligos

(Foxp3-1, 2, 3). (C) Expression of RNA 24 hours post siRNA transfection for different oligos (DUSP1: D1-1,2, DUSP4: D4-1,2, RGS1: R-1,2,3, Helios: H1-1, 2, 3). (D-E) In vitro micro-suppression assay using human PBMC (LeukoPak). (D) Representative figure of the *in vitro* suppression assay (preliminary). Tresponder cells (naïve CD8 T cells: 2000 / well) were analyzed for their proliferation based on the dilution of CTV dye. (B) Quantitative plots represent percent suppression at the indicated Treg:T responder ratio. A representative experiment of a total of three independent replicates is shown. (N = 3 per group, repeated 2x.) % Suppression = (1-(DI of the sample)/(DI of the average of "No Treg"))*100 (*DI=division index).

(Note: (A-C): Summer rotation medical student Victoria Huang (my mentee).)

# FIGURES FOR CHAPTER IV

# Figures Human TIL-Treg part

Yuki Muroyama

# Figure IV-1

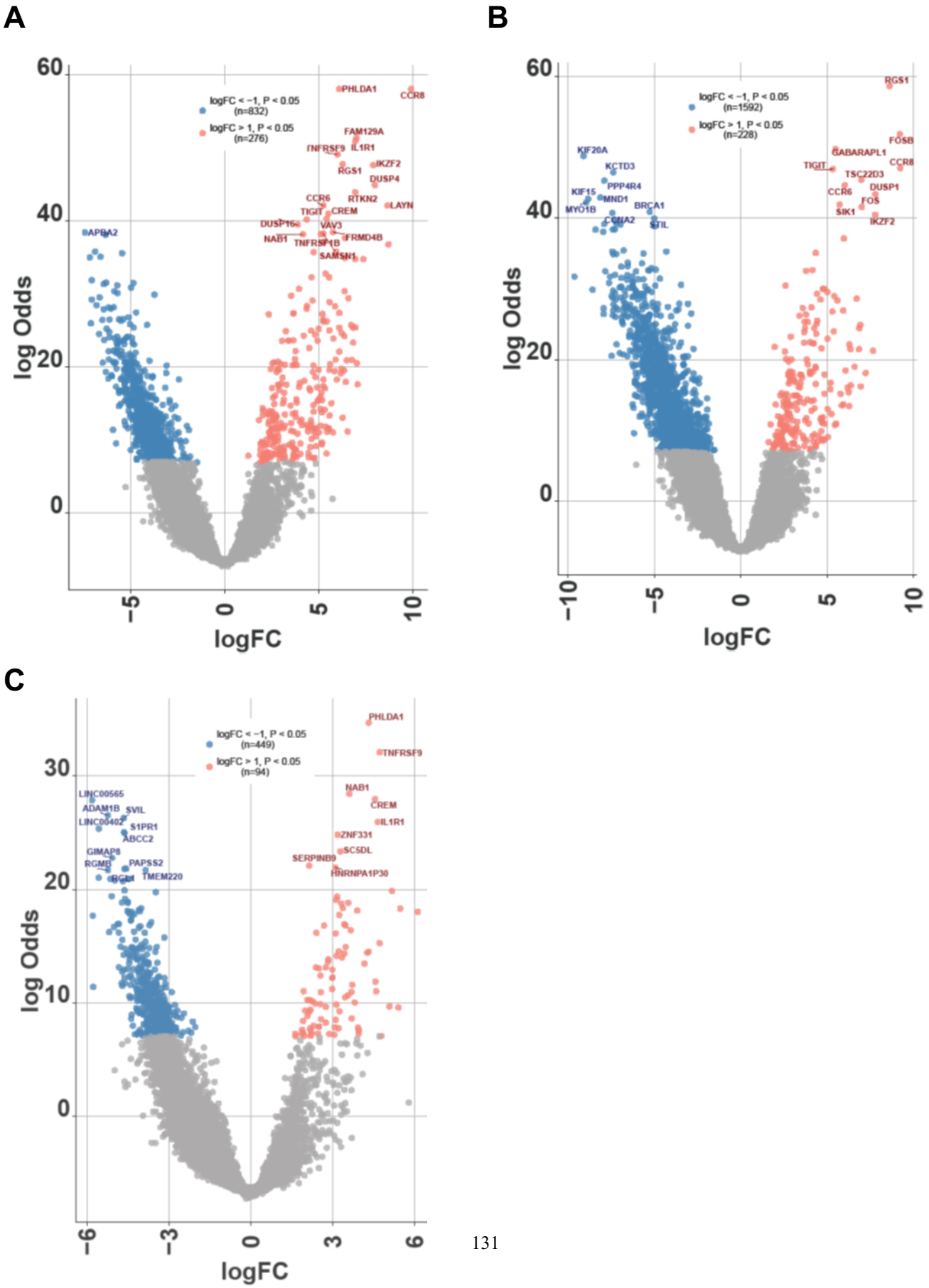
A
logFC < −1, P < 0.05
(n=832)
logFC > 1, P < 0.05
(n=276)
PHLDA1
CCR8
FAM129A
TNFRSF9
IL1R1
IKZF2
RGS1
DUSP4
CCR6
RTKN2
LAYN
TIGIT
CREM
DUSP16
VAV3
APBA2
NAB1
TNFRSF1B
FRMD4B
SAMSN1
log Odds
logFC
B
logFC < −1, P < 0.05
(n=1592)
logFC > 1, P < 0.05
(n=228)
RGS1
FOSB
KIF20A
GABARAPL1
KCTD3
TIGIT
CCR8
TSC22D3
PPP4R4
KIF15
CCR6
DUSP1
MND1
MYO1B
BRCA1
FOS
SIK1
CCNA2
STIL
IKZF2
log Odds
logFC
C
logFC < −1, P < 0.05
(n=449)
logFC > 1, P < 0.05
(n=94)
PHLDA1
TNFRSF9
NAB1
LINC00565
CREM
ADAM1B
SVIL
IL1R1
LINC00402
S1PR1
ZNF331
ABCC2
SC5DL
GIMAP8
SERPINB9
RGMB
PAPSS2
HNRNPA1P30
BCL11
TMEM220
log Odds
logFC

# Figure IV-2

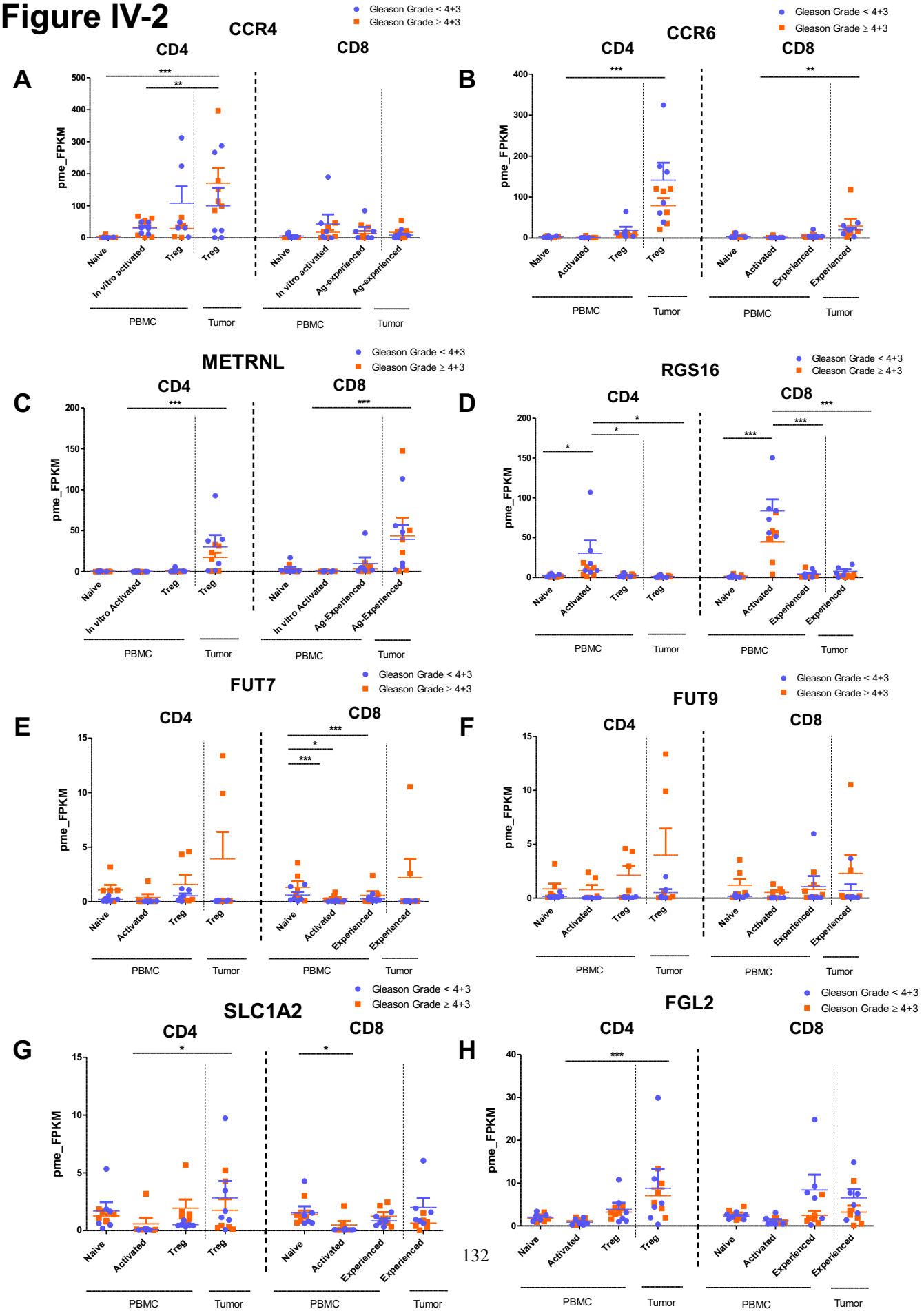
A
CCR4
CD4
CD8
Gleason Grade < 4+3
Gleason Grade ≥ 4+3
pme_FPKM
Naive
In vitro activated
Treg
Treg
In vitro activated
Ag-experienced
Ag-experienced
PBMC
Tumor
B
CCR6
Activated
Experienced
C
METRNL
In vitro Activated
Ag-Experienced
D
RGS16
E
FUT7
F
FUT9
G
SLC1A2
H
FGL2

# Figure IV-3

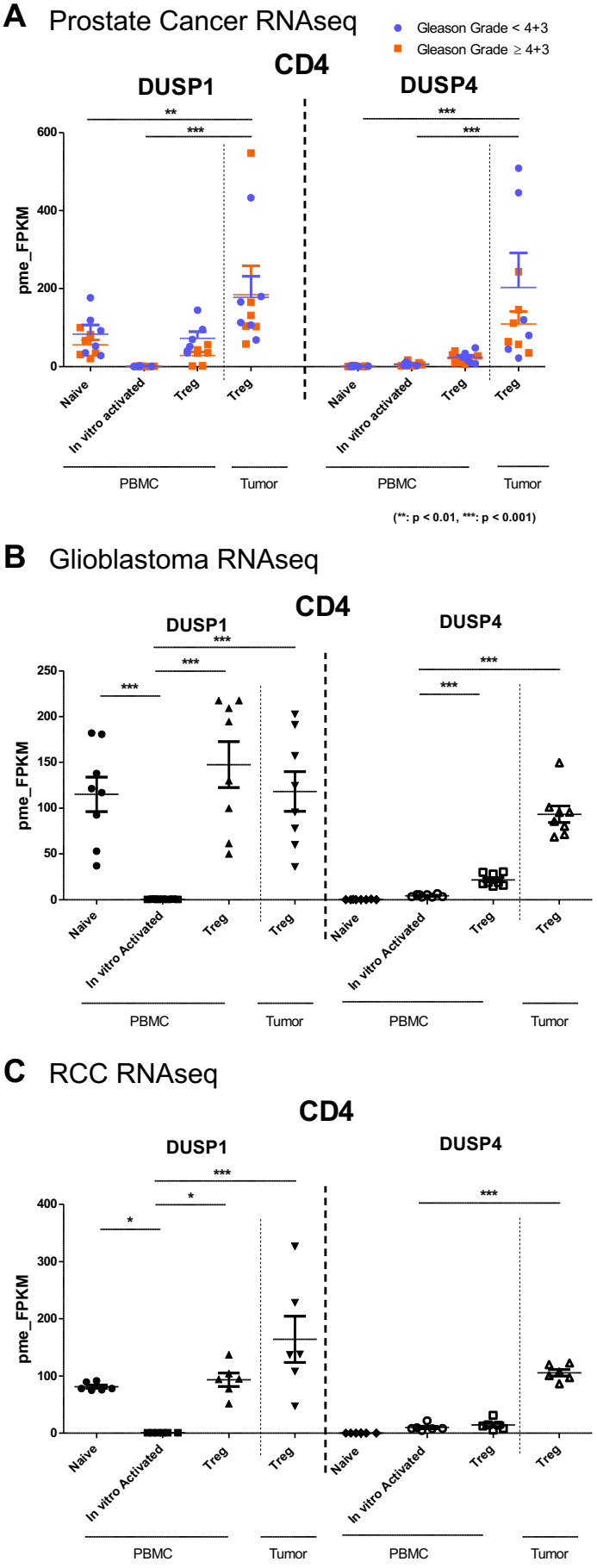
A Prostate Cancer RNAseq
Gleason Grade < 4+3
Gleason Grade ≥ 4+3
CD4
DUSP1
DUSP4
pme_FPKM
Naive
In vitro activated
Treg
Treg
PBMC
Tumor
(**: p < 0.01, ***: p < 0.001)
B Glioblastoma RNAseq
In vitro Activated
C RCC RNAseq

**Figure IV-3 Continued**

**D** Human qPCR (PBMC)

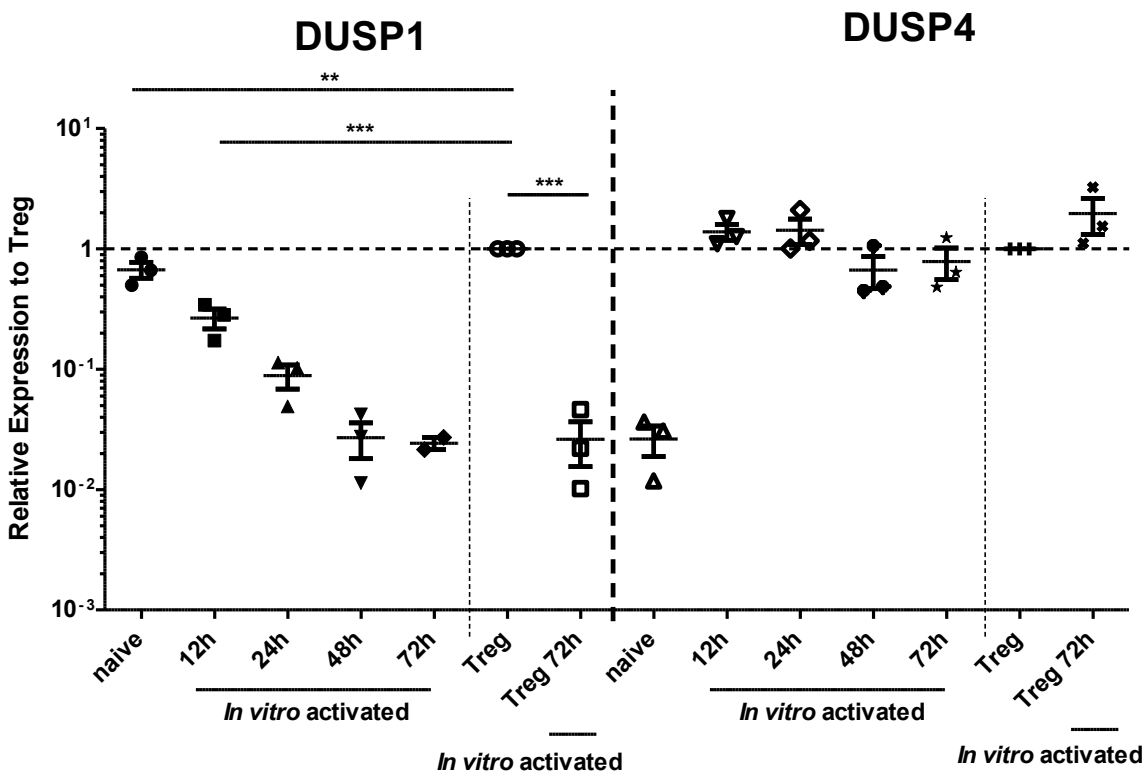


**E** Mouse qPCR (spleen)

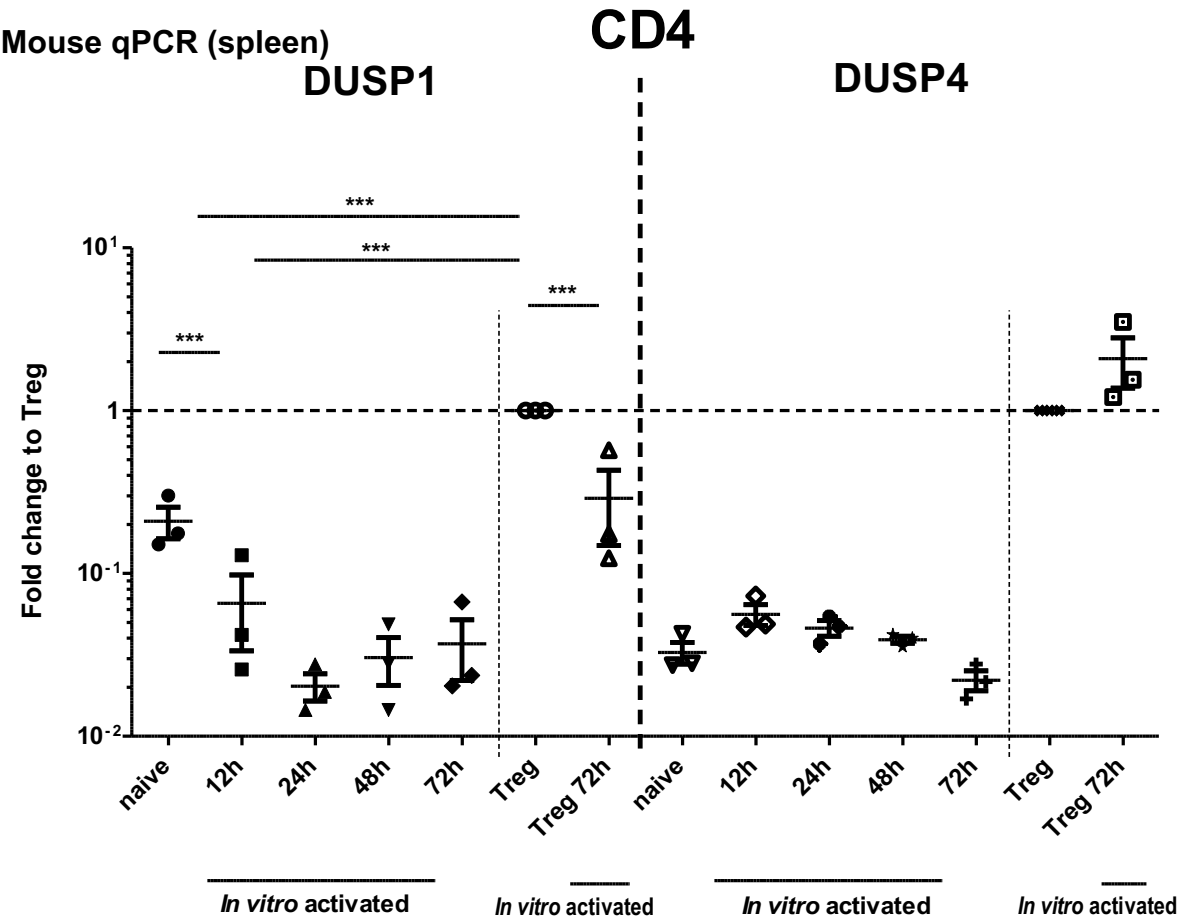

# Figure IV-4

**A** Prostate Cancer RNAseq

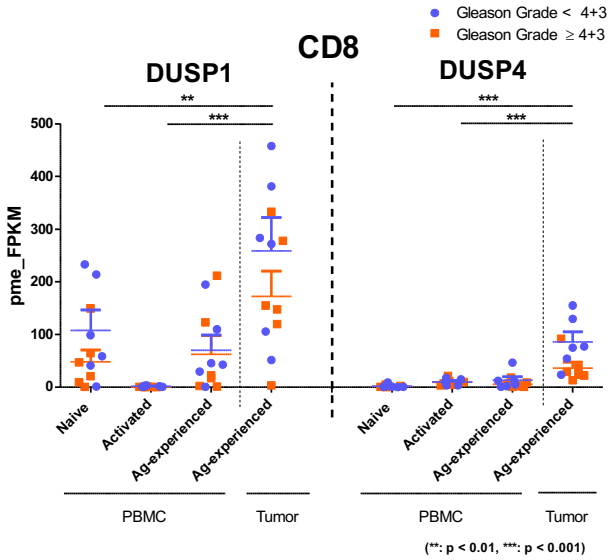


**B** Glioblastoma RNAseq

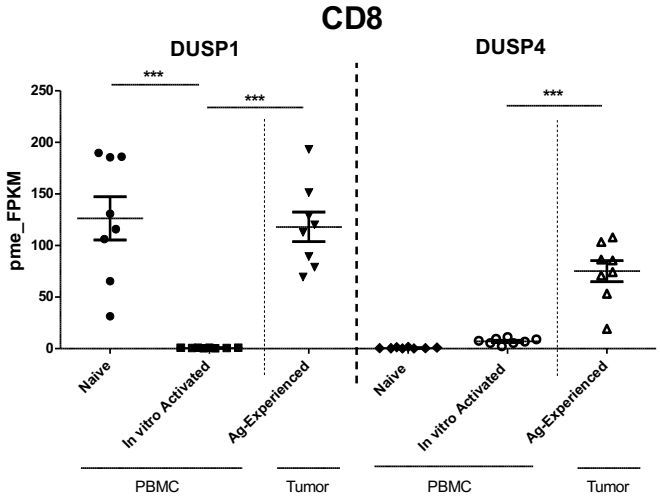


**C** RCC RNAseq

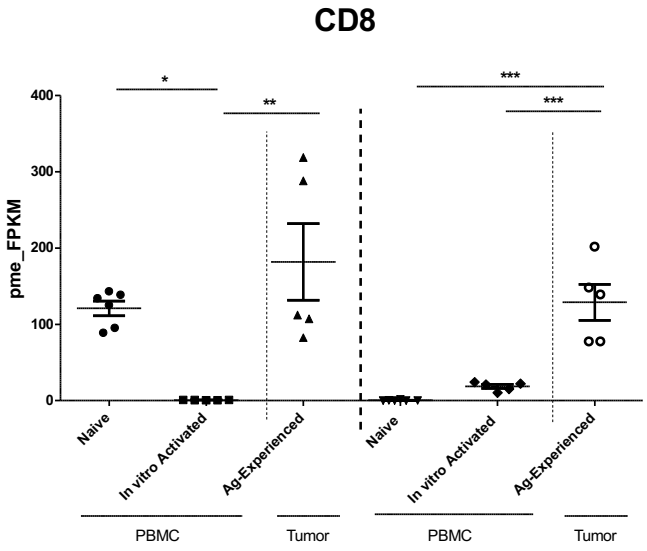

D Human qPCR (PBMC)

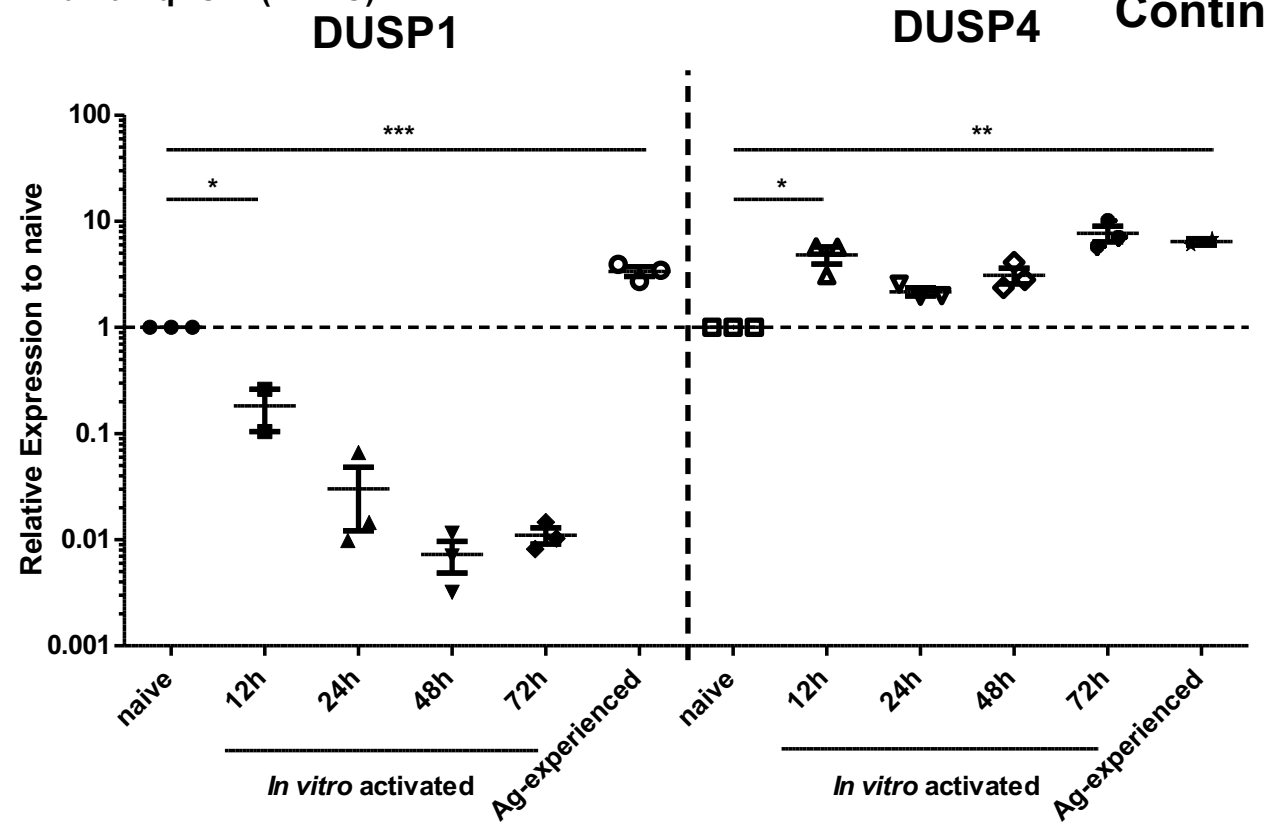


E Mouse qPCR (spleen)

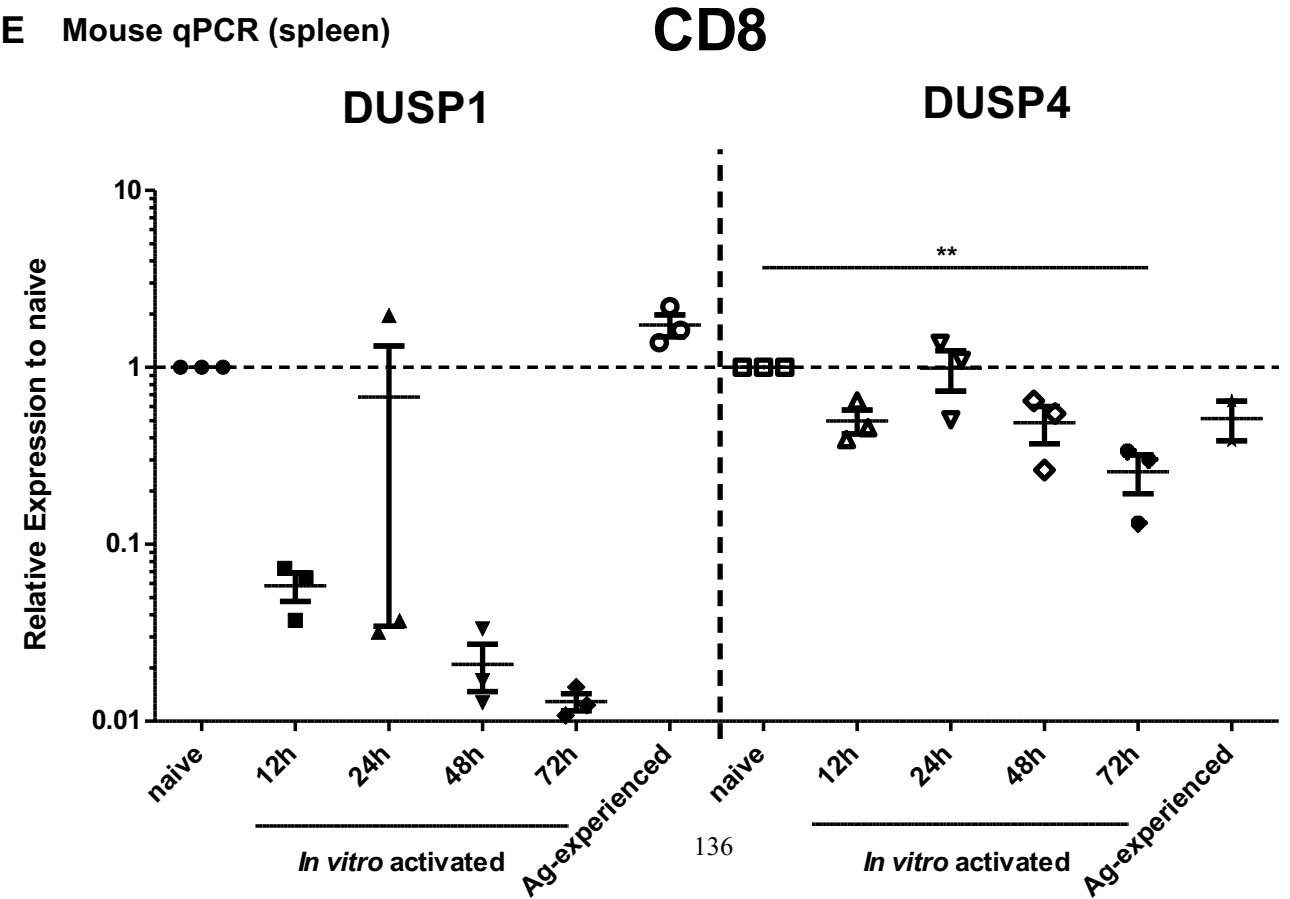

# Figure IV-5

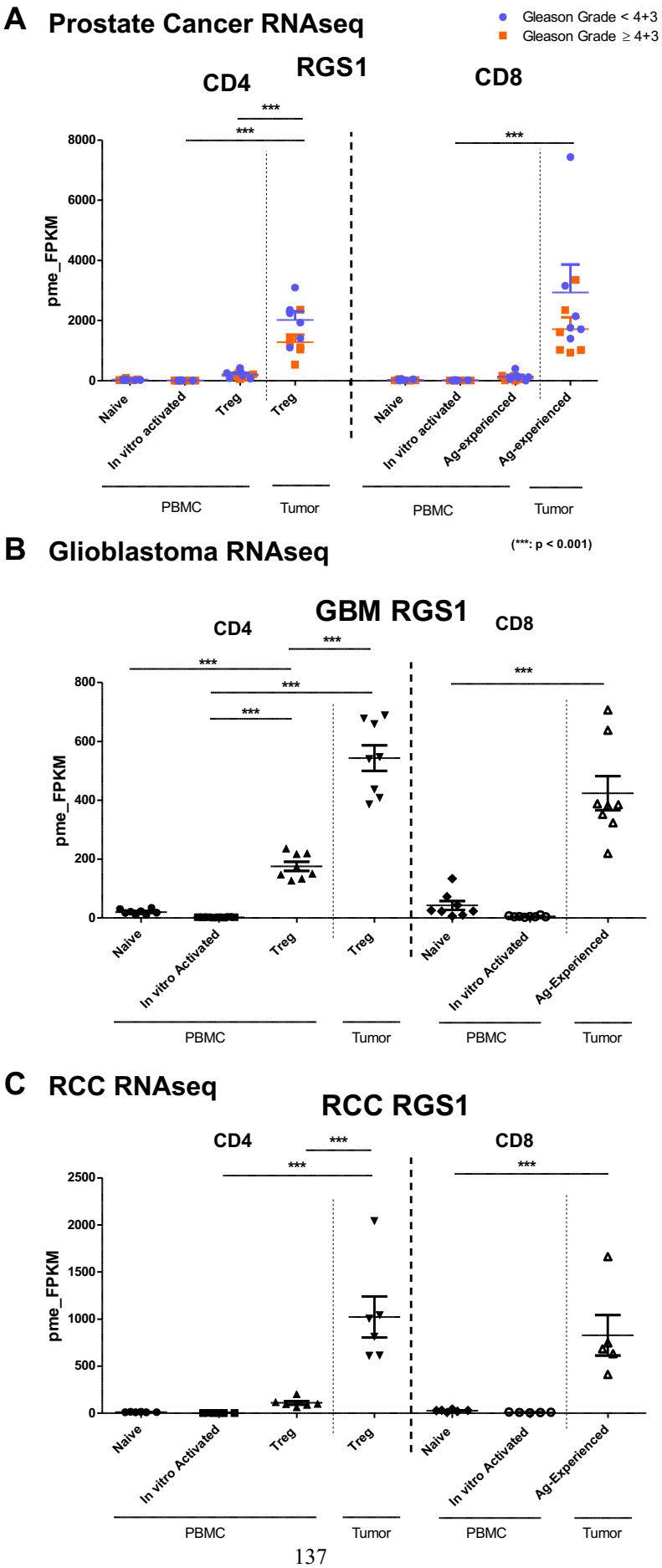
A Prostate Cancer RNAseq
Gleason Grade < 4+3
Gleason Grade ≥ 4+3
RGS1
CD4
CD8
pme_FPKM
8000
6000
4000
2000
0
***
Naive
In vitro activated
Treg
Treg
Naive
In vitro activated
Ag-experienced
Ag-experienced
PBMC
Tumor
PBMC
Tumor
(***: p < 0.001)
B Glioblastoma RNAseq
GBM RGS1
CD4
CD8
800
600
400
200
0
Naive
In vitro Activated
Treg
Treg
Naive
In vitro Activated
Ag-Experienced
PBMC
Tumor
PBMC
Tumor
C RCC RNAseq
RCC RGS1
CD4
CD8
2500
2000
1500
1000
500
0
Naive
In vitro Activated
Treg
Treg
Naive
In vitro Activated
Ag-Experienced
PBMC
Tumor
PBMC
Tumor

**Figure IV-5 Continued**

**D** Human qPCR (PBMC)

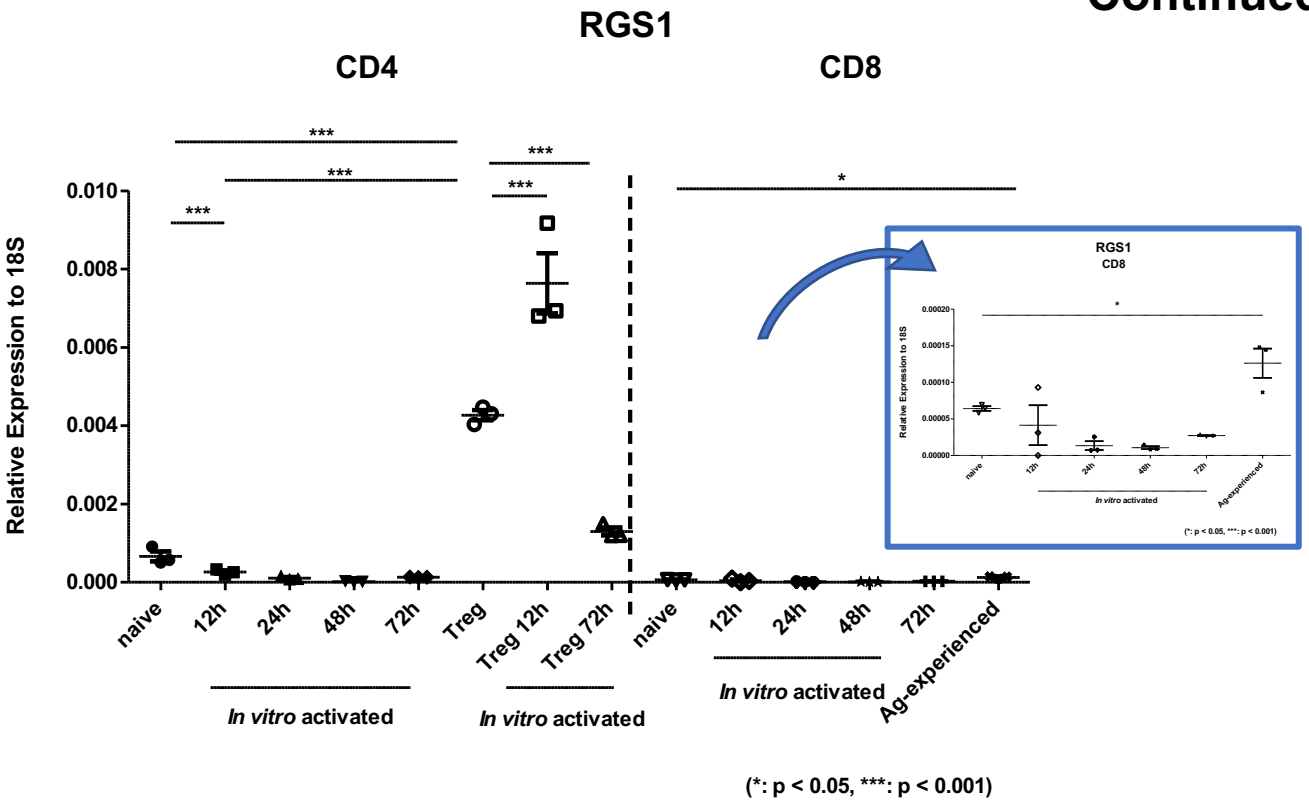


(*: $p < 0.05$, ***: $p < 0.001$)

**E** Mouse qPCR (spleen)

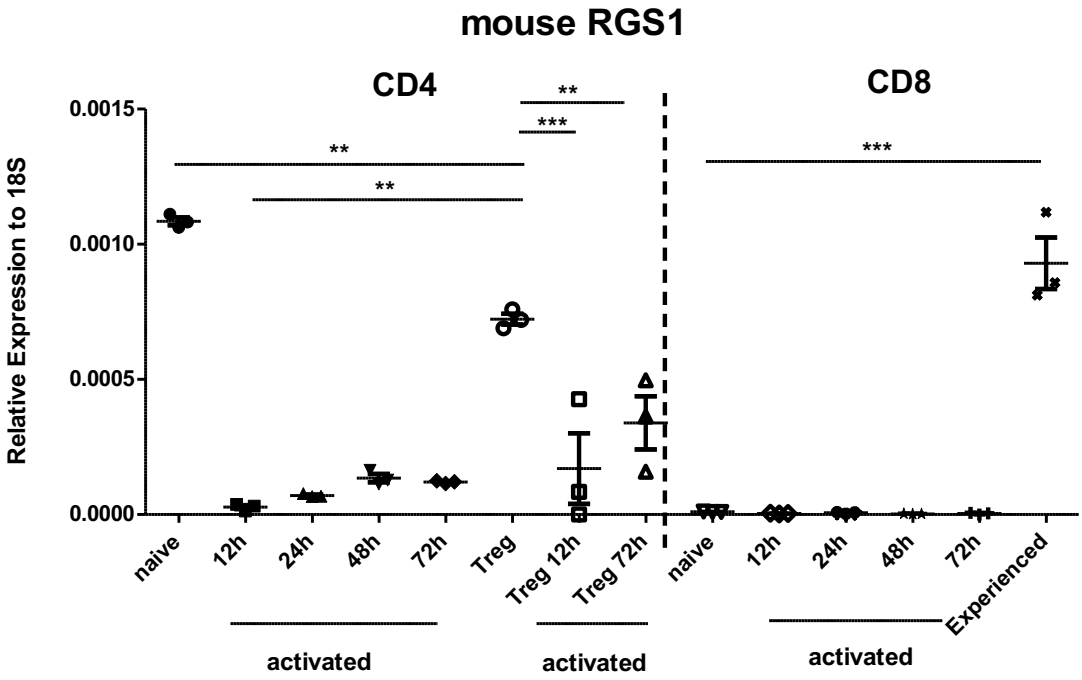

A

# Figure IV-6

Wildtype Locus of the Dusp1 Gene

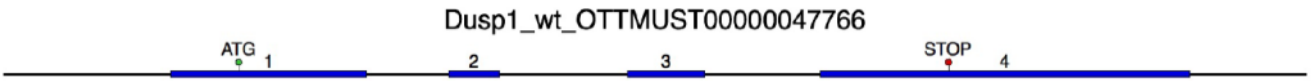


Gene Targeted Locus of the Dusp1 Gene

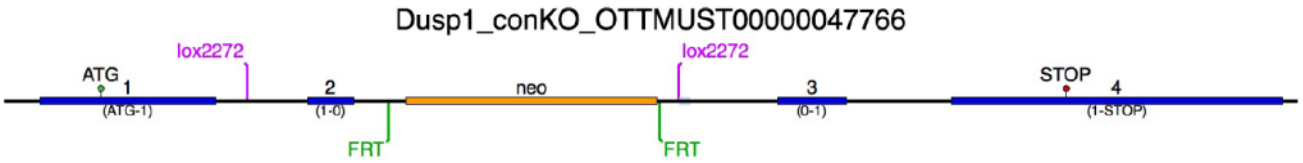


Gene Targeted Locus after flp mediated neo removal

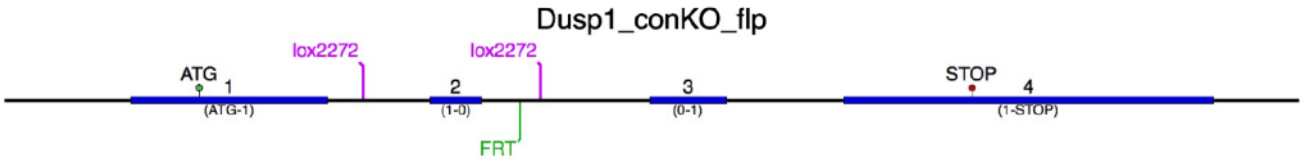


Gene Targeted Locus after Cre mediated deletion of exon 2

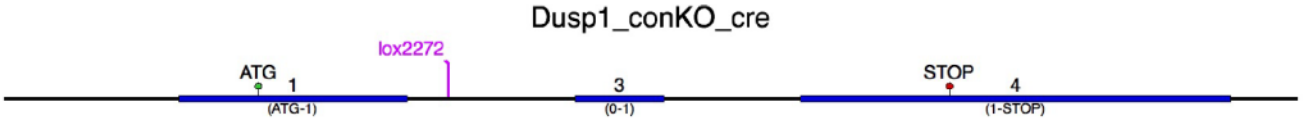


Figure IV-6: Gene-targeting strategy to create Dusp1 floxed mice.

B

**Figure IV-6 Continued**

Wildtype Locus of the Rgs1 Gene

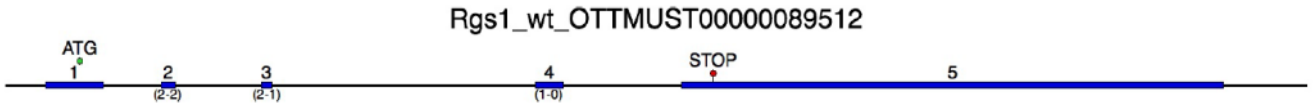


Gene Targeted Locus of the Rgs1 Gene

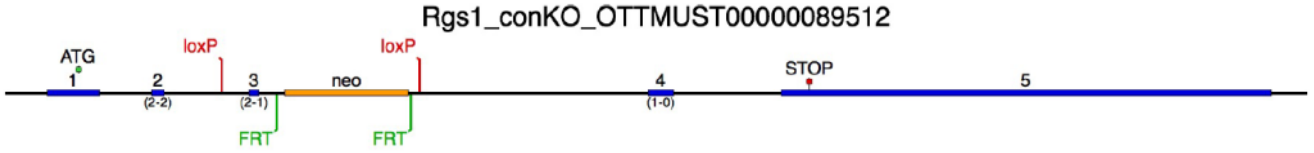


Gene Targeted Locus after flp mediated neo removal

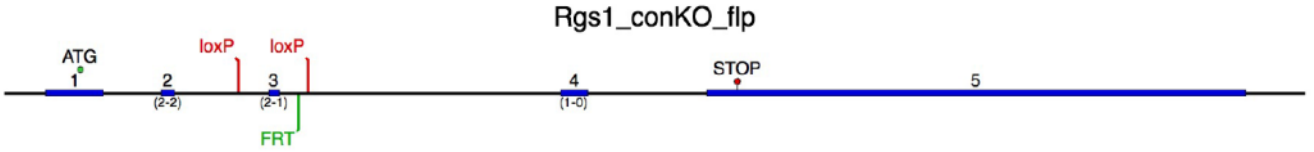


Gene Targeted Locus after Cre mediated deletion of exon 3

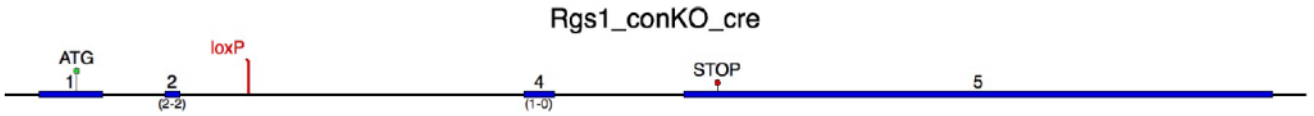


Figure IV-6: Gene-targeting strategy to create Rgs1 floxed mice.

# Supplementary Figures for Chapter IV:

# “Novel Treg-associated targets from human TIL”

**Supplementary Figure IV-1**

(A, B: modified from Nirschl, Muroyama, Drake et al.)

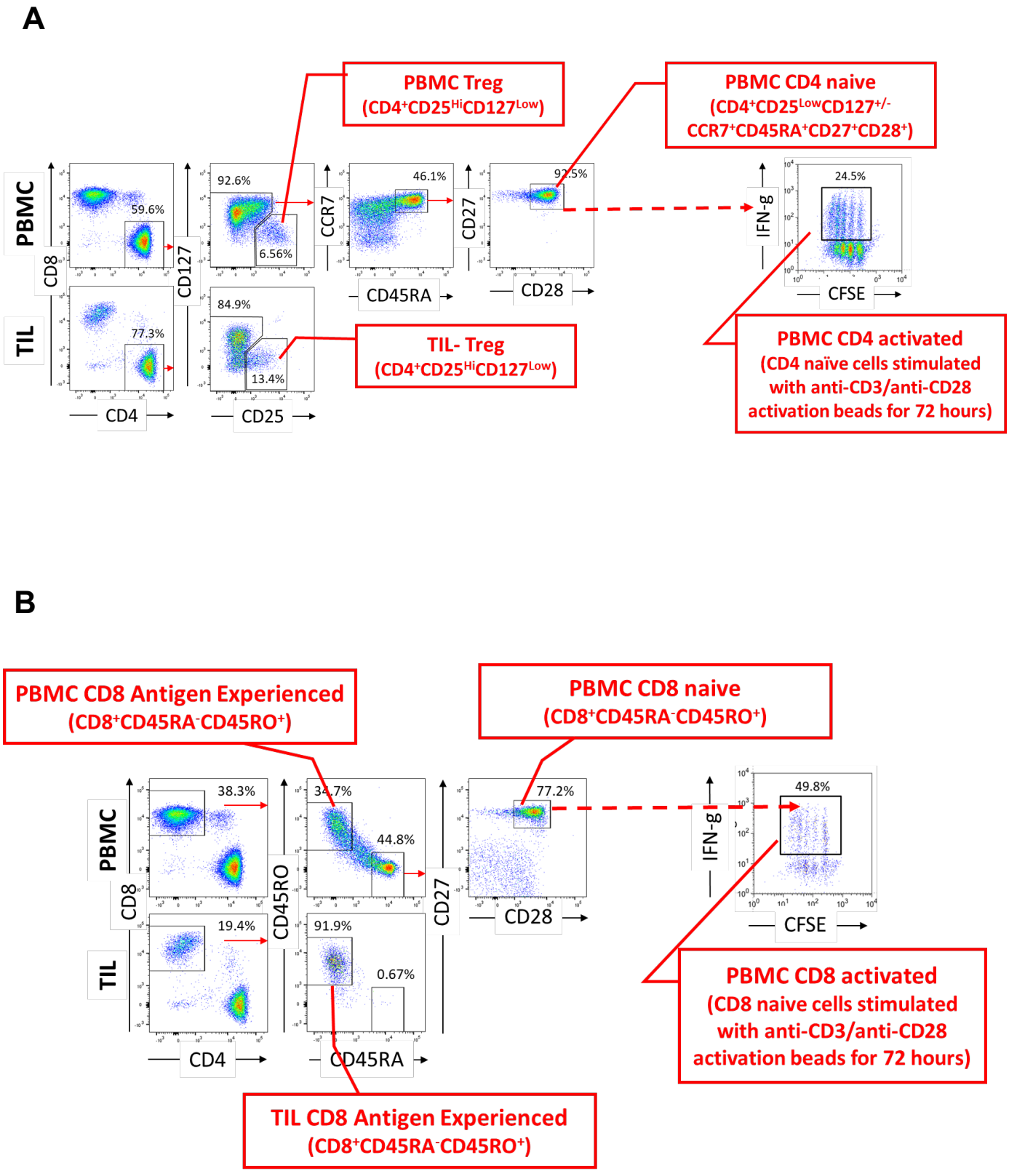

**A** Human qPCR (with tumor: prostate Ca sample not good)

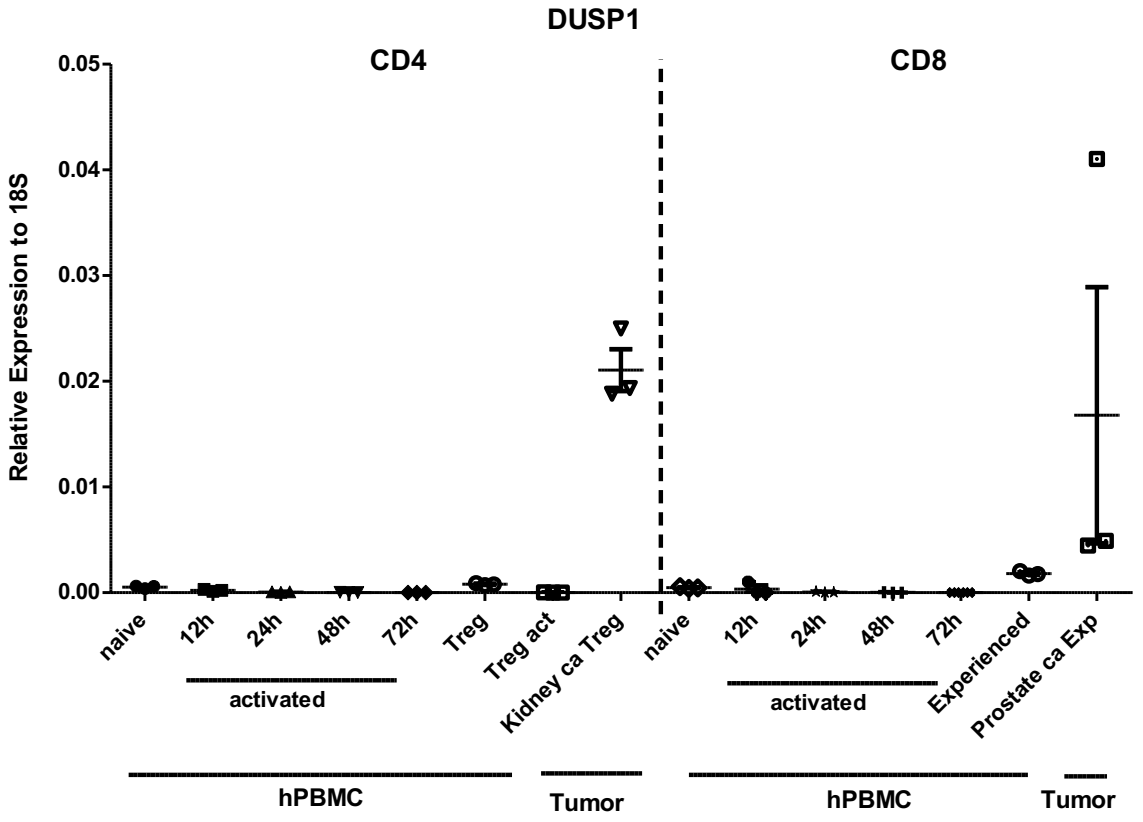


**B**

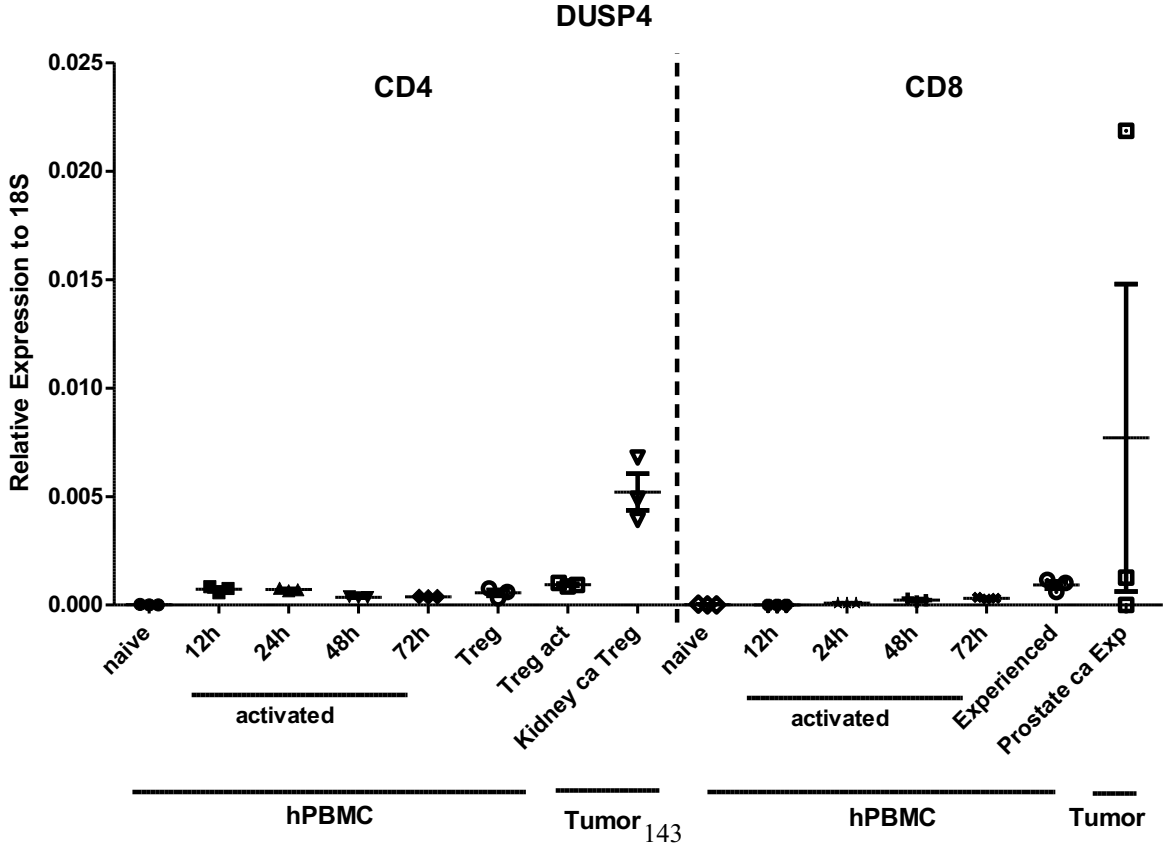

# A Gating strategies of tumor-bearing GFP-Foxp3 mouse

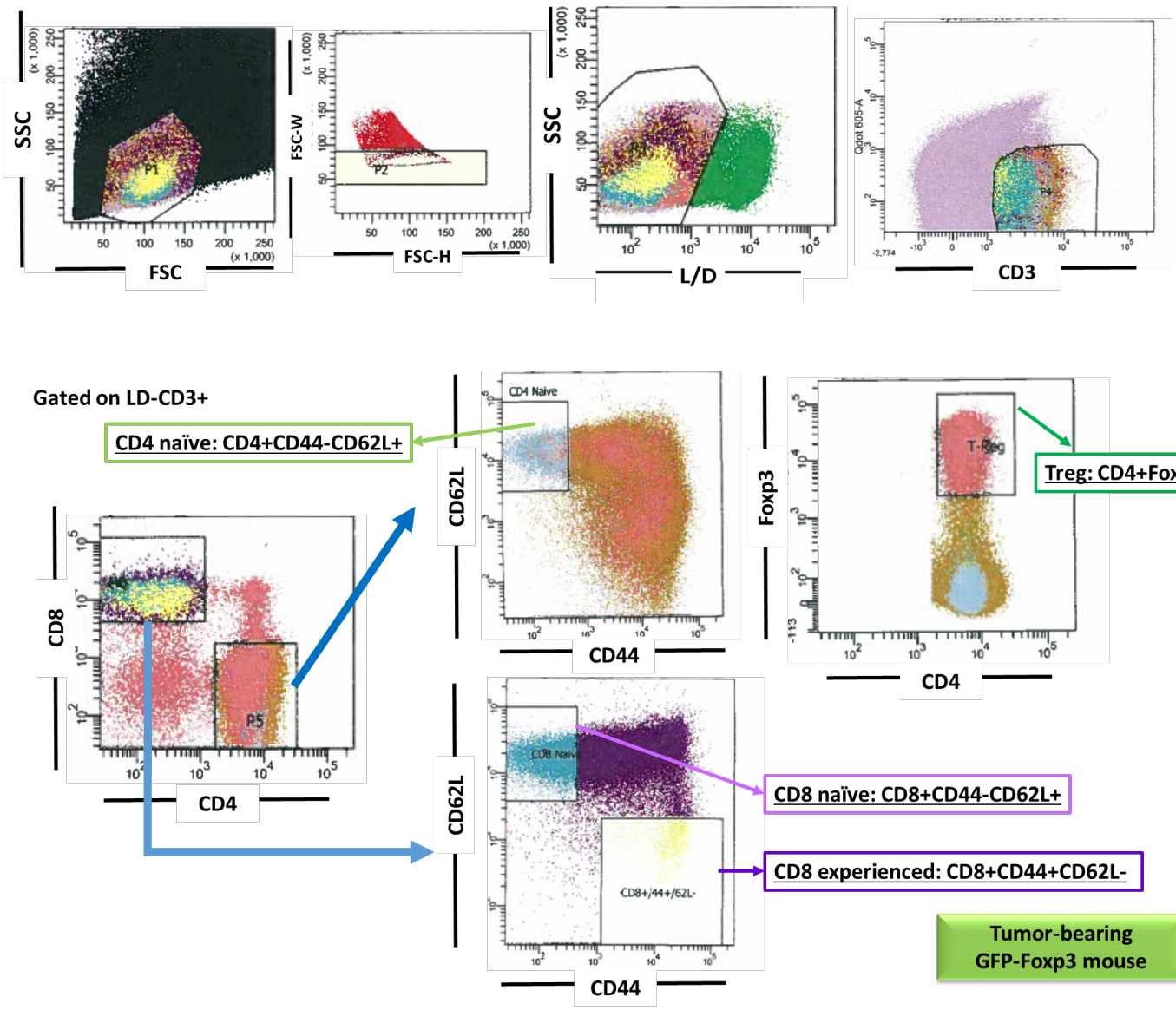

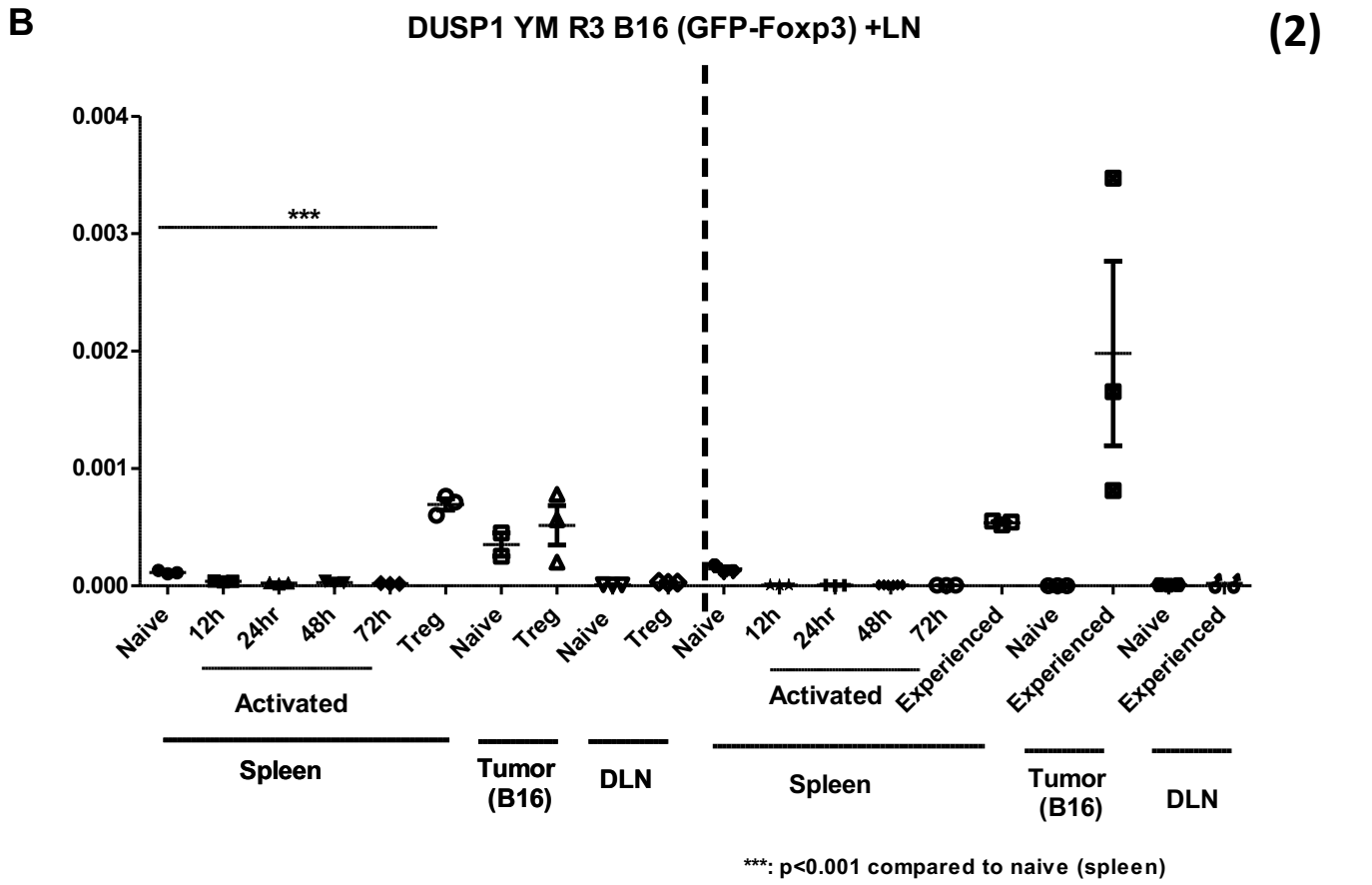


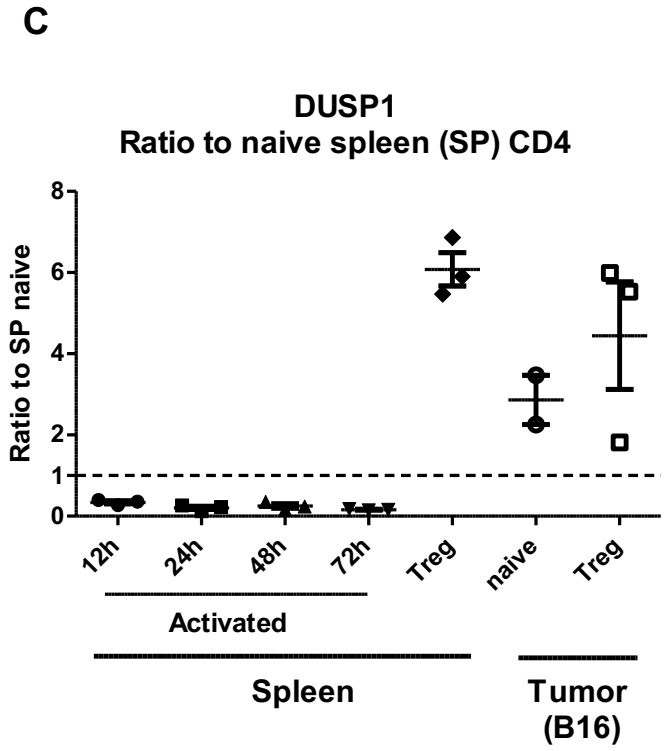


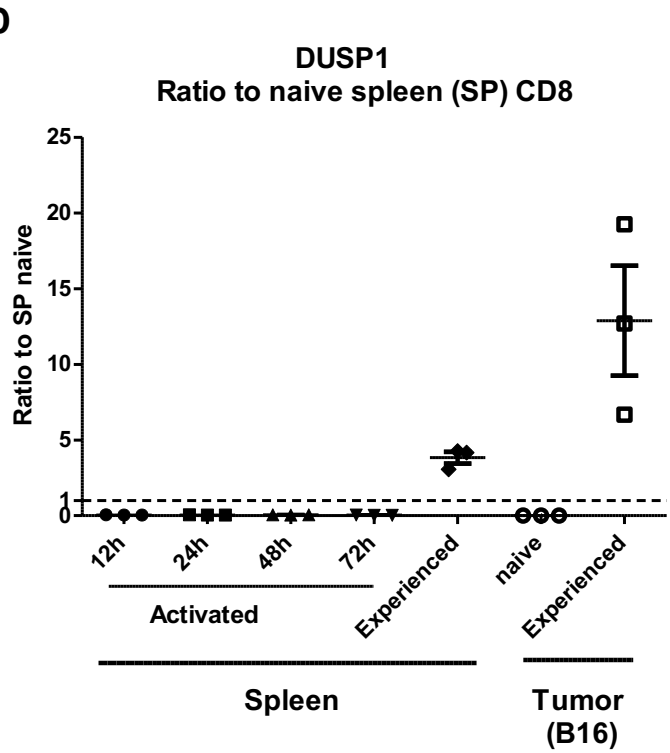




CT>34 in tumor

E

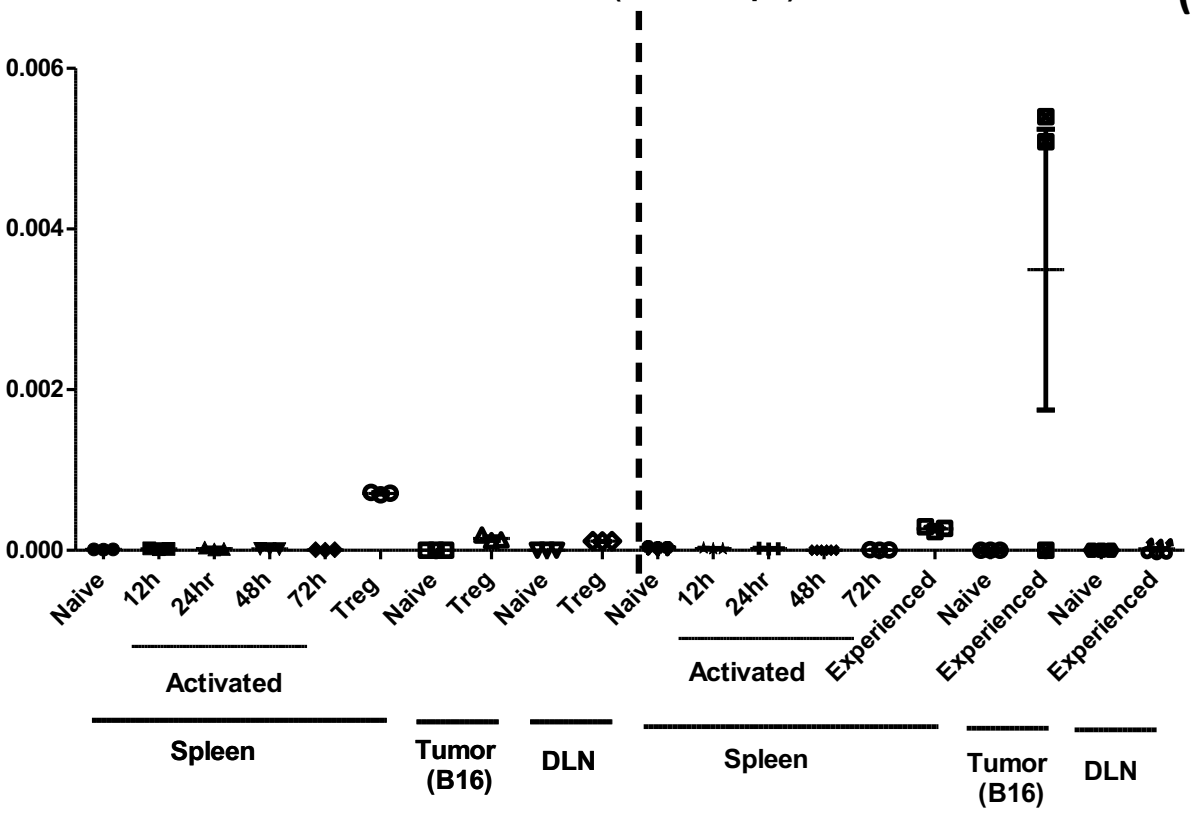
DUSP4 YM R3 B16 (GFP-Foxp3)+LN
0.006
0.004
0.002
0.000
Naive
12h
24hr
48h
72h
Treg
Naive
Treg
Naive
Treg
Naive
12h
24hr
48h
72h
Experienced
Naive
Experienced
Naive
Experienced
Activated
Activated
Spleen
Tumor (B16)
DLN
Spleen
Tumor (B16)
DLN

F

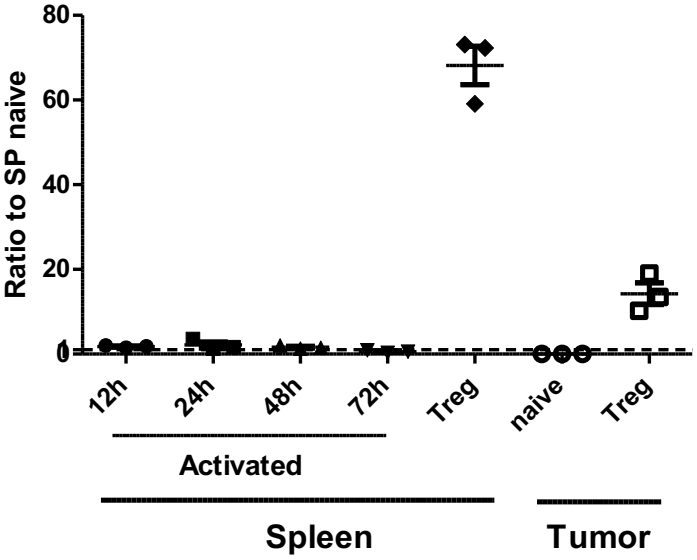
DUSP4
Ratio to naive spleen (SP) CD4
Ratio to SP naive
80
60
40
20
0
12h
24h
48h
72h
Treg
naive
Treg
Activated
Spleen
Tumor (B16)

G

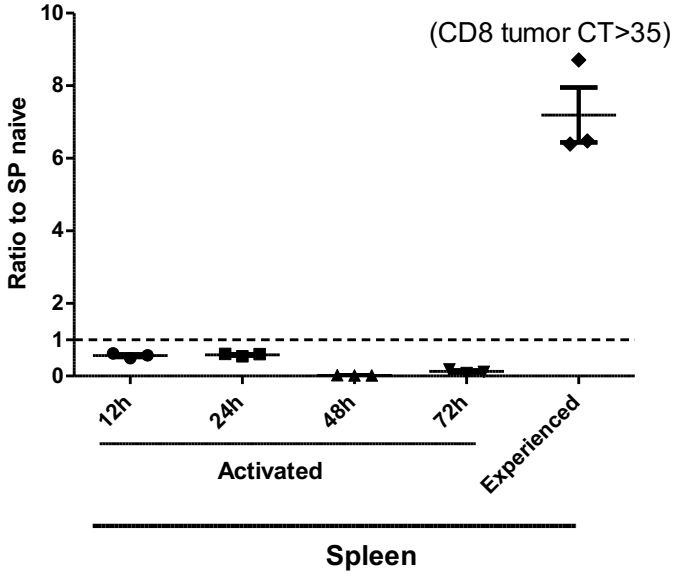
DUSP4
Ratio to naive spleen (SP) CD8
(CD8 tumor CT>35)
Ratio to SP naive
10
8
6
4
2
1
0
12h
24h
48h
72h
Experienced
Activated
Spleen

# Supplementary Figure IV-3 (4)

H

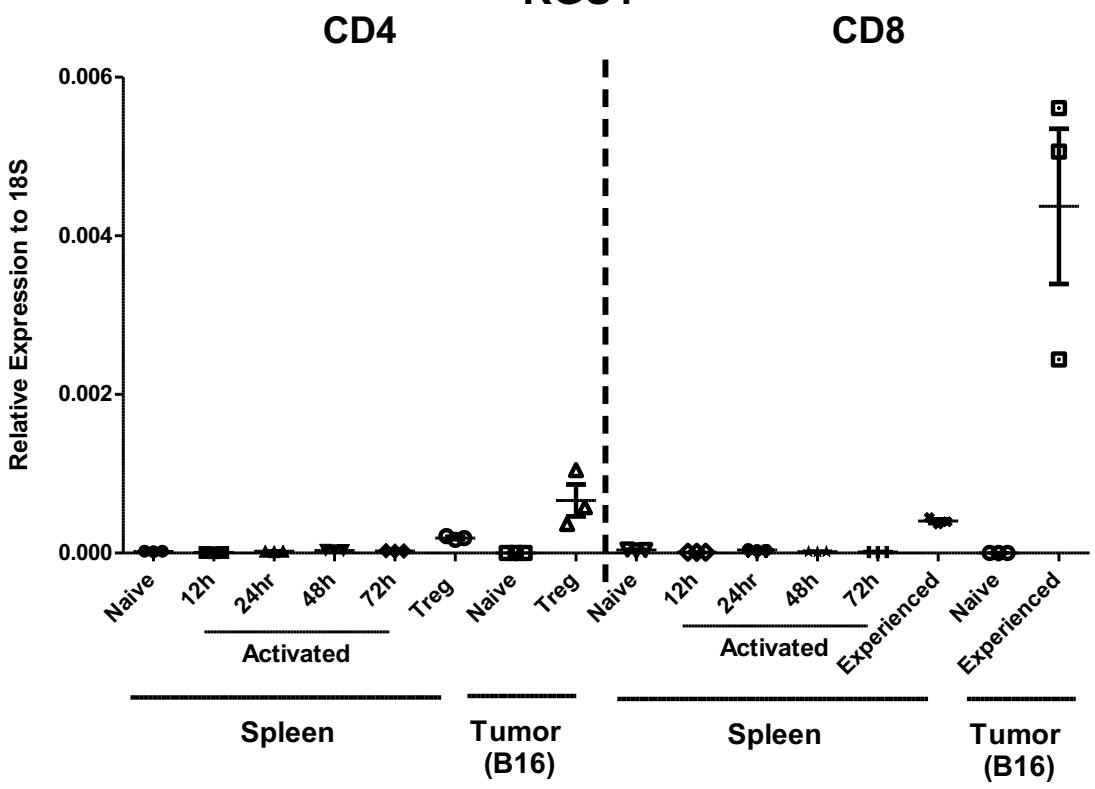


***: p<0.001, compared to naive (spleen)

I

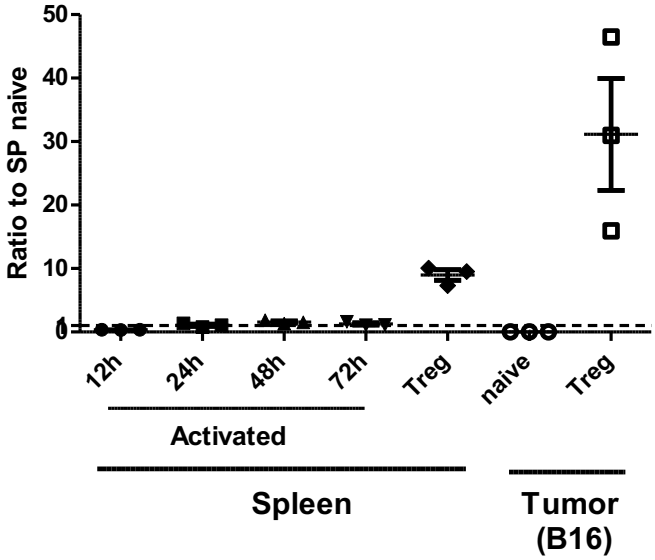


J

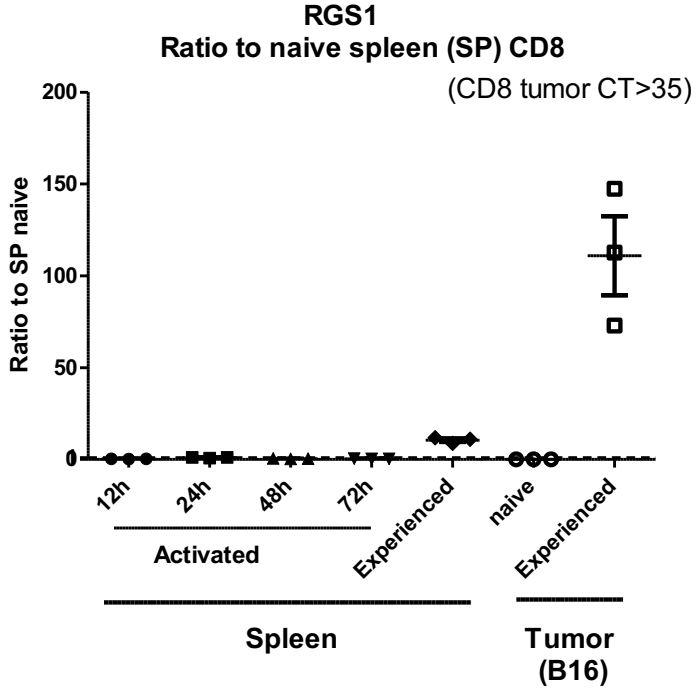




CT>34 in tumor

# Supplementary Figure IV-3 (5)

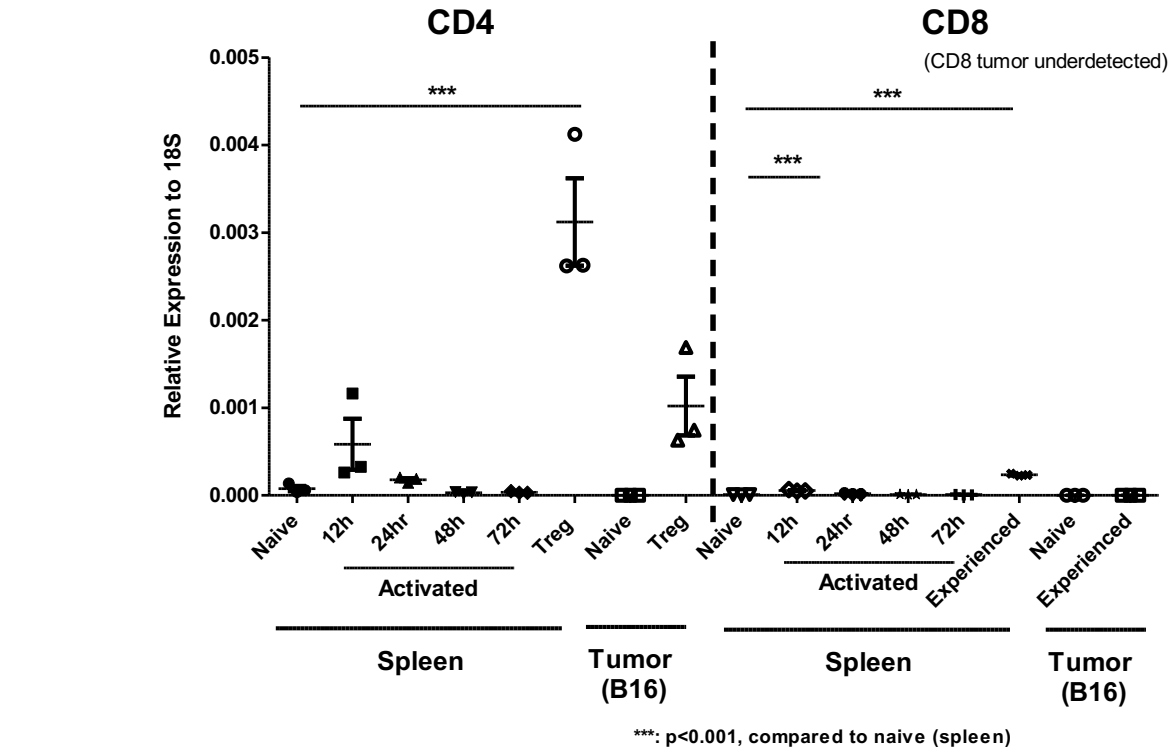


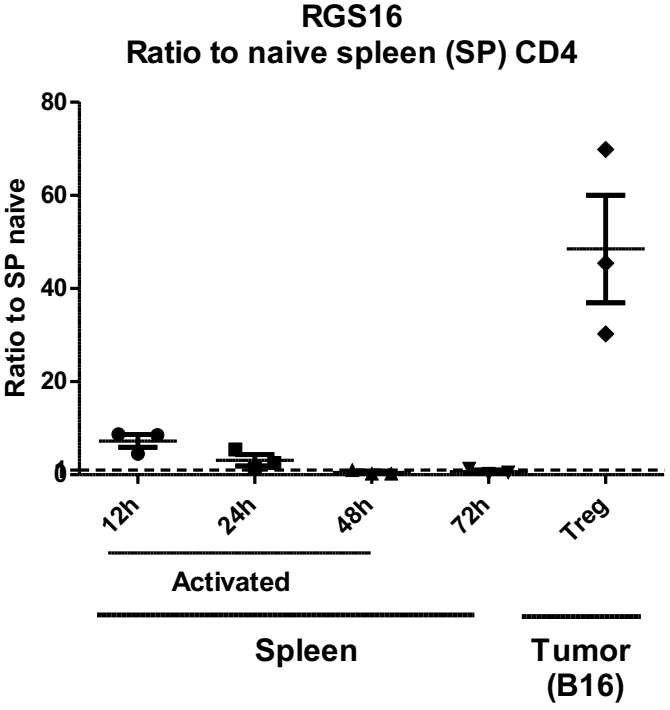


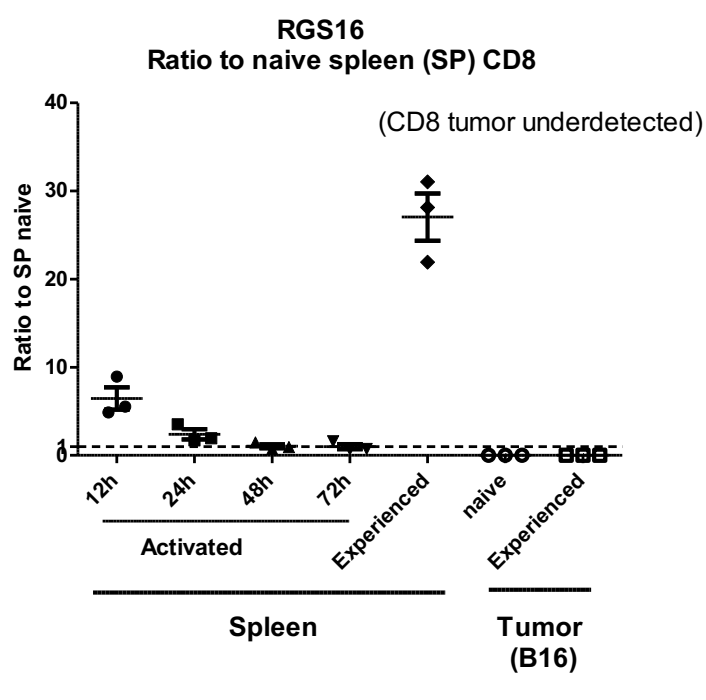




CT>34 in tumor

## Supplementary Figure IV-4

A-C: Victoria Huang: Summer rotation medical student (my mentee)

**A** Human PBMC (LeukoPak)

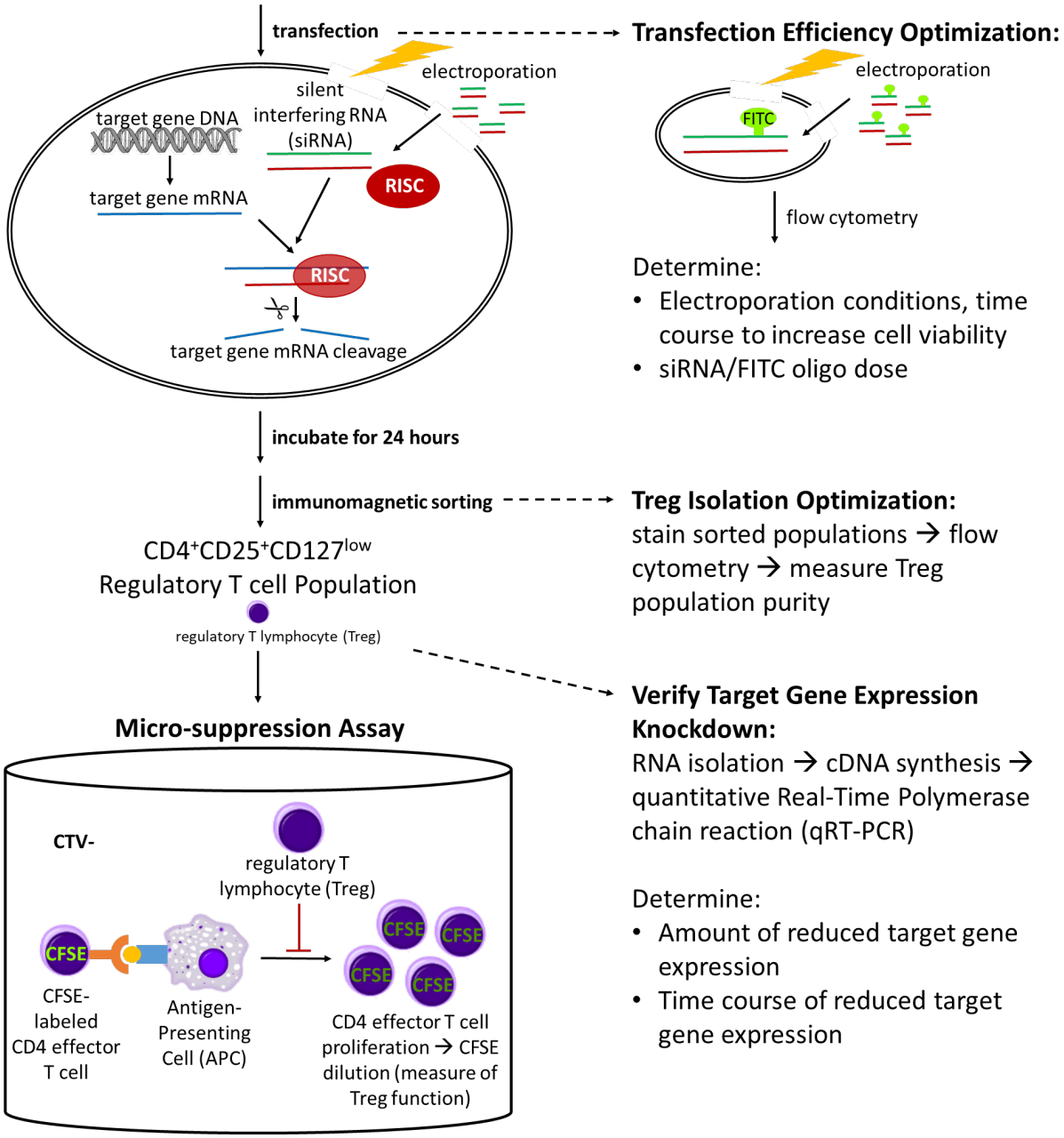

# Supplementary Figure IV-4 (Continued)

**B**

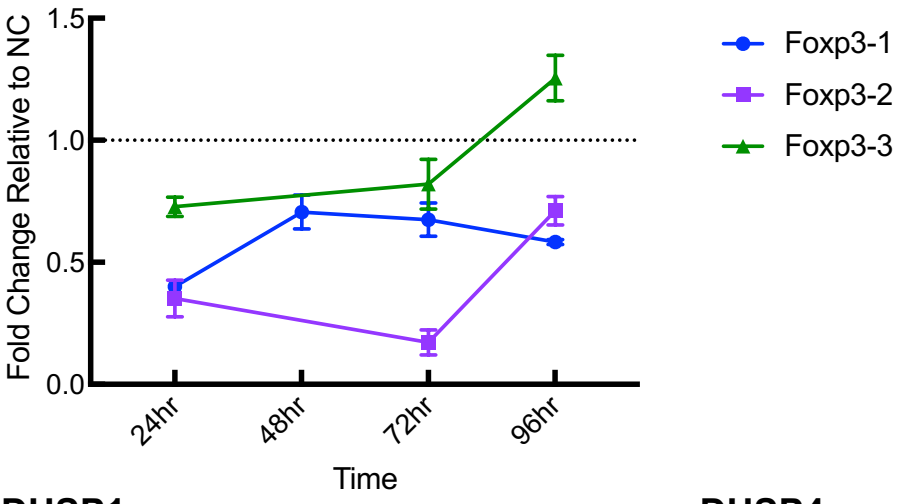


**C**

**DUSP1**

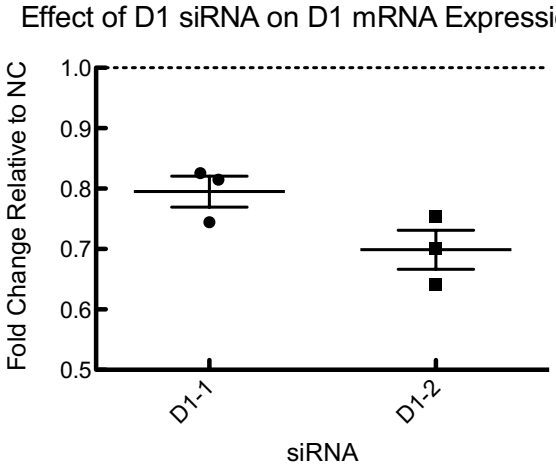


**DUSP4**

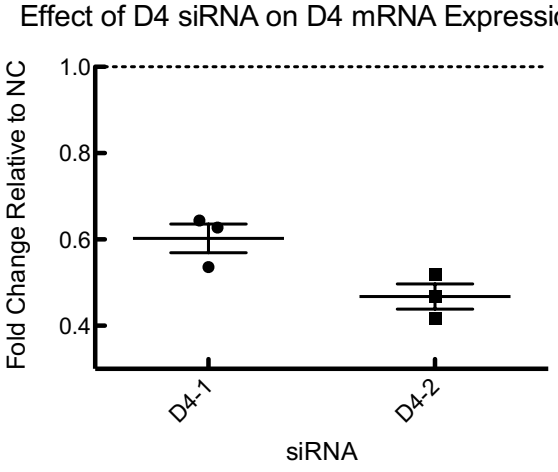


**RGS1**


**Helios**

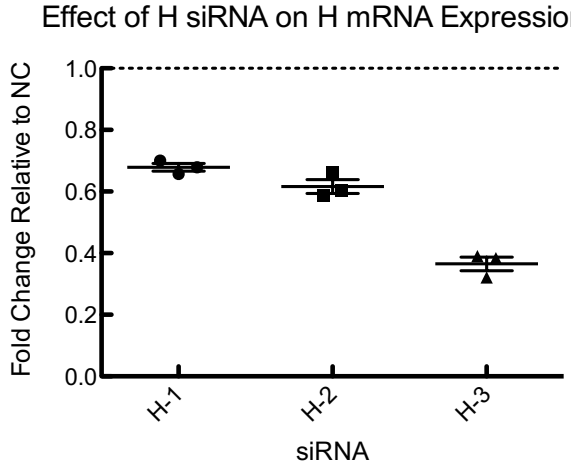

# Supplementary Figure IV-4 (Continued)

**D**

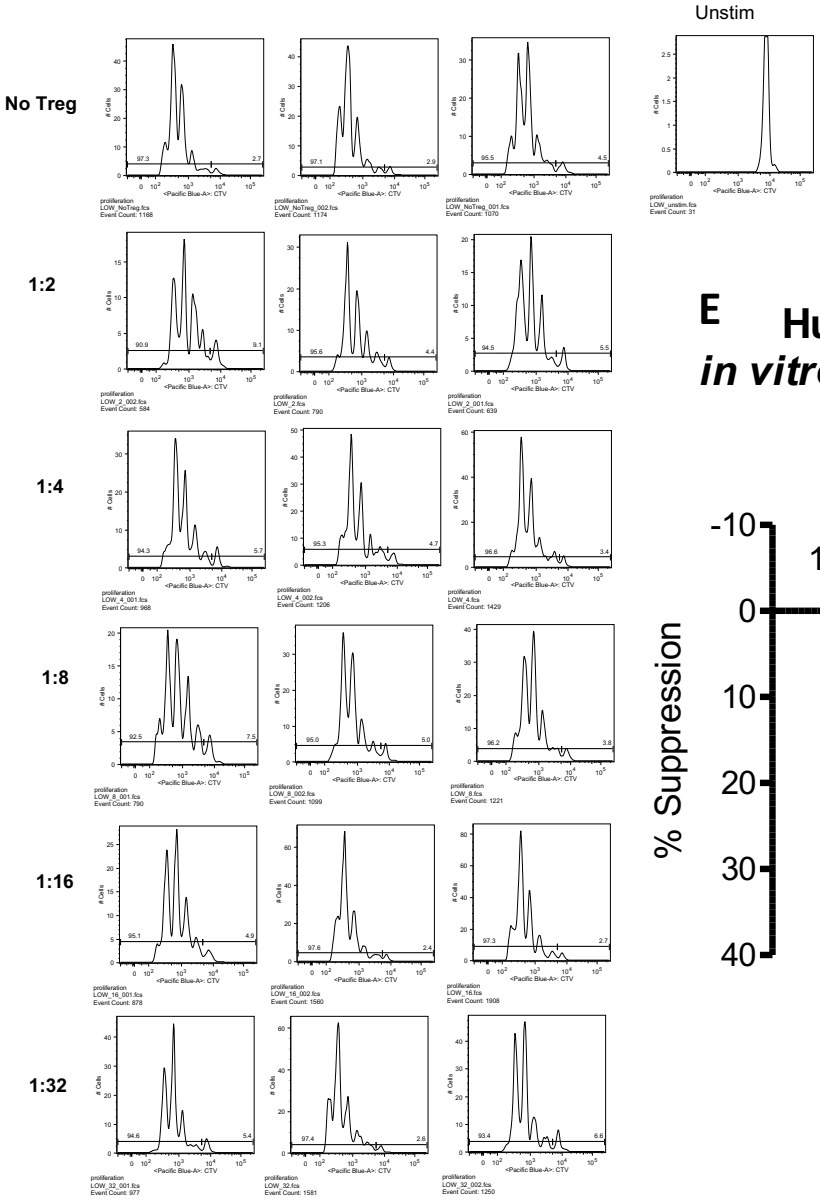


**E** **Human PBMC (Leukopak)**
***in vitro* (micro-)suppression assay**

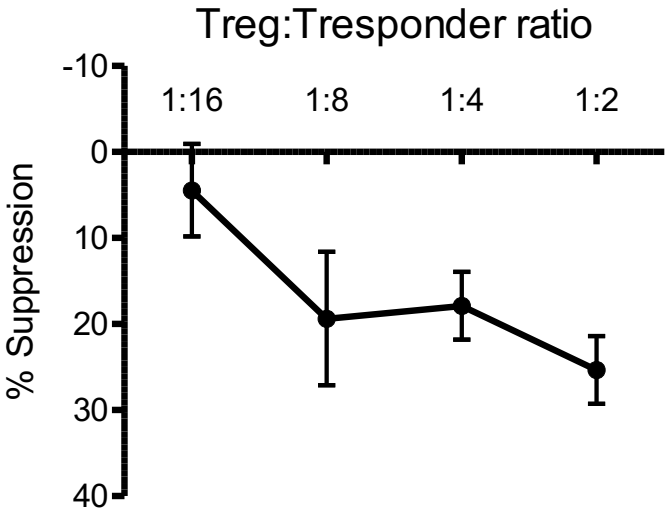


% Suppression
= (1-(DI of the sample)/(DI of the average of "No Treg"))*100
(*DI=division index)

# CURRICULUM VITAE

CURRICULUM VITAE FOR Ph.D. CANDIDATES

The Johns Hopkins University School of Medicine

Yuki Muroyama, MD — 11/06/2017

Name — Date of thisversion

**EDUCATION AND TRAINING:**

**EDUCATION:**

| | | |
|---|---|---|
| Ph.D. | 2013 – 2017 | Johns Hopkins University, School of Medicine, Baltimore, MD<br>Ph.D. in Immunology expected 2017<br>Thesis advisors: Dr. Charles G. Drake, M.D., Ph.D. and Dr. Drew M. Pardoll, M.D., Ph.D.<br>Thesis title: "Tumor-infiltrating Regulatory T cells – Phenotype and Expansion by Radiation Therapy" |
| M.D. | 2005 – 2011 | The University of Tokyo, School of Medicine, Tokyo, Japan |

**TRAINING:**

| | | |
|---|---|---|
| Resident | 2013 | Division of Rheumatic Disease, National Center for Global Health<br>and Medicine, Tokyo, Japan |
| Resident | 2011 – 2013 | The University of Tokyo Hospital, Tokyo, Japan |
| Research Rotation | 2010 | University of Pennsylvania, Pulmonary, Allergy and Critical Care Division<br>Advisor: Dr. Reynold Panettieri, M.D.<br>Project: "Vitamin D and narrow spectrum kinase inhibitors modulate<br>inflammatory mediator release in a model of steroid-insensitivity and viral exposure." |

**AWARDS AND HONORS:**

1. 2017 American Association of Immunologists (AAI) Trainee Abstract Award, May 2017.
2. 1st prize Young Investigator Award for Oral Presentation, 20th Annual Translational Research Cancer Centers Consortium (TRCCC) Meeting, February 2017
3. Best poster presentation award, Graduate Immunology program annual retreat, Johns Hopkins University, School of Medicine, September 2016.

**SCHOLARSHIPS AND FUNDINGS:**

1. Japan Student Services Organization (JASSO), Japanese Ministry of Education and Science (2013-2016)
2. Scholarship from the University of Tokyo for overseas research clerkship, 2010

3. Helped writing RO1 grant for Dr. Charles Drake (Radiotherapy increases functionally suppressive regulatory T cells in the tumor microenvironment)

**PUBLICATIONS:**

1. Muroyama Y, Pardoll DM, Drake CG et al. Stereotactic Radiotherapy Increases Functionally Suppressive Regulatory T cells in the Tumor Microenvironment. *Cancer Immunology Research* **5**, 992-1004, doi:10.1158/2326-6066.cir-17-0040 (2017).
2. Muroyama Y*, LaFleur M*, Drake CG and Sharpe AH. Inhibitors of the PD-1 Pathway in Tumor Therapy. *J. Immunol.* 2018 (in press)
3. Marsiscano AE, …Muroyama Y, …Drake CG et al. Elective nodal irradiation attenuates synergy with immunotherapy. *Clinical Cancer Research* (in submission)
4. Nirschl TR, …Muroyama Y, …Drake CG et al. Understanding the Phenotype and Function of Prostate Infiltrating T-Regulatory Cells (in submission)
5. Muroyama Y, Jo T, Nagase T et al. A case of lung hepatoid adenocarcinoma with brain metastasis and highly elevated alpha-fetoprotein levels. (in preparation)

(*: co-first authors)

**PRESENTATIONS:**

**INVITED TALKS AND ORAL PRESENTATIONS:**

1. Muroyama Y, Drew M. Pardoll and Charles G. Drake et al., American Association of Immunologists (AAI) annual meeting, May 2017
2. Muroyama Y, Drew M. Pardoll and Charles G. Drake et al., 20th Annual Meeting of the Translational Research Cancer Centers Consortium (TRCCC), February 2017.
3. Muroyama Y, Jo T, Nagase T et al., Joint conference of the Japanese Respiratory Society Kanto Division and the Japanese Tuberculosis Society Kanto Division, September 2012.
4. Muroyama Y, Rose N et al., Invited talk at the Clinical Immunology Research Course at the University of Tokyo, School of Medicine, July 2014

**POSTER PRESENTATIONS AND PUBLISHED ABSTRACTS:**

1. Muroyama Y, Drew M. Pardoll and Charles G. Drake et al., American Society for Radiation Oncology (ASTRO) immunotherapy workshop, June 2017.
2. Muroyama Y, Drew M. Pardoll and Charles G. Drake et al., Annual meeting of the American Association of Immunologists (AAI), May 2017. *The Journal of Immunology* 2017;198(1 Supplement): 204.19-.19.
3. Muroyama Y, Drew M. Pardoll and Charles G. Drake et al., Keystone Symposia Conference, Cancer Immunology and Immunotherapy, March 2017.
4. Muroyama Y, Drew M. Pardoll and Charles G. Drake et al., 20th Annual Meeting of the Translational Research Cancer Centers Consortium (TRCCC), February 2017.
5. Muroyama Y, Drew M. Pardoll and Charles G. Drake et al., Graduate Immunology program annual retreat, Johns Hopkins University, School of Medicine, September 2016.

6. Muroyama Y, Drew M. Pardoll and Charles G. Drake et al., Graduate Immunology program annual retreat, Johns Hopkins University, School of Medicine, September 2015.
7. Okudaira R, Muroyama Y, Nagase T et al., Academic research meeting for the respiratory function imaging, January 2013.
8. Koziol-White C, Banerjee A, Muroyama Y, Panettieri RA, et al. Presentation at the American Thoracic Society International Conference, May 2011. *American Journal of Respiratory and Critical Care Medicine* 183: A24142, 2011

**TEACHING EXPERIENCE, SERVICE:**

1. Mentoring medical student Victoria Huang (Persky Award Recipient, and the awardee of the top 3 podium presentation award in medical school research symposium), summer research project, Johns Hopkins University, School of Medicine (January 2016 – February 2017).
2. Lecture, presentation and forum at Clinical Immunology Research Course at the University of Tokyo, School of Medicine, July 2014

**LABORATORY SKILLS:**

Flow-cytometry, mouse tumor models, *in vitro* micro-suppression assay, regulatory T cell *in vitro* suppression assay, ELISA, Western blot, PCR, siRNA, animal breeding and genotyping, human tumor and blood sample processing

**REFERENCES:**

**1: Dr. Charles G. Drake, M.D., Ph.D.**
Thesis advisor (primary)
Columbia University Medical Center, Division of Hematology / Oncology
177 Fort Washington Avenue, suite 6GN-435, New York, NY 10032
E-mail: cgd2139@cumc.columbia.edu
Phone: (212) 305-2055

**2: Dr. Drew M. Pardoll, M.D., Ph.D.**
Thesis advisor (co-advisor)
The Johns Hopkins University School of Medicine
CRB-I, Room 444, 1650 Orleans Street, Baltimore, Maryland 21231
E-mail: dmpardol@jhmi.edu
Phone: (410) 955-7866

**3: Dr. Jonathan D. Powell, M.D., Ph.D.**
Thesis committee member
The Johns Hopkins University School of Medicine
CRB-I, Room 443, 1650 Orleans Street, Baltimore, Maryland 21231
E-mail: poweljo@jhmi.edu
Phone: (410)502-7887